LBL-21171

Lawrence Berkeley Laboratory
UNIVERSITY OF CALIFORNIA

EARTH SCIENCES DIVISION

Received by OSTI
JUN 0 9 1986

MATHEMATICAL MODELS OF THERMAL AND CHEMICAL TRANSPORT IN GEOLOGIC MEDIA

C.-H. Lai
(Ph.D. Thesis)

December 1985

DO NOT MICROFILM
COVER

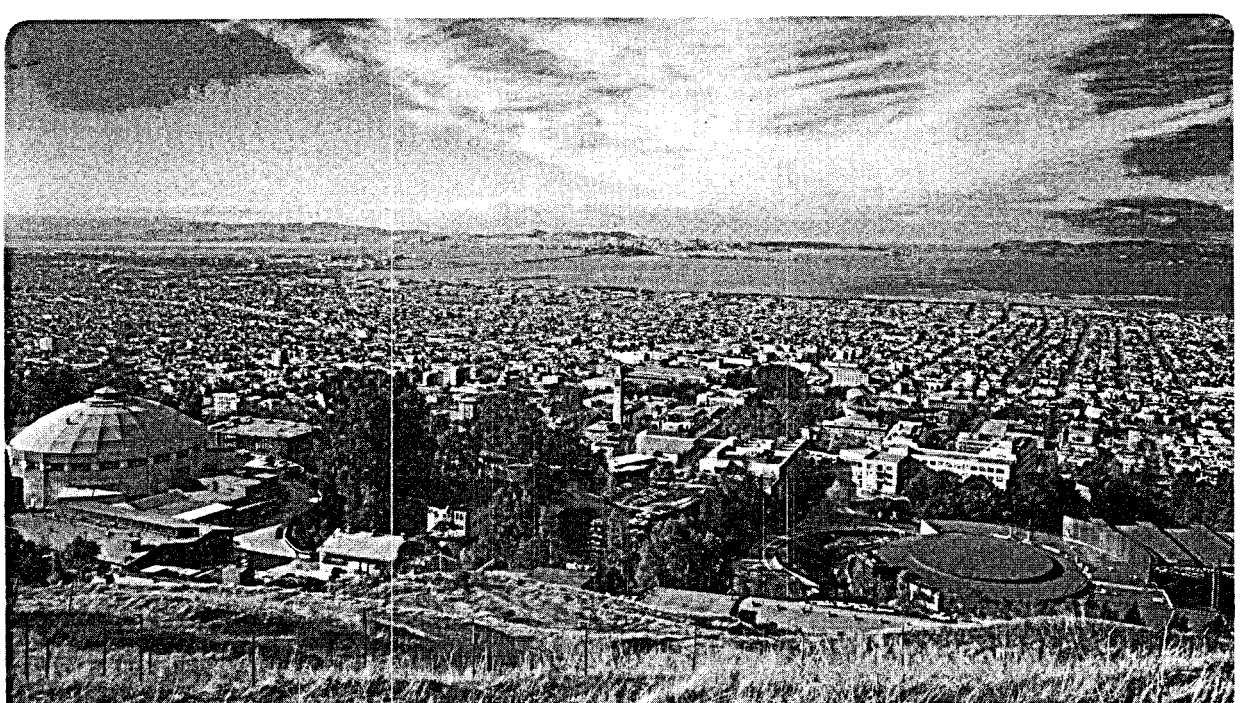

DISTRIBUTION OF THIS DOCUMENT IS UNLIMITED

Prepared for the U.S. Department of Energy under Contract DE-AC03-76SF00098

DISCLAIMER

This report was prepared as an account of work sponsored by an agency of the United States Government. Neither the United States Government nor any agency Thereof, nor any of their employees, makes any warranty, express or implied, or assumes any legal liability or responsibility for the accuracy, completeness, or usefulness of any information, apparatus, product, or process disclosed, or represents that its use would not infringe privately owned rights. Reference herein to any specific commercial product, process, or service by trade name, trademark, manufacturer, or otherwise does not necessarily constitute or imply its endorsement, recommendation, or favoring by the United States Government or any agency thereof. The views and opinions of authors expressed herein do not necessarily state or reflect those of the United States Government or any agency thereof.

DISCLAIMER

Portions of this document may be illegible in electronic image products. Images are produced from the best available original document.

LEGAL NOTICE

This book was prepared as an account of work sponsored by an agency of the United States Government. Neither the United States Government nor any agency thereof, nor any of their employees, makes any warranty, express or implied, or assumes any legal liability or responsibility for the accuracy, completeness, or usefulness of any information, apparatus, product, or process disclosed, or represents that its use would not infringe privately owned rights. Reference herein to any specific commercial product, process, or service by trade name, trademark, manufacturer, or otherwise, does not necessarily constitute or imply its endorsement, recommendation, or favoring by the United States Government or any agency thereof. The views and opinions of authors expressed herein do not necessarily state or reflect those of the United States Government or any agency thereof.

Lawrence Berkeley Laboratory is an equal opportunity employer.

MASTER

LBL--21171

DE86 011302

MATHEMATICAL MODELS OF THERMAL AND CHEMICAL TRANSPORT IN GEOLOGIC MEDIA

Cheng-Hsien Lai

Earth Sciences Division
Lawrence Berkeley Laboratory
University of California
Berkeley, California 94720

Ph.D. Thesis
Department of Material Science and Mineral Engineering
University of California
Berkeley, California 94720

December 1985

This work was supported by the U.S. Department of Energy under Contract Number DE-ACO3-76SF00098.

DISTRIBUTION OF THIS DOCUMENT IS UNLIMITED

MATHEMATICAL MODELS OF THERMAL AND CHEMICAL TRANSPORT IN GEOLOGIC MEDIA

Cheng-Hsien Lai

Department of Material Science and Mineral Engineering
University of California, Berkeley
Berkeley, California 94720

ABSTRACT

Semi-analytical and numerical methods are used to investigate thermal and chemical transport processes in geologic media. The work is divided into two parts: (1) development of semi-analytical models for the analysis of uncoupled isothermal and nonisothermal fluid flow in naturally fractured media, and (2) development of a high resolution numerical code to address coupled nonisothermal chemical transport in geologic media.

A semi-analytical model is developed for well test data analysis in naturally fractured reservoirs. A simple approximate analytical solution for pressure build-up and drawdown tests is developed. Methods based on the approximate solution are developed for the evaluation of important reservoir properties. Type curves for nonisothermal fluid flow in naturally fractured media are developed to design injection systems for maximum energy in hydrothermal systems.

An accurate finite difference method for the solution of a convection-diffusion type equation is developed. The method consists of a novel combination of an explicit second-order Godunov method and the operator splitting technique. The accuracy of the numerical method is investigated. The results shows that, in con-

trast to conventional finite difference methods, the present method can significantly reduce numerical diffusion errors and grid orientation effects. In particular, the method guarantees no spurious oscillations near fronts for high Peclet numbers.

The method is incorporated in a two-dimensional code to investigate free convection in a porous slab and kinetic silica-water reactions in geothermal systems. The effects of pressure- and temperature-dependent fluid properties on the details of convection solutions are addressed. The results show that the overall heat transfer behavior is not strongly affected by relaxing the Boussinesq approximation. However, the mass flux and temperature distributions are significantly affected by the pressure- and temperature-dependent fluid properties. The results obtained from the simulation of silica-water reactions illustrate that the precipitation of silica plays a definite role in the reduction of permeability and flow rate. A multicomponent model considering the variations of pressure, temperature and silica concentration is developed to interpret the evolution of geothermal systems during exploitation. This model can provide information on the interaction between the hot reservoir and adjacent cold aquifers, which is impossible by conventional methods.

P. A. Witherspoon

Thesis Committee Chairman

MATHEMATICAL MODELS OF THERMAL AND CHEMICAL TRANSPORT IN GEOLOGIC MEDIA

Table of Contents

Table of Contents i

List of Figures vi

List of Tables x

Notation xi

Acknowledgments xii

CHAPTER 1: INTRODUCTION 1

CHAPTER 2: LITERATURE REVIEW

2.1. Fluid Flow in Geologic Media 8

2.1.1. Fluid Flow in a Single Fracture 8

2.1.2. Fluid Flow in Fracture Networks 11

2.1.3. Fluid Flow in Double Porosity Media 12

2.2. Miscible Displacement 18

2.2.1. Miscible Displacement in a Capillary Tube 18

2.2.2. Miscible Displacement in Geologic Media 19

2.3. Numerical Methods 22

CHAPTER 3: ANALYTICAL STUDIES OF TRANSPORT IN NATURALLY FRACTURED RESERVOIRS

3.1. Introduction 27

3.2. Verification of the MINC Approximation 27

3.2.1. Fluid Flow in a Porous Cube 28

3.2.2. Fluid Flow in a Rectangular Porous Slab 32

3.3. Pressure Transient Analysis of Naturally Fractured Reservoirs 37

3.3.1. Basic Model 39

3.3.2. Mathematical Model 39

3.3.3. Asymptotic Solutions 44

3.3.4. Numerical Verification of the Present Model 46

3.3.5. Comparison Between Models for Naturally Fractured Reservoirs 46

3.4. Pressure Transient Analysis with New Model 49

3.4.1. Well Test Data Analysis for Infinite Reservoirs 49

3.4.2. Horner Pressure Build-Up Analysis for Infinite Reservoirs 58

3.4.3. Pressure Drawdown Behavior in Reservoirs with Closed or Constant Pressure Outer Boundary 60

3.4.4. Application of New Model to Field Data 64

3.5. Thermal Propagation in Naturally Fractured Reservoirs 68

3.5.1. Basic Model 68

3.5.2. Mathematical Model 69

3.5.3. Thermal Front Propagation 72

3.5.4. Design of Injection Systems 78

3.6. Conclusions 79

CHAPTER 4: NUMERICAL MODEL FOR THERMAL AND CHEMICAL TRANSPORT

4.1. Introduction 82

4.2. Numerical Simulator PTC 83

4.3. Mathematical Model 83

4.3.1. Conservation of Mass 84

4.3.2. Conservation of Energy 87

4.3.3. Conservation of Chemical Species 88

4.4. Solution Procedures 89

4.5. Method for Controlling Numerical Diffusion Errors And Grid Orientation Effects 92

4.6. Validation of the Numerical Method 99

4.6.1. One-Dimensional Convection with Longitudinal Dispersion 99

4.6.2. Two-Dimensional Convection with Longitudinal and Transverse Dispersion 103

4.7. Grid Orientation Effects 106

4.7.1. Convection with Flow Field Oblique to Computational

Grid 110

4.7.2. Chemical Transport Processes in Five-Spot Well Configurations 112

4.8. Conclusions 116

CHAPTER 5: APPLICATIONS

5.1. Introduction 120

5.2. Natural Convection in a Porous slab 123

5.3. Reactive Silica Transport in a Single Fracture 138

5.3.1. Kinetic Model of Silica-Water Reactions 139

5.3.2. Effects of Silica Deposition on Transient Flow Behavior 141

5.4. Multiple-Component Modeling of Geothermal Systems 149

5.5. Conclusions 157

CHAPTER 6: CONCLUSIONS AND RECOMMENDATIONS

6.1. Conclusions 159

6.2. Recommendations 161

REFERENCES 163

APPENDICES

APPENDIX A: Derivation of the Governing Equations for Fluid Flow in Naturally Fractured Media 175

APPENDIX B: Simultaneous Solution for Pressures of the Fracture and Rock Matrix 178

APPENDIX C: Asymptotic Solution for Pressures of an Infinite Reservoir 181

APPENDIX D: Approximate Solution for the Pressure of an Infinite Reservoir 183

APPENDIX E: The Solution of Temperatures for the Fracture and Rock 185

List of Figures

Figure 2-1 Idealized Model of Naturally Fractured Reservoirs.

Figure 2-2 Computational Mesh to Model Transport Processes in a Fractured Porous Medium Employed by the MINC Approximation.

Figure 3-1 One-Dimensional Approximation of Fluid Flow in Rock Matrix Block.

Figure 3-2 Pressure Distributions in a Porous Cube Calculated Using the One-Dimensional Approximation and the Exact Solution (Labeled 3D Model).

Figure 3-3 Comparison Between the Flow Rate From a Cube Using the One-Dimensional Solution and the Exact Solution.

Figure 3-4 Basic Model for a Rectangular Porous Slab Using the One-Dimensional Approximation.

Figure 3-5 Comparison Between the Flow Rate from a Rectangular Porous Slab Using the One-Dimensional Solution and the Exact Solution (Labeled 2D Model).

Figure 3-6 Comparison Between Numerical and Semi-Analytical Solutions.

Figure 3-7 Comparison Between Warren and Root and the Present Solution for an Infinite Reservoir.

Figure 3-8 Pressure Drawdown Behavior without Wellbore and Skin Effects.

Figure 3-9 Effects of Wellbore Storage on Pressure Drawdown Behavior.

Figure 3-10 Effects of Wellbore Storage and Skin on Pressure Drawdown Behavior.

Figure 3-11 Comparison Between Warren and Root and the Present Solutions for a Closed Reservoir.

Figure 3-12 Effects of Outer Boundary Conditions on Pressure Behavior.

Figure 3-13 Pressure Build-Up Analysis.

Figure 3-14 Type Curves for Thermal Front Movement in Naturally Fractured Reservoirs.

Figure 3-15 Temperature Profiles in Fractures and Rock Matrix; $\tau = 0.1$.

Figure 3-16 Temperature Profiles in Fractures and Rock Matrix; $\tau = 1.0$.

Figure 4-1 Fluid Motion in a Porous Space R (W is a Subregion of R).

Figure 4-2 The Mass Flow Rate Across the Unit Surface Area.

Figure 4-3 The Symbols of Numerical Computations in Two Dimensions.

Figure 4-4 Solutions at the Front Where First-Order or Second-Order Differencing (the Limiter $\Delta^s T_{i,j}$) is Used.

Figure 4-5 Comparison Between Analytical and Numerical Solutions Using a Second-Order Godunov Method.

Figure 4-6 Comparison Between Results Using a Second-Order Godunov Method (Monotonize Upwind/Central Differencing Method) and a Conventional First-Order Upwind Difference Method.

Figure 4-7 Schematic Illustration of a Convection-Diffusion Problem with Longitudinal and Transverse Dispersion.

Figure 4-8 Comparison Between Numerical and Approximate Analytical Solutions for a Convection-Diffusion Problem with Longitudinal and Transverse D.spersion.

Figure 4-9 Schematic Illustration of a Benchmark Problem for a Flow Field Oblique to the Computational Grid at 45^0.

Figure 4-10 Comparison of Numerical Solutions and the Approximate Solution for the Grid Orientation Problem.

Figure 4-11 Comparison Between Numerical Solutions for Chemical Transport in Injection-Production Wells with a Five-Spot Pattern.

Figure 4-12 Solutions for Chemical Transport in Injection-Production Wells with a Five-Spot Pattern Using the Code RESSQ.

Figure 4-13 Solutions for Chemical Transport in Injection-Production Wells with a Five-Spot Pattern Using a Second-Order Godunov Method (with Physical Dispersion).

Figure 5-1 The Rectangular Porous Slab Considered for the Natural Convection Problem.

Figure 5-2 The Computational Mesh Used in the Natural Convection Problem.

Figure 5-3a The Distribution of Mass Flux in the Porous Slab for Rayleigh Number of 25.

Figure 5-3b The Distribution of Mass Flux in the Porous Slab for Rayleigh Number of 50.

Figure 5-3c The Distribution of Mass Flux in the Porous Slab for Rayleigh Number of 100.

Figure 5-3d The Distribution of Mass Flux in the Porous Slab for Rayleigh Number of 200.

Figure 5-4a The Distribution of Isotherm Contours in the Porous Slab for Rayleigh Number of 25.

Figure 5-4b The Distribution of Isotherm Contours in the Porous Slab for Rayleigh Number of 50.

Figure 5-4c The Distribution of Isotherm Contours in the Porous Slab for Rayleigh Number of 100.

Figure 5-4d The Distribution of Isotherm Contours in the Porous Slab for Rayleigh Number of 200.

Figure 5-5 Silica Concentration and Permeability Profiles along the Fracture for the Low Pressure Drop Case.

Figure 5-6 Silica Concentration and Permeability Profiles along the Fracture for the High Pressure Drop Case.

Figure 5-7 Flow Rate Declines along the Fracture under Isotherm Conditions for Low Pressure Drop (Case 1) and High Pressure Drop (Case 2).

Figure 5-8 Silica Concentrations Compared with Temperature and Permeability Profiles along the Fracture without Heat Transfer from the Rock Matrix.

Figure 5-9 Silica Concentrations Compared with Temperature and Permeability Profiles along Fractures with Heat Transfer form Rock Matrix.

Figure 5-10 A Simplified Conceptual Model of the Ellidaar Geothermal Field in Iceland.

Figure 5-11 The Computational Mesh Used in the Modeling of the Ellidaar Geothermal Field in Iceland.

Figure 5-12 Annual Production Rates for the Ellidaar Geothermal Field. The Broken Line Shows the Average Flow Rate Used in the Coupled Modeling.

Figure 5-13 Comparison Between Calculated and Observed Pressure Decline at the Ellidaar Geothermal Field in Iceland.

Figure 5-14 Comparison Between Calculated and Observed Temperature Decline at the Ellidaar Geothermal Field in Iceland.

Figure 5-15 Comparison Between Calculated and Observed Silica Concentration Decline at the Ellidaar Geothermal Field in Iceland.

List of Tables

Table 3-1 Data for Pressure Build-Up Test.

Table 3-2 Parameters Used for Design of Injection Systems.

Table 5-1 Input Parameters for Natural Convection Problem.

Table 5-2 Nusselt Number as a Function of Rayleigh Number for Aspect Ratio of 0.3.

Table 5-3 The Equilibrium Constants for Silica-Water Reactions.

Table 5-4 The Rate Constants for Silica-Water Reactions.

Notation

A	Length of a rectangle	L
A_r	Surface reaction area for silica-water reactions	L^2
A_z	Cross section area in the z direction	L^2
A_z	Cross section area in the z direction	L^2
b	Fracture aperture	L
$\bar{b}$	Effective fracture aperture	L
B	Width of a rectangle	L
$\bar{B}$	Formation volume factor	
c	Sum of the compressibility of fluid and rock	$T/(ML^2)$
c_1	Storativity of rock matrix	$T/(ML^2)$
c_2	Storativity of fracture	$T/(ML^2)$
c_f	Specific heat of fluid	$L^3/(TK)$
c_r	Specific heat of rock	$L^3/(TK)$
C	Concentration	M/L^3
C_c	A constant for the cubic law	
C_D	Dimensionless storativity	
C_{eq}	Equilibrium concentration	M/L^3
C_S	Concentration of fluid sources	M/L^3
C_w	Wellbore storage coefficient	
$\bar{C}$	Dimensionless concentration	
D	Side length of a cube	L
D_{ij}	Dispersion coefficient	L^2/T

D_l	Longitudinal dispersion coefficient	L^2/T
D_m	Molecular diffusion constant	L^2/T
D_{num}	Numerical diffusion constant	L^2/T
D_t	Transverse dispersion coefficient	L^2/T
D_x	Numerical diffusion constant in the x direction	L^2/T
D_y	Numerical diffusion constant in the y direction	L^2/T
E	Total energy in geologic media	M/T
g	Gravitational acceleration	L/T^2
h	Formation thickness	L
H	Width of a porous slab	L
I_0	Modified Bessel function of the first kind, zero order	
$I_{1/2}$	Modified Bessel function of the first kind, 1/2 order	
I_1	Modified Bessel function of the first kind, first order	
$I_{3/2}$	Modified Bessel function of the first kind, 3/2 order	
k	Permeability of a porous medium	L^2
$\underline{k}$	Rate constants for silica-water reactions	
k_1	Permeability of rock matrix	L^2
k_2	Permeability of fracture	L^2
K_0	Modified Bessel function of the second kind, zero order	
K_1	Modified Bessel function of the second kind, first order	
K_h	Effective heat conductivity of geologic media	$ML^2/(T^2K)$
$\underline{K}$	Equilibrium constant for silica-water reactions	
$\bar{K}$	Dimensionless permeability	
L	Length of a system or a porous slab	L

M_r	Mass of water for silica-water reactions	M
$\bar{n}$	Unit outward normal vector	
Nu	Nusselt number	
p	Laplace parameter	
P	Pressure	M/LT^2
P_1	Pressure of rock matrix	M/LT^2
P_2	Pressure of fracture	M/LT^2
P_b	Pressure at the boundary	M/LT^2
P_D	Dimensionless Pressure	
P_{Df}	Dimensionless Pressure of wellbore	
P_i	Initial Pressure	M/LT^2
P_{wf}	Flowing well pressure	M/LT^2
P_{DS}	Dimensionless shut-in pressure	
$\bar{P}_{D1}$	Dimensionless pressure of rock matrix in the Laplace domain	
$\bar{P}_{D2}$	Dimensionless pressure of fractures in the Laplace domain	
$\bar{P}_{Df}$	Dimensionless pressure of wellbore in the Laplace domain	
Pe	Peclet number	
q	Volumetric flow rate	L^3/T
q_D	Dimensionless volumetric flow rate	
q_m	Mass injection rate	M/T
$\bar{q}_{cond}$	Conductive heat flux	$ML/(T^2K)$

$\bar{q}_{conv}$	Convective heat flux	$ML/(T^2K)$
Q	Mass flow rate at the entrance	L^3/T
Q_i	Initial mass flow rate at the entrance	L^3/T
Q_h	Total heat flow rate per unit thickness	ML^2/T^2
r	Radial distance	L
r_D	Dimensionless radial distance	
r_e	External radius of a system	L
r_{ed}	Dimensionless external radius	
r_i	Internal radius of a system	L
r_t	Radius of a tube	L
r_w	Wellbore radius	L
R	Any domain in geologic media	
Ra	Rayleigh number	
S	Skin factor	
S_A	Bounded surface area for a volume	L^2
S_i	Symbol for any dependent variables	
t	time	T
t_e	Time for uniform energy sweep	T
t_D	Dimensionless time	
T	Temperature	K
T_0	Initial temperature	K
T_1	Temperature of rock	K
T_2	Temperature of fracture	K
T_b	Temperature at the boundary	K

T_C	Temperature at the cold wall	K
T_D	Dimensionless temperature	
T_{D1}	Dimensionless temperature of rock matrix	
T_{D2}	Dimensionless temperature of fracture	
T_H	Temperature at the hot wall	K
T_i	Temperature of injected fluid	K
T_{ref}	Referenced temperature	K
T_S	Temperature of fluid sources	K
$\overline{T}$	Dimensionless temperature	
$\overline{u}$	Average velocity of the cross section in a tube	L/T
v_m	Seepage velocity in the m direction	L/T
v_n	Seepage velocity in the n direction	L/T
v_x	Darcy's velocity in the x direction	L/T
v_y	Darcy's velocity in the y direction	L/T
$\overline{v}$	Darcy's velocity	L/T
$\overline{v}_c$	Convective mass flux	$M/(TL^2)$
$\overline{v}_T$	Convective heat flux	$ML/(T^2K)$
$\overline{v}_t$	Total seepage velocity	L/T
$\lvert\overline{v}_t\rvert$	Magnitude of total seepage velocity	
V_e	Any volume element in geologic media	
$\overline{V}$	Vector of total velocity	
$\lvert\overline{V}\rvert$	Magnitude of total velocity	
W	Any subregion of the domain W	
$\overline{W}$	Width of a system	L

x	x coordinate	
x'	Dimensionless x distance	
y	y coordinate	
y'	Dimensionless y distance	
z	z coordinate	
z'	Dimensionless z distance	
α_{ijmn}	Geometric tensor in porous media	L^2
α_l	Longitudinal dispersivity	L^2
α_t	Transverse dispersivity	L^2
β	Fluid thermal expansivity	1/K
$\overline{\beta}$	The aspect ratio of a rectangle	
ξ	Dimensionless radial distance	
ξ_c	Radial distance for uniform energy sweep	L
ϵ	Rock compressibility	$T/(ML^2)$
ϕ	Porosity of geologic media	
ϕ_1	Porosity of rock matrix	
ϕ_2	Porosity of fracture	
γ	Euler's constant	
$\overline{\gamma}$	Rock thermal expansivity	1/K
θ	Ratio of the energy content of the fracture to that of of the rock	
λ	Inter-porosity flow factor defined by Warren and Root	
$\overline{\lambda}$	Inter-porosity flow factor	
μ	Fluid viscosity	M/LT

ψ_1	Dimensionless temperature of rock in the Laplace domain	
ψ_2	Dimensionless temperature of fracture in the Laplace domain	
ρ_f	Fluid density	M/L^3
ρ_r	Rock density	M/L^3
ρ_{ref}	Referenced fluid density	M/L^3
σ_c	Chemical capacity per unit volume	M/L^3
σ_T	Thermal capacity per unit volume	M/TK
τ	Dimensionless time	
ω	Ratio of storativity	
η	Dimensionless vertical distance	
ς	Fluid compressibility	T/ML^2

Acknowledgments

I would first like to express my deepest gratitude to Professor P. A. Witherspoon, my research advisor, for his guidance, advise and support during this work. I should appreciate Dr. C. F. Tsang for his invaluable help, advise and inspiration. Many sincere thanks are due to Professor W. H. Somerton for his help and critical review of this work.

Through many helpful discussions on nonisothermal chemical transport in geologic media, Dr. G. S. Bodvarsson has significantly contributed to this work. I convey to him my gratitude for this and his many suggestions. I extend my gratitude to Drs. K. Pruess and M. Lipmann for their stimulating discussions and suggestions. My special thanks are due to Dr. P. Colella for his discussions and suggestions on the second-order Godunov method for hyperbolic equations. I would also like to thank S. Benson, C. Doughty, K. Karasaki, and A. Verma for their help and discussions.

I am grateful to M. Bodvarsson. She carefully revised and edited this manuscript.

This work was supported through U. S. Department of Energy Contract No. DE-AC03-76SF00098 by the Assistant Secretary for Conservation and Renewable Energy, Office of Renewable Technology, Division of Geothermal Technology.

Finally, I would like to thank my parents for their help and encouragement.

CHAPTER 1

INTRODUCTION

The role of nonisothermal chemical transport in geologic media has received considerable attention in recent years, because of its importance in such problems as exploitation of hydrothermal resources, underground storage of nuclear waste materials, and enhanced oil recovery processes. To obtain an integrated analysis of the transport processes in geologic media, an appropriate physical and mathematical model of the system is indispensable. However, most transport models have been founded on the assumption of a homogeneous, isotropic porous medium. In geologic media, high permeability and secondary porosity may occur in naturally fractured and jointed formations, and this makes the analysis of transport processes much too complicated for conventional homogeneous formation models.

In addition to the complexity of geologic media, chemical transport is often coupled with hydrological, and thermal processes. Heat and chemical species carried by the flowing fluids can alter the flow field significantly. The fluid properties depend greatly on temperature, and chemical reactions causing precipitation or dissolution of minerals can change important medium properties such as porosity and permeability. These coupled processes generally exhibit non-linear behavior; thus numerical methods become the only viable means to address these problems. However, there are some problems that must be addressed when a numerical code is developed. These include the development of an accurate method to control numerical diffusion errors and the computational efficiency of the method.

The control of numerical diffusion errors is one of the major challenges in numerical modeling of transport processes dominated by convection forces. The substantial amounts of numerical diffusion errors inherent in conventional finite difference methods may cause incorrect computational results. For example, numerical diffusion errors can result in erroneous predictions of breakthrough times in tracer tests or enhanced oil recovery processes and, more seriously, cause the physics of the processes to be lost. To avoid numerical instabilities, any explicit numerical method must satisfy stability conditions. This is to say that no more than one pore volume of material can be put through a computational grid in one time step, which can result in enormous computations to simulate problems for long time periods. Where there are no time step restrictions, implicit methods allow one to take large size time steps in numerical simulations. However, a large size time step will introduce artificial diffusion from the temporal truncation errors, and produce an inaccuracy in numerical computations. Also, implicit methods for solving a set of nonlinear equations require one to solve a large system of algebraic equations simultaneously, which can lead to matrices that are too large to be inverted quickly even for the super computer. It is known that in using conventional explicit and/or implicit finite difference methods, it is very difficult to avoid numerical diffusion errors unless a very fine grid is used. This means these methods become difficult to model chemical transport in large scale geologic systems, if highly resolved solutions are required. Therefore, one objective of this work was to develop a cost-effective numerical method to handle these problems.

The present study is divided into two parts. The first part deals with the semi-analytical methods used to analyze uncoupled isothermal and nonisothermal fluid flow in naturally fractured reservoirs. A naturally fractured reservoir model is presented that considers transient inter-porosity flow for a cubic-shaped rock matrix, as proposed by Barenblatt et al. (1960) and Warren and Root (1963). They employed a quasi-steady assumption for inter-porosity flow rather than a transient assumption. Other investigators (Kazemi, 1969; Boulton and Streltsova, 1977; Streltsova, 1982; Serra et al. 1982; Javandel and Witherspoon, 1983) proposed layered models to consider transient inter-porosity flow in naturally fractured reservoirs. Since the surface interaction area for a given volume is different for the present model and the layered model, the intensity of inter-porosity flow of the two models should be different. In contrast to the layered model, inter-porosity flow between the rock matrix and fractures should be handled as a three-dimensional problem and involves more mathematical complexities. However, it is shown that a simple one-dimensional approximate model, developed from the method of "multiple interaction continua" (MINC) (Pruess and Narasimhan, 1982), can be used to accurately account for transient inter-porosity flow.

Based on the present model, a semi-analytical method for the analysis of well test data from naturally fractured reservoirs is developed. The method considers the wellbore storage and skin effects during pressure drawdown and build-up tests for several different boundary conditions. The boundary conditions include the cases of constant rate production in infinite and finite systems as well as a system with a constant pressure outer boundary. Solutions for the pressures

in the fractures and rock matrix can be obtained using the Laplace transformation technique. Because the solutions in the Laplace domain are too complicated to be inverted into real space by analytical means, a numerical method is employed. However, a simple approximate solution in real space for the analysis of the transient pressure behavior without wellbore storage and skin effects in an infinite system is developed. Ershaghi and Aflaki (1985) applied this approximate solution and developed a technique to generalize the so-called "half slope" observed in the transition period of the pressure drawdown test. Methods, based on the approximate solution, analyzing the important reservoir properties such as storativity, transmissibility, inter-porosity flow factor, and ratio of storativity are developed. The results show that the inter-porosity flow factor and storativity ratio calculated from the present model are much smaller than those obtained by the original Warren and Root model (1963). A quantitative analysis of the effects of wellbore storage and skin on the transient pressure behavior shows a large discrepancy between the present model and the Mavor and Cinco-Ley model (1979). This is because the Mavor and Cinco-Ley model (1979) considered a quasi-steady assumption for the interaction between the rock matrix and fractures.

Because nonisothermal fluid flow in naturally fractured media is a topic of interest in the geothermal field, various theoretical studies based on the layered models (Lauwerier, 1955; Bodvarsson, 1969; Bodvarsson and Tsang, 1982) have been done. These studies showed that injection of water into geothermal reservoirs during exploitation can greatly enhance the energy recovery from the resource. Injection will help maintain reservoir pressure and provide water that

will extract residual heat contained in the reservoir rocks. However, experience gained through commercial scale reinjection has shown that the injection operation must be carefully designed. Horne (1981) reports declines in enthalpy of produced fluids at several Japanese fields due to injection. This interference is attributed to rapid flow of the injected "cold" water through fractures, as evidenced by high tracer velocities. This indicates that fundamental studies of cold water movement in fractured geothermal reservoirs are needed, before confidence in the design of commercial reinjection operations can be established. A semi-analytical model for the analysis of injection flow rates and the injection locations in naturally fractured reservoirs is developed. The purpose of this work is to design injection systems to obtain maximum energy recovery from geothermal reservoirs.

The second part of this investigation is to study the coupled nonisothermal chemical transport processes in geologic media by numerical methods. As the basic equation describing the processes is a convection-diffusion type equation, conventional finite difference methods may not be suited for solving this type of equation; they will either introduce substantial amounts of numerical diffusion errors or give spurious oscillations near fronts when convection force is dominant. To overcome these difficulties, a new method is developed. The method consists of a novel combination of an explicit second-order Godunov method (Van Leer, 1977; Colella, 1984) and the operator splitting technique (Strang, 1968). By means of operator splitting, the convection-diffusion equation can be split into two parts and solved in two steps. The first part, solved by a second-order Godunov method, is a pure hyperbolic equation, which only considers the convection equation. The second part, solved by the conventional central difference

method, is a parabolic type equation, which omits the convection term from the convection-diffusion equations. The results show that with this new approach, the numerical diffusion errors and grid orientation effects can be significantly reduced. In particular, the method guarantees no oscillations near fronts for high Peclet numbers.

The method has been incorporated in a two-dimensional code to investigate free convection in a porous slab and to simulate kinetic reactions of silica-water in geothermal systems. The natural convection problem in a porous slab subjected to horizontal temperature differences has long been of some interest to hydrologists and heat transfer engineers, and it has posed many difficult and fundamental questions. These include theoretical investigations of overall heat transfer rate from one hot vertical wall to the other vertical cold wall, and mass flux and temperature distributions in the system. The effects of pressure- and temperature-dependent fluid properties on the the convection solutions, which have not been considered by previous workers, are also investigated in the present study. Numerical predictions of the overall heat transfer rate, mass flux and temperature distributions are obtained for Rayleigh numbers of 25, 50, 100, and 200, respectively. The results show that the overall heat transfer behavior in the medium is not strongly affected by relaxing the Boussinesq approximation, but the mass flux and temperature distributions are significantly affected by the pressure- and temperature-dependent fluid properties.

In order to investigate the effects of silica precipitation on transient fluid flow behavior, the kinetics of silica-water reactions, as proposed by Rimstidt and

Barnes (1980), are incorporated in the code. The results obtained from the simulation of silica-water reactions illustrate that the precipitation of silica plays a definite role in the reduction of permeability and flow rate. Furthermore, to address the performance of geothermal reservoirs during production, a multi-component model including pressure, temperature, and silica concentration is employed. This model has been applied to the Ellidaar geothermal field in Iceland to obtain good estimates of reservoir volume, permeability and porosity. The model also gives information on the interaction between the active hot reservoir and adjacent cold aquifers, which is not possible with conventional methods.

CHAPTER 2

LITERATURE REVIEW

2.1. Fluid Flow in Geologic Media

The main driving force in transport processes in geologic media is fluid flow. A review of this process is necessary in order to understand the complexities of the development of a physical model for transport processes in such media. At the microscopic level, fluid flow through a void space in such media is governed by the same fundamental laws for the conservation of mass, and momentum that are derived from continuous mechanics. The complex geometric configurations and boundary conditions in geologic media make it very difficult to investigate fluid flow at the microscopic level. Therefore, the basic law usually employed in describing the macroscopic behavior of fluid flow in geologic media is Darcy's law, which was developed from experimental investigations of the overall behavior of flow in porous media. This law defines permeability as an intrinsic material property that describes the ability of a given medium to transmit fluids.

2.1.1. Fluid Flow in a Single Fracture

Because the topology of fractured media is different from that of porous media, Darcy's law may not be adequate for describing the fluid motion in such media. For a single fracture separated by two smooth, parallel surfaces, the macroscopic flow rate in the fracture is governed by the cubic law. The law is derived from the solution of the Navier-Stokes equation for steady laminar flow of incompressible Newtonian fluids through two parallel plates (Lomize, 1951; Snow, 1965; Romm, 1966; Schlichting, 1968; Iwai, 1976) given by

$$q = C_c b^3 \nabla P \tag{2.1}$$

where q is volumetric flow rate, b is the aperture of the plates and P is pressure. C_c in Eq. 2.1 is dependent on the system geometries and fluid properties. For rectangular and radial coordinate systems, C_c is expressed as

$$C_c = -\frac{\overline{W}}{L}\frac{\rho_f\, g}{12\mu} \tag{2.2}$$

and

$$C_c = -\frac{2\pi}{\ln(\frac{r_e}{r_i})}\frac{\rho_f\, g}{12\mu} \tag{2.3}$$

where $\overline{W}$ is the system width, L is the system length, r_e is the system external radius, r_i is the system internal radius, ρ_f is fluid density, μ is fluid viscosity, and g is gravitational acceleration. The cubic law has been extensively applied to fluid flow in a single fracture of natural rocks (Louis, 1969; Sharp, 1970; Iwai, 1976).

Since rough surfaces of a natural rock fracture may have some degree of contact under stressed conditions, the resulting tortuous flow path could affect the cubic law. To study this problem, Witherspoon et al. (1980) experimentally investigated flow test in three different rock types (Iwai, 1976), and found that the cubic law seems to be valid whether the fractures are open or closed. However, the constant C_c in Eq. 2.1 must be divided by a factor f to take into account roughness effects. Raven and Gale (1985) investigated fluid flow behavior in natural rocks by subjecting different sized sample to various normal stresses. They indicated that fracture flow rate is decreased with increasing sample size and with each additional loading cycle. The deviation of the relation

between fracture flow rate and fracture deformation from behavior predicted by a parallel plate model is increased with sample size and number of loading cycles. To confirm their experimental results, they suggested that further work on measurement of fracture roughness with load-deformation and stress-permeability tests on different sample sizes is required. More recently, Pyrak et al. (1985) developed a new experimental technique to investigate fluid flow behavior in natural rock fractures under stressed conditions. The preliminary results showed that this new technique enables one to determine the flow paths and contact area between the fracture surfaces under various effective stresses.

Tsang and Witherspoon (1981) developed a theoretical model to address the effects of normal stress on fluid flow in a single fracture with rough surfaces. To analyze the macroscopic flow behavior in a single fracture with rough surfaces, they developed a modified cubic law, in which the averaged apertures along the longitudinal and transverse directions to the macroscopic flow were used. The averaged apertures were obtained from stress-displacement measurements of intact rock and fractured rock; the fluid flow was then calculated from the modified cubic law. The validity of this theoretical model was verified with Iwai's experimental work (1976), and they found that the predicted flow rates from the model agree well with the experimental results. Later, Tsang and Witherspoon (1983) computed the normal stress-displacement and stress-fluid flow for a single fracture with known roughness profiles using a theoretical model (Tsang and Witherspoon, 1981). They found qualitative correlations between the roughness profile and normal stress-displacement and stress-fluid flow.

2.1.2. Fluid Flow in Fracture Networks

For fluid flow through fractured formations, two approaches are usually employed; that is, the discrete and continuous approaches. The discrete approach considers that the fractured formations consist of the distributed fractures with finite apertures, and each fracture can transmit fluids only when it intersects other conducting fractures. The continuous approach assumes that the distributed fractures are of infinite extent so that no fracture dead ends exist, and the global fluid flow in the system behaves as that in an equivalent porous medium. Based on the intrinsic permeability tensor of a single infinite fracture with arbitrary orientation and aperture for a given coordinate system, Snow (1969) developed a mathematical model to compute the intrinsic permeability tensor of a rock mass contributed by a fracture network.

Some investigators (Parsons, 1966; Caldwell, 1971, 1972) used the discrete approach to study fluid flow in fracture networks by means of electric analog models which are based on the analogy between Ohm's law and the cubic law. By comparing the measured electrical potential distributions with theoretical solutions for different values of permeability tensor, the overall permeability of the system may be obtained. To address whether a fracture network can be represented by an equivalent porous medium, Long et al. (1982) and Long (1983) developed a method to generate random fracture distributions, and used a discrete approach to study flow behavior in such a system. The effects of fracture density, fracture aperture, fracture orientation, and sample sizes were considered in their studies. These investigators showed that permeability ellipses cal-

culated from a simulated flow test in fracture networks may not exist, and this implies that a fracture network may not be represented by an equivalent porous medium. Their results also showed that a fracture network will behave more like a porous medium when the system has a high fracture density with rather uniform fracture apertures and nonuniform fracture orientations. Later, Long and Witherspoon (1985) further considered the effects of the degree of interconnection between fractures on the global permeability of a fracture network. They found that fracture networks with longer but less dense fractures behave more like porous media than do networks with shorter but more dense fractures. Because the main emphasis of these investigators is to determine the role of fractures in fluid flow behavior in geologic media, they assume the rock matrix to be impermeable; no interaction between the rock matrix and fractures is considered. However, the fraction of the total volume occupied by fractures (fracture porosity) is very small, and can not provide substantial amounts of fluids. Thus, it seems necessary to assess the potential of prolific hydrothermal and petroleum fractured reservoirs to account for the storativity of the rock matrix and its interaction with the fractures. Another approach commonly used to investigate fluid flow in fractured formations in the hydrology and petroleum field is reviewed in the next section.

2.1.3. Fluid Flow in Double Porosity Media

Using an alternative continuous approach, Barenblatt et al. (1960) and Warren and Root (1963) proposed the so-called "double porosity" model, as shown in Figure 2-1. This model assumes that fractured reservoirs behave like two-porosity

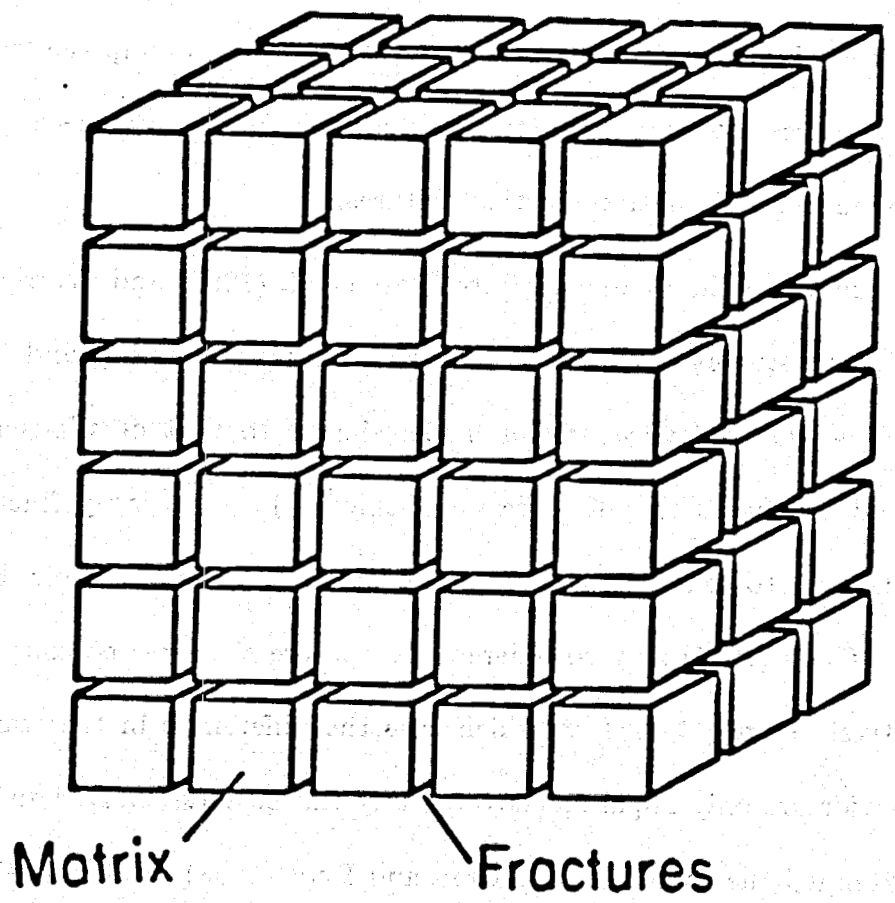

-- XBL 833-8668 --

Figure 2-1 Idealized Model of Naturally Fractured Reservoirs.

media; one medium (the rock matrix), separated by three sets of orthogonal fractures, has a high storage capacity and low permeability, and the other (the fractures) has a low storage capacity and high permeability. Therefore, a basic characteristic of "double porosity" reservoirs (naturally fractured reservoirs) is that the fractures provide the main conduits for fluid transport in the system, while the rock matrix provides gradual fluid drainage to the fractures. To investigate fluid flow in "double porosity" reservoirs, the approach employed by Barenblatt et al. (1960) and Warren and Root (1963) is to lump the fractures and the rock matrices into two different continua, and further assume a quasi-steady flow between the rock matrix and the fractures.

Subsequent to the studies of Barenblatt et al. (1960) and Warren and Root (1963), various studies have been published on the applicability and extension of their models. Odeh (1965) used a model similar to that of Warren and Root (1963), and concluded that the pressure behavior in a naturally fractured reservoir is identical to that of a homogeneous porous medium reservoir. However, in his study, Odeh (1965) only considered cases where the inter-porosity flow factor was relatively large ($\geq 10^{-3}$), in which case the differences in the transient pressure behavior are only apparent at very early times. Later, Mavor and Cinco-Ley (1979) extended the solution by Warren and Root (1963) to include the effects of wellbore storage and skin. Chen and Jian (1980) developed analytical solutions for fluid flow in two-dimensional and radial flow systems with finite domains using the method of separation of variables. Bourdet and Gringarten (1980), and Gringarten (1982) introduced an alternative analysis of well test data from new type curves that included wellbore storage and skin effects.

Many workers have developed models that do not require the approximation of quasi-steady fluid flow between the rock matrix and the fractures. However, due to the three-dimensional nature of the model considered by Barenblatt et al. (1960) and Warren and Root (1963), the treatment of transient inter-porosity flow is mathematically very difficult, and has been accomplished only by drastic simplification of matrix block geometry. Kazemi (1969), Boulton and Streltsova (1977), Deruyck (1982), Streltsova (1982) and Serra et al. (1982), considered a slab model, whereas de Swan (1976), Najurieta (1980), and Cinco-Ley and Fernando Samaniego (1982), considered models based on spherically shaped matrix blocks. Javandel and Witherspoon (1983) developed an analytical solution for a partially penetrating well in a two-layer aquifer. At early times, their solution is identical to that of a single layer aquifer. At later times, the slope of a semi-log plot of drawdown versus time is only a function of the sum of the transmissivitiy of the two layers. Barker (1984) defined exact and approximate block-geometry functions to treat regular and irregular matrix geometries, respectively. The regular rock matrix geometries included an infinite slab, infinite cylinder, sphere, rectangular parallel pipe, and infinite hollow cylinder.

The slab model is applicable to layered reservoirs as well as to reservoirs with predominantly horizontal fractures. However, in the slab model one-dimensional fluid flow in the layers is assumed. This approximation is only valid if the permeability contrast between layers is large. The pressure transient behavior observed in wells located in naturally fractured reservoirs may be strongly affected by the local heterogeneous properties. In this circumstance, the naturally fractured model may not give satisfactory interpretations of the test

data (Benson and Lai, 1985; Karasaki et al. 1985); different models, which may consist of a naturally fractured and a conventional models, are necessary to take into account the effect of local heterogeneous properties.

Pruess and Narasimhan (1982) have developed an extension of the double porosity method, referred to as "multiple interacting continua" (MINC) method, to model heat transfer in highly fractured porous media by the integral finite difference method (Edwards, 1972; Narasimhan and Witherspoon, 1976). The MINC approximation assumes that, due to high permeability and low storativity of the fractures, any changes of thermodynamic conditions in a fractured porous media will propagate rapidly in the fracture network, while migrating slowly in low permeability rock matrix. Therefore, the changes of thermodynamic conditions in the rock matrix blocks will depend primarily on the distance to the nearest fracture. In light of this and neglecting gravity effects, fluid and heat flow in the rock matrix blocks may be treated by a one-dimensional approximation. This concept is applicable to regular as well as irregular matrix blocks (Pruess and Karasaki, 1983). In numerical simulations, the MINC method partitions rock matrix blocks into sets of nested volume elements (Figure 2-2). Thus, the interactions between fractures and the rock matrix can be described by one-dimensional mass and energy conservation equations. However, the accuracy of this approximation should be tested and justified (Pruess et al., 1982). The verification of the MINC approximation and the application of the concept of this approximation to isothermal or nonisothermal fluid flow in naturally fractured reservoirs are presented in Chapter 3.

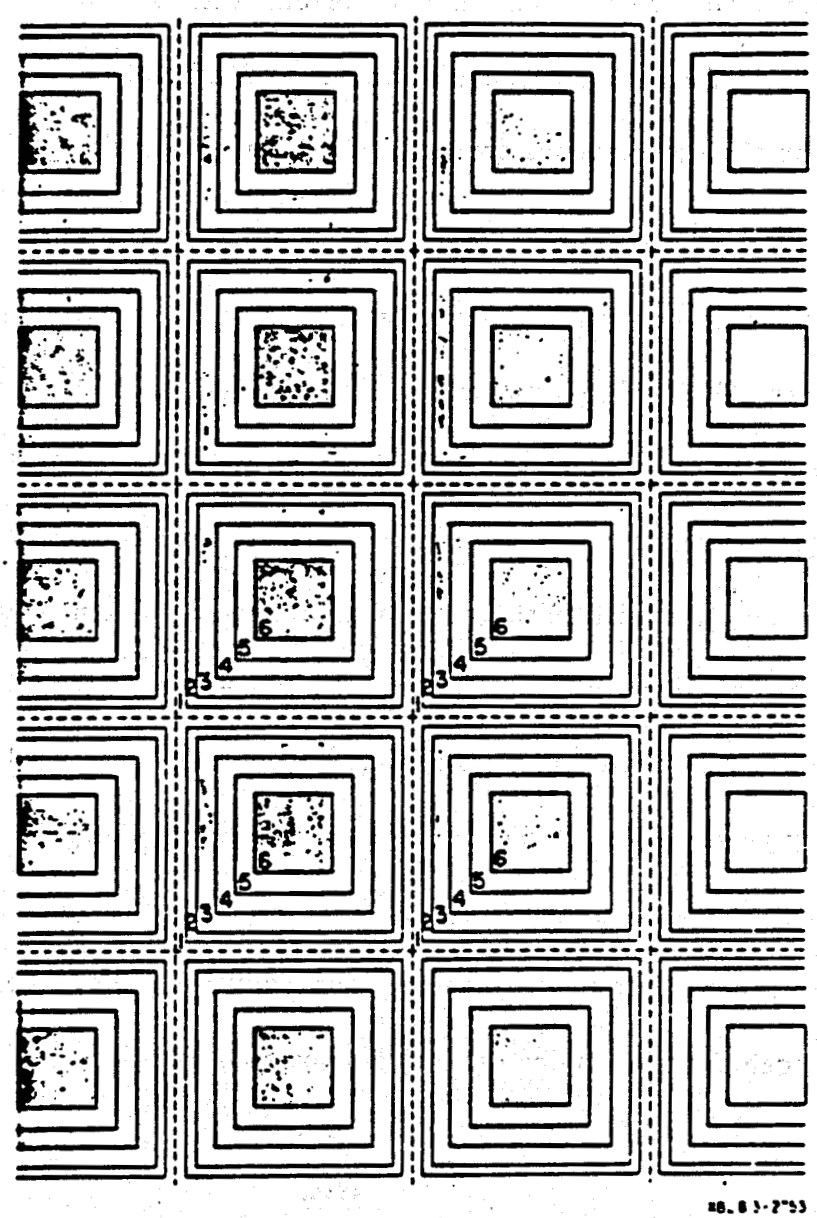

Figure 2-2 Computational Mesh to Model Transport Processes in a Fractured Porous Medium Employed by the MINC Approximation.

2.2. Miscible Displacement

The present study considers miscible displacement, since it is of more concern to hydrologists and petroleum engineers in extensive investigations of recoverable energy from hydrothermal and petroleum reservoirs, and pollutant migration in geologic formations. The phenomenon of miscible displacement can be illustrated by the simultaneous processes of molecular diffusion and dispersion.

2.2.1. Miscible Displacement in a Capillary Tube

At a microscopic level, dispersion in porous or fractured media results from the combined effects of molecular diffusion, distribution of pore velocity within single pores or fractures, and the variable velocities along the tortuous pathlines. Since the geometric structure of porous or fractured media is very complicated, a satisfactory simple model of the process as in such a system does not yet exist. Simplified models, however, may help one to better understand the mechanisms of the process. One of the simplest models for porous or fractured media is a single capillary tube. Taylor (1953) investigated the dispersion process under steady state laminar flow in a capillary tube and showed that for a sufficiently large time the process can be described by the Fickian convection-dispersion process. The dispersion coefficient in Taylor's theory is expressed as

$$D_l = \frac{r_t^{\,2}\bar{u}^2}{48D_m} \tag{2.4}$$

where r_t is radius of the capillary tube, and $\bar{u}$ is the mean velocity of flow in the cross section of the tube. Later, Gill and Sankarasubramanian (1970, 1971) used the series expansion method to generalize Taylor's theory. They showed that the

dispersion coefficient is not a constant, but a time dependent quantity leading asymptotically to Taylor's dispersion theory. A more complicated dispersion process in a capillary tube that included chemical reactions with catalytic walls was investigated by Dang (1983). He found that the length of the tube required for the dispersion model to be valid is increased when chemical reactions occur.

2.2.2. Miscible Displacement in Geologic Media

One method of analyzing the behavior of dispersion in porous media is to statistically model the random motion of marked fluid particles. This allows one to obtain a macroscopic description of dispersion. Analyzing the average distance traveled by a tracer in porous media, Bear (1961) showed that the dispersion coefficient, D_{ij}, is a second rank tensor and is linearly proportional to the components of the seepage velocity. Based on Bear's results, Scheidegger (1961) demonstrated that the dispersion coefficient is expressed as

$$D_{ij} = \alpha_{ijmn} \frac{v_m v_n}{|\overline{v}_t|} \tag{2.5}$$

where α_{ijmn} is the geometric tensor of porous media, v_m and v_n are seepage velocities in the m and n directions, respectively, and $|\overline{v}_t|$ is the magnitude of absolute seepage velocity. For an isotropic porous medium, all components of α_{ijmn} are zero except for

$$\begin{gathered} \alpha_{iiii} = \alpha_l, \ \alpha_{iijj} = \alpha_t \\ \alpha_{ijij} = \alpha_{ijji} = 1/2\,(\alpha_l - \alpha_t), \ i \neq j \end{gathered} \tag{2.6}$$

where α_l and α_t are longitudinal and transverse dispersivity, respectively. When the velocity is coincident with one of the principal axes of the dispersion tensor,

one obtains

$$D_l = \alpha_l \, |\overline{v}_t|, \; D_t = \alpha_t \, |\overline{v}_t| \tag{2.7}$$

Because dispersion is such a complex phenomenon, depending on system properties, flow field, initial and boundary conditions of the system, it is very difficult to evaluate. However, one may gain insight into the properties of dispersivity in porous media through the analysis of Taylor's theory. For example, consider a hypothetical porous medium tube made of continuous stratified layers so that the velocity distributions under steady state in the cross section of the tube are the same as those in the capillary tube. The overall behavior of the dispersion processes in the hypothetical system should be identical to that observed in the capillary tube. In one-dimension, comparing Eqs. 2.4 and 2.7, one can obtain longitudinal dispersivity given by

$$\alpha_l = \frac{r_t^{\,2} \, |\overline{u}|}{48 D_m} \tag{2.8}$$

From the results of Gill and Sankarasubramanian (1970, 1971) for the dispersion process in a capillary tube, one also expects that the dispersivity given by Eq. 2.8 must be a time-dependent quantity asymptotically approaching the constant. This can also explain why the Fickian convection-dispersion processes is not valid for modeling miscible displacement in porous medium at early times, and why the dispersion coefficient is strongly dependent on the scale studied.

Gelhar et al. (1979) studied solute transport in vertically discrete stratified porous media and showed that this type of heterogeneous permeability leads to the Fickian convection-dispersion process for a sufficiently large time. Later,

Gelhar and Axness (1983) developed a three-dimensional solute transport model in heterogeneous porous media. They found that the conventional Fickian convection-dispersion transport model is valid for a large field. Matheron and de Marsily (1980) countered that the Fickian convection-dispersion model may not be always valid for a stratified porous medium with flow parallel to the bedding. However, if a mean flow component is added perpendicular to the layers, the Fickian convection-dispersion processes will be valid for sufficiently large times.

To determine whether the behavior of solute transport in a fracture system can be represented by that in an equivalent porous medium (ie., the Fickian convection-dispersion process is valid). More recently, Endo (1984) extended Long's discretized fracture model (1983) to address mechanical transport in fracture systems on a microscopic scale. He found that for some fracture systems, fluid flow can be predicted using equivalent porous media, but it may not be possible to predict transport using equivalent porous media. At present, for a complicated system involving transient flow field and reactive chemical species, no theoretical model of the global dispersion processes is available, and most numerical models (Rubin and James, 1973; Valocchi et al., 1981; Jennings et al., 1982; Schulz and Reardon, 1983) assume that the Fickian convection-dispersion processes is valid or consider only the convection process for multiple reactive solute transport.

When applicable, the Fickian convection-dispersion processes for chemical transport in geologic media involves two steps. The first step in the modeling procedure is to simulate hydraulic head distributions. This usually needs consider-

able adjustment of permeability distributions until the simulated head distributions are quite similar to those observed in the field. The second step is to simulate chemical concentration distributions using the simulated fluid flow distributions and trial and error adjustments of the values of longitudinal and transverse dispersivities until the simulated chemical migration pattern is similar to that observed in the field. This approach, using a two-dimensional computer code, has been employed to simulate chemical plume migrations in porous or fractured media by Robertson and Barraclough (1973), Pinder (1973), and Konikow and Bredeheoft (1974). Longitudinal and transverse dispersivities obtained from the above simulation studies are in the range of 10 to 100 m, which is as much as several orders of magnitude larger than dispersion coefficients measured in laboratory tests (Fried, 1975; Anderson, 1979).

2.3. Numerical Methods

In a variety of reservoir engineering problems, such as nonisothermal reactive chemical transport, the inhomogeneity of reservoir properties and the nonlinearity of the governing equations make these problems unsolvable by exact analytical techniques. Thus, numerical methods become the indispensable means to obtain solutions of these problems. For practical field applications, the traditional convection-diffusion equations arising from the conservation laws are usually dominated by the convection term, leading to solutions with steep fronts. The most common numerical methods for reservoir engineering problems are those based on difference operators. Computational experience has shown that the central difference method is well adapted to solving the problems with relatively

smooth solutions. However, when the solution has very steep fronts due to strong convection forces, higher-order or central difference methods may suffer from unphysical oscillations (Peaceman, 1977; Hald, 1984). Price et al. (1968) showed that when solving the convection-diffusion equation

$$\frac{\partial S_i}{\partial t} + Pe \frac{\partial S_i}{\partial x} = \frac{\partial^2 S_i}{\partial x^2} \tag{2.9}$$

with a central difference method, unphysical oscillations can be avoided by specifying the computational grid such that $Pe\ \Delta x \leq 2$. S_i is any dependent variable (concentration or temperature) and Pe is the dimensionless Peclet number given by

$$Pe = \frac{|\overline{V}|L}{D_m} \tag{2.10}$$

where $|\overline{V}|$ is the magnitude of absolute velocity, L is a system length, and D_m is a diffusion constant.

In practice, the use of the central difference method without numerical oscillation solutions results in too much computational effort to be implemented. Thus, the alternative usually employed is to use the first-order upwind difference method, which introduces numerical diffusion to avoid oscillations. Such numerical diffusion may be so dominant that the physical diffusion will be obscured. At this point, it is clearly understood that the accuracy of numerical schemes for the convection-diffusion equation is strongly dependent on whether the method used can accurately model the convection term. To eliminate the numerical diffusion errors, particle tracking methods (Garder et al., 1964; Redell and Sunada, 1970;

Bredehoeft and Pinder, 1973; Ahlstrom et al., 1977) were extensively used to simulate solute transport in the petroleum and hydrology field. The basic idea behind these methods is to assign several particles representing the concentration on each computational grid and each particle moves with fluid velocity during each time increment. Thus, the new concentration on each grid point can be interpolated by the concentration of the particles, which move from the neighboring grids. The main drawback of these methods is that the scheme is not well satisfied by the conservation of mass if the particles are not enough. Neuman (1981) proposed an adaptive Eulerian-Lagrangian scheme to avoid many particles required in numerical simulations. He tested various linear problems under a uniform flow field, and showed that the method is capable of handling the entire range of Peclet numbers. However, the applicability of this method to problems under a nonuniform flow field and with nonlinear interactions needs further investigation.

Different approaches based on modified characteristic method eliminate numerical diffusion errors and reduce grid orientation effects in reservoir simulations as shown by Glimm et al. (1983), Ewing et al. (1983), and Jensen and Finlayson (1983). Computational experience with these methods is limited to incompressible problems, and the algorithms arising in implementation are different from those of finite difference codes. Therefore, these techniques are beyond the scope of the present study. Another method to avoid numerical diffusion errors is the random choice method (Glimm's method or sampling method). The method, based on Glimm's constructive existence proof (1965), was developed by Chorin (1976, 1977) into a numerical method with the random

number sequence to solve systems of nonlinear hyperbolic equations. Colella (1982) improved the sampling procedure using the van der Corput sequence to obtain more accurate solutions. This numerical method has been applied to petroleum reservoir simulations (Concus and Proskurowski, 1979; Anderson and Concus, 1980; Glimm et al., 1981; Sethian et al. 1983; Li, 1983). Due to the inherent nature of the sampling sequence, the error introduced by this method is that of front position; the front location is off the exact location by one grid block or less. During this work, this method was tested with several convection problems and found that it indeed possesses some attractive features. The scheme is simple and accurate for nonreactive chemical transport under a uniform flow field. However, the scheme leads to errors in the conservation of chemical species when modeling reactive chemical transport under a nonuniform flow field.

To reduce numerical diffusion errors, Larson (1982) developed a variably timed flux updating method, which belongs to the class of flux-corrected transport methods (Boris and Book, 1973, 1976; Boris et al., 1975; Zalesak, 1979). Except for linear problems, Larson's method appears to introduce oscillations to the solution. Recently, an upwind-type of explicit, second-order finite-difference scheme (Godunov type scheme) with flux limiters to avoid spurious oscillations of the solutions around discontinuities was developed for systems of nonlinear hyperbolic equations arising from gas dynamics (Van Leer, 1977; Roe, 1981; Chakravarthy and Osher, 1983). Sweby (1984) investigated these independently proposed second-order accurate schemes and showed how they relate to each other. From several test cases, including linear advection problems and shock

tube problems, Sweby found that for linear problems, Roe's limiter is most appropriate, followed by Van Leer's, and Chakravarthy and Osher's. For the nonlinear problem (shock tube problem), Van Leer's limiter can obtain a solution nearly as accurate as Roe's, but less susceptible to numerical oscillations. Harten et al. (1983) provided an extensive review of upwind differencing and Godunov type schemes for hyperbolic conservation laws. Colella et al. (1983) applied Van Leer's scheme to solve the one-dimensional Buckley-Leverett equation, and showed that numerical diffusion errors can be significantly reduced by this numerical scheme. More recently, Colella (1984), Colella and Woodward (1984), and Colella (1985) substantially refined Van Leer's scheme. These include computational processes to extend one-dimensional problems to multidimensional problems for systems of nonlinear hyperbolic equations without time splitting, and to improve the accuracy at discontinuities of the solution using a fourth-order accurate difference scheme. In two-dimensions, Van Leer's fourth-order accurate scheme involves 7×7 block of grid points for the solution of each nodal point, resulting in complicated computational procedures. This scheme has not been considered in the present study. The refined version of Van Leer's second-order accurate scheme (without time splitting) was successfully applied to problems of petroleum and hydrothermal reservoir simulations (Bell and Shubin, 1985; Lai et al., 1985) to reduce numerical diffusion errors and grid orientation effects. This numerical scheme is linked with the operator splitting technique for the numerical model of nonisothermal chemical transport in geologic media presented in Chapter 4.

CHAPTER 3

ANALYTICAL STUDIES OF TRANSPORT PROCESSES IN NATURALLY FRACTURED RESERVOIRS

3.1. Introduction

In order to develop a sound plan for the exploitation of a hydrothermal or petroleum resource, reliable information about in-situ conditions of the resource is required. Such information may be obtained from isothermal and nonisothermal well testing, and may be used to predict and evaluate future production scenarios. A physical model of a geologic formation is usually represented by either a porous medium or fractured porous medium model, depending on which model can successfully interpret transport phenomena in the hydrological resource.

In the last two decades considerable work has been devoted to the analysis of isothermal and nonisothermal fluid flow in naturally fractured reservoirs. The need for new methods of analysis arose because of the distinct differences in transport phenomena observed between homogeneous porous reservoirs and fractured reservoirs. In this work, semi-analytical models for the analysis of the well test data and thermal propagation in naturally fractured reservoirs are developed. The models are based on the verification of the MINC approximation, which is presented in the following section.

3.2. Verification of the MINC Approximation

Modeling of inter-porosity flow between fracture and rock matrix in fractured porous media is difficult, especially for irregular rock matrix geometries.

Thus, to model transport processes in double-porosity media most workers have done more or less drastic simplification of rock matrix block geometries. With the MINC approximation, modeling of transport processes in double-porosity media does not require any simplification of block geometries. However, the inherent feature of one-dimensional inter-porosity flow between the rock matrix and fracture by the MINC approximation needs verifications. For example, in most types of matrix block geometry, the mass and heat flow are not perpendicular to the fracture surfaces, especially near fracture intersections ("corners"), and hence can not strictly be considered one-dimensional. To study this "corner" effect, some idealized geometrical configurations and simple boundary conditions are considered, for which the exact solutions as well as solutions based on the MINC approximation are available in analytical and semi-analytical form.

3.2.1. Fluid Flow in a Porous Cube

The test case considered is for isothermal, slightly compressible fluid flow in a porous cube (or, equivalently, heat conduction in an impermeable cube). A constant pressure, P_i, is maintained at the cube surfaces, and an initial pressure of zero is assumed everywhere. With the MINC approximation, fluid flow in a cube can be approximated by a one-dimensional model, as shown in Figure 3-1. The basic model represents one-sixth of a cube, with the surface area for flow decreasing from D^2 (D is the side length of the cube) at the edges of the cube to zero in the center. Thus, the total mass flow at the cube surfaces will be six times that given by the one-dimensional model. This one-dimensional approximation leads to a differential equation, whose form is identical to the heat conduction equation in

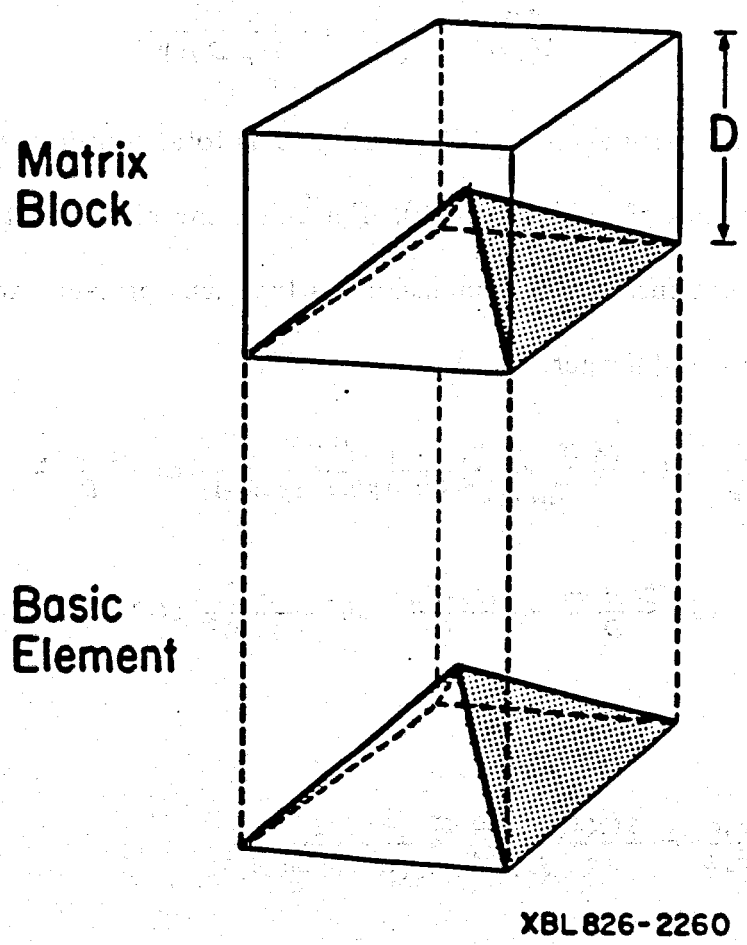

Figure 3-1 One-Dimensional Approximation of Fluid Flow in Rock Matrix Block.

a system with spherical geometry. The dimensionless pressure and flow rate for this problem using the one-dimensional approximation is given by Carslaw and Jaeger (1959)

$$P_D = \frac{P}{P_b} = 1 - \frac{D}{\pi z}\sum_{n=1}^{\infty}\frac{(-1)^n}{n}\sin\frac{2n\pi z}{D}\exp\{-\frac{4n^2\pi^2 kt}{\phi\mu c D^2}\} \tag{3.1}$$

and

$$q_D = \frac{q\mu}{kP_b D} = 24\sum_{n=1}^{\infty}\exp\{-\frac{n^2\pi^2 kt}{\phi c\,\mu(D/2)^2}\} \tag{3.2}$$

where k is intrinsic permeability, ϕ is porosity, c is total compressibility (ie., sum of the compressibility of fluid and rock). For this same problem, it can be solved exactly in three-dimension. The dimensionless transient pressure and flow rate is given by (Carslaw and Jaeger, 1959)

$$P_D = \frac{P}{P_b} = 1 - \frac{64}{\pi^3}\sum_{l=1}^{\infty}\sum_{m=1}^{\infty}\sum_{n=1}^{\infty}\frac{(-1)^{l+m+n-3}}{(2l-1)(2m-1)(2n-1)}\cos\frac{(2l-1)\pi x}{D}$$

$$\cos\frac{(2l-1)\pi y}{D}\cos\frac{(2l-1)\pi z}{D}\exp\{-\frac{k\pi^2 t}{\phi\mu c D^2}[(2l-1)^2+(2m-1)^2+(2n-1)^2]\} \tag{3.3}$$

and

$$q_D = \frac{q\mu}{kP_b D} = \frac{24\times 64}{\pi^4}\sum_{l=1}^{\infty}\sum_{m=1}^{\infty}\sum_{n=1}^{\infty}\frac{1}{(2l-1)^2(2m-1)^2}$$

$$\exp\{-\frac{\pi^2}{4}[(2l-1)^2+(2m-1)^2+(2n-1)^2]\frac{kt}{\phi c\,\mu(D/2)^2}\} \tag{3.4}$$

In the above equations, (x, y, z) coordinates are measured from the center of the cube, and parallel to the edges. The dimensionless pressures at a distance $z = 0.3D$ for the MINC approximation and for the exact solution are plotted versus dimensionless time in Figure 3-2. The figure clearly indicates that in the

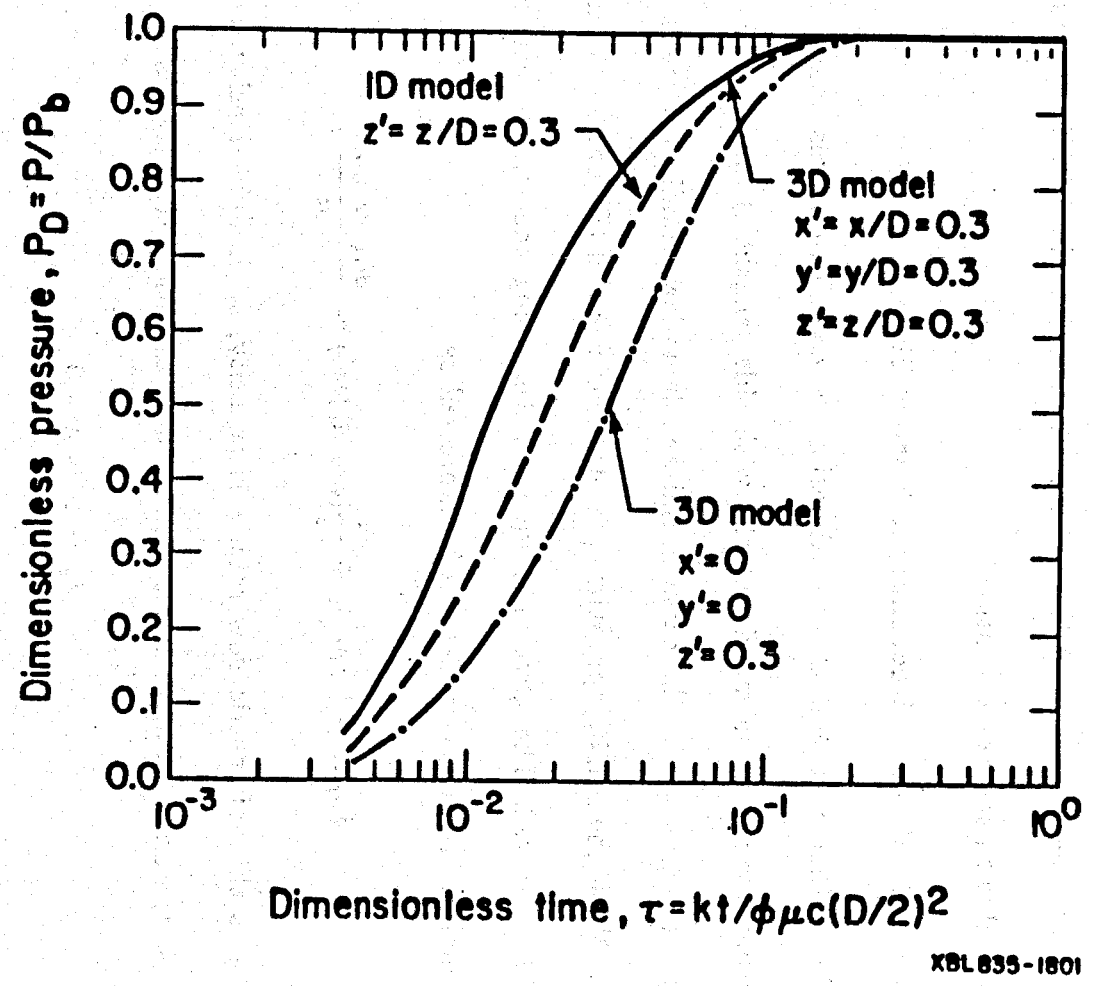

Figure 3-2 Pressure Distributions in a Porous Cube Calculated Using the One-Dimensional Approximation and the Exact Solution (Labeled 3D Model).

center of the plane $z = 0.3D$ (ie., for $x' = \frac{x}{D} = y' = \frac{y}{D} = 0$) the pressures using the MINC approximation are somewhat higher than the exact pressures, but at corner of that plane ($x' = y' = 0.3$) they are somewhat lower. The discrepancies are not large (about 10-15%). What really matters, however, is not the detailed pressure distributions inside the cube, but the flow rate at the cube surfaces, which can affect the global transport processes in fractures. Figure 3-3 shows that the flow rate at the cube surfaces using the MINC approximation agrees well with the exact solution.

3.2.2. Fluid Flow in a Rectangular Porous Slab

To further test MINC approximation, a comparison was made for two-dimensional rectangular matrix blocks with side lengths A and B for different aspect ratios $\overline{\beta} = A/B$. The same initial and boundary conditions are used as in case 1. With the MINC approximation, the basic model (Figure 3-4) of a rectangle will be solved. The governing equation describing the mass conservation in the domain of the basic model can be expressed as

$$q \rho_f A_z - \{ q \rho_f A_z + \frac{\partial}{\partial z}(q \rho_f A_z) dz \} = \frac{\partial (A_z \, dz \, \phi \rho_f)}{\partial t} \tag{3.5}$$

where q is the volumetric flow rate, ϕ is porosity, ρ_f is fluid density, t is time, and A_z is the cross section surface area in the z direction expressed as

$$A_z = 4z + A - B \tag{3.6}$$

Substituting Eq. 3.6 and the Darcy's law ($q = -\frac{k}{\mu}\frac{\partial P}{\partial z}$) into Eq. 3.5, the governing equation describing slightly compressible fluid flow in the domain of the basic

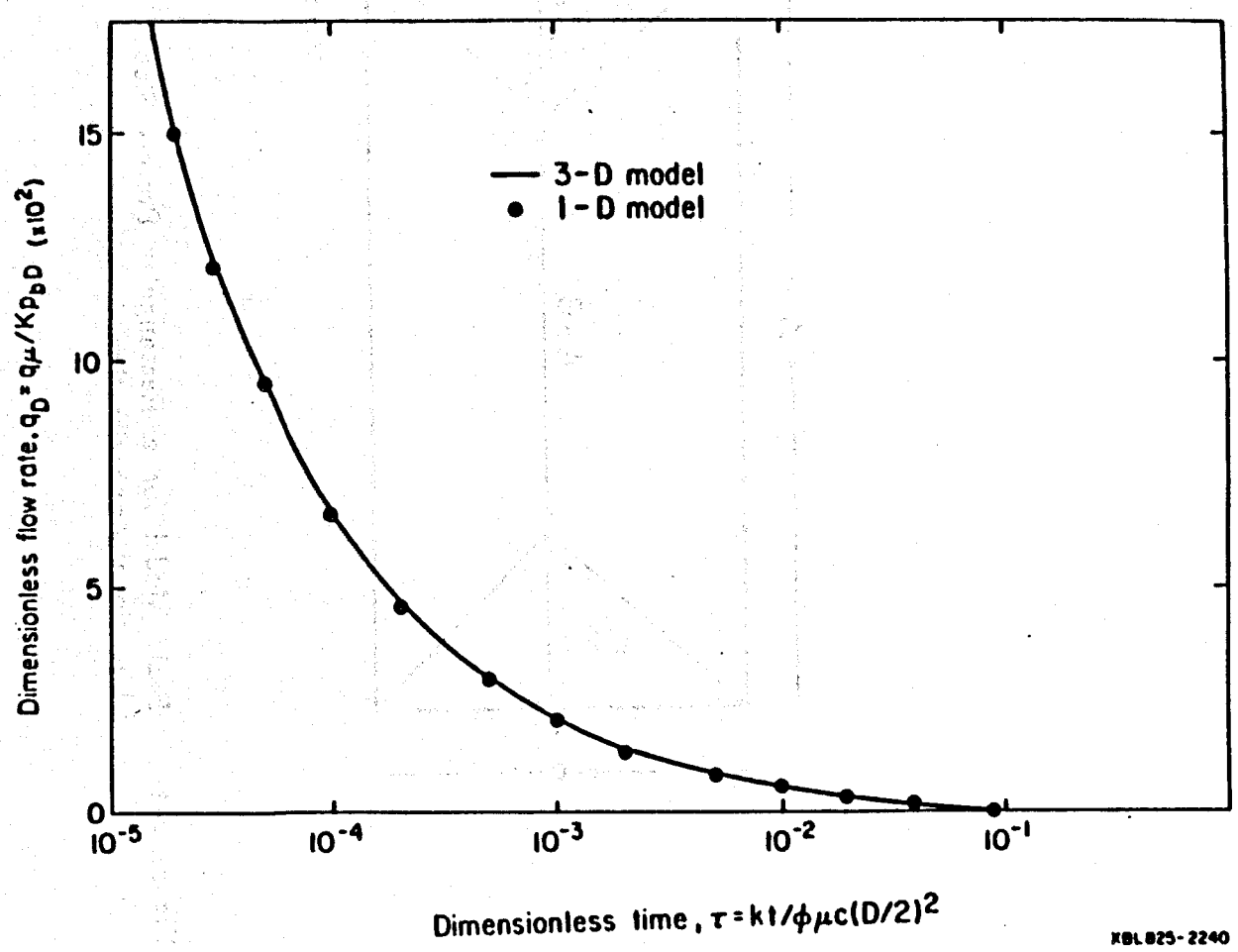

Figure 3-3 Comparison Between the Flow Rate From a Cube Using the One-Dimensional Solution and the Exact Solution.

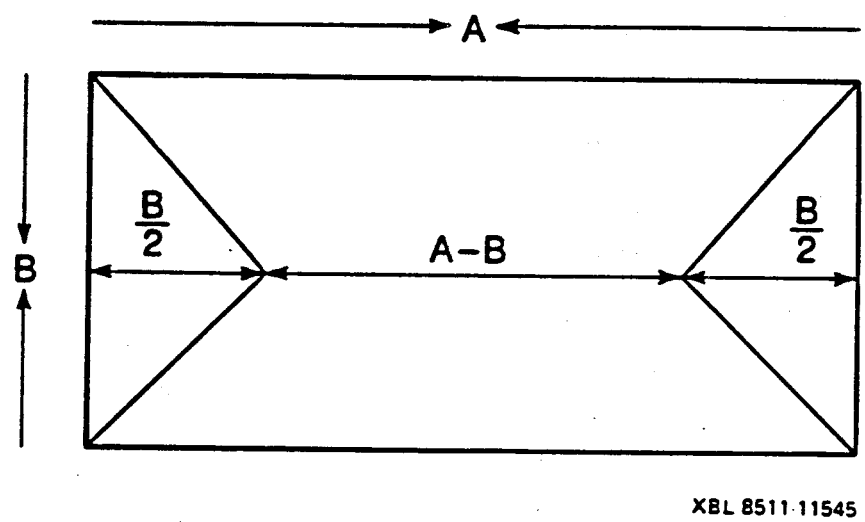

Figure 3-4 Basic Model for a Rectangular Porous Slab Using the One-Dimensional Approximation.

model can be expressed as

$$\frac{\partial^2 P}{\partial z^2} + \frac{1}{z + \frac{1}{4}(A - B)} \frac{\partial P}{\partial z} = \frac{\phi \mu c}{k} \frac{\partial P}{\partial t} \tag{3.7}$$

The initial and boundary conditions are

$$P\ (z, 0) = 0 \tag{3.8}$$

$$P\ (\frac{B}{2}, t) = P_b \tag{3.9}$$

$$\frac{\partial P}{\partial z}\Big|_{z=0} = 0 \tag{3.10}$$

In terms of dimensionless parameters, the governing equation and the initial and boundary conditions can be written as

$$\frac{\partial^2 P_D}{\partial \eta^2} + \frac{1}{\eta} \frac{\partial P_D}{\partial \eta} = \frac{\partial P_D}{\partial t_D} \tag{3.11}$$

$$P_D = 0 \tag{3.12}$$

$$P_D\ (\eta = \frac{A + B}{4B}, t_D) = 1 \tag{3.13}$$

$$\frac{\partial P_D}{\partial \eta}\Big|_{\eta = \frac{A-B}{4B}} = 0 \tag{3.14}$$

where

$$P_D = \frac{P}{P_b} \tag{3.15}$$

$$\eta = \frac{z + 1/4(A - B)}{B} \tag{3.16}$$

$$\tau = \frac{kt}{\phi \mu c B^2} \tag{3.17}$$

In the Laplace domain, the solution of Eq. 3.7 subject to the given initial and boundary conditions is

$$\bar{P}_D = \frac{1}{p} \frac{K_1(\sqrt{p}\frac{A-B}{4B}) I_0(\sqrt{p}\,\eta) + K_0(\sqrt{p}\,\eta) I_1(\sqrt{p}\frac{A-B}{4B})}{K_1(\sqrt{p}\frac{A-B}{4B}) I_0(\sqrt{p}\frac{A+B}{4B}) + K_0(\sqrt{p}\frac{A+B}{4B}) I_1(\sqrt{p}\frac{A-B}{4B})} \tag{3.18}$$

where p is the Laplace parameter. The dimensionless volumetric flow rate at the surface of the rectangle can be obtained from Eq. 3.18 by evaluating the pressure gradient at the surface. The result is expressed as

$$\bar{q}_D = 2(\frac{A}{B}+1)\frac{1}{\sqrt{p}} \frac{K_1(\sqrt{p}\frac{A-B}{4B}) I_1(\sqrt{p}\frac{A+B}{4B}) - K_1(\sqrt{p}\frac{A+B}{4B}) I_1(\sqrt{p}\frac{A-B}{4B})}{K_1(\sqrt{p}\frac{A-B}{4B}) I_0(\sqrt{p}\frac{A+B}{4B}) + K_0(\sqrt{p}\frac{A+B}{4B}) I_1(\sqrt{p}\frac{A-B}{4B})} \tag{3.19}$$

where q_D is $\frac{q\mu}{kP_b}$. In this study, the solution for the dimensionless flow rate in real space is obtained by numerical inversion of Eq. 3.19 (Stehfest, 1972). The exact solution for this two-dimensional problem is given by Carslaw and Jaeger (1959)

$$P_D = 1 - \frac{16}{\pi^2} \sum_{l=1}^{\infty} \sum_{m=1}^{\infty} \frac{(-1)^{l+m-2}}{(2l-1)(2m-1)} \cos\frac{(2l-1)\pi x}{A} \cos\frac{(2m-1)\pi y}{B}$$

$$\exp\{-\frac{k\pi^2 t}{\phi \mu c}[\frac{(2l-1)^2}{A^2} + \frac{(2m-1)^2}{B^2}]\} \tag{3.20}$$

and

$$q_D = \frac{64}{\pi^2}\sum_{l=1}^{\infty}\sum_{m=1}^{\infty}\{\frac{A}{B}\frac{1}{(2l-1)^2} + \frac{B}{A}\frac{1}{(2m-1)^2}\}\exp\{-\frac{k\pi^2 t}{\phi\mu c}[\frac{(2l-1)^2}{A^2} + \frac{(2m-1)^2}{B^2}]\} \tag{3.21}$$

Figure 3-5 shows that the dimensionless volumetric flow rate across the surface of the rectangle obtained from the MINC approximation for different aspect ratios ($\bar{\beta}$) compares well with the exact solution. The agreement becomes close when the aspect ratio is increased, because this will diminish the corner effects neglected by the MINC approximation. These test results indicate that the pressure (or temperature) distributions inside a rock matrix predicted by the MINC approximation are not exact. However, this approximation can accurately represent fragment inter-porosity flow in fractured porous media. This provides a rationale for the method, based on this approximation, for the analysis of well test data and thermal propagation in naturally fractured reservoirs that will be presented in the following sections.

3.3. Pressure Transient Analysis of Naturally Fractured Reservoirs

The original geometrical configurations (Figure 2-1) of a rock matrix, as proposed by Barenblatt et al (1960) and Warren and Root (1963) for double porosity media, is used for the present study. Fully transient inter-porosity flow between the rock matrix and fractures is considered (Lai, et al., 1983). In the following discussion, description of the mathematical model and verification of the solution using a numerical model is presented. Type curves will be given for the cases of constant rate production in infinite and finite systems as well as a system with a constant pressure outer boundary. The effects of wellbore storage and skin will be illustrated. Finally, application of the model will be demonstrated through

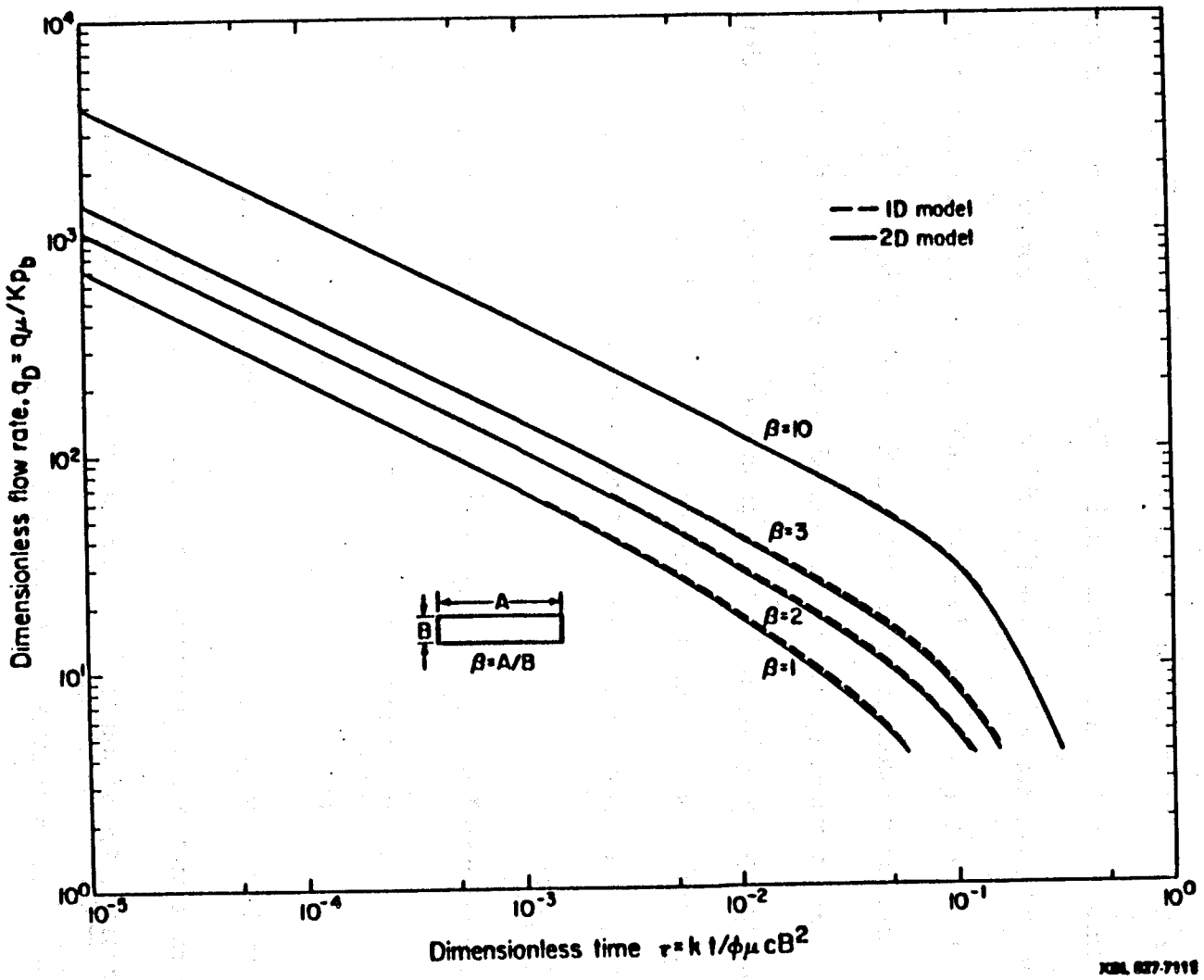

Figure 3-5 Comparison Between the Flow Rate from a Rectangular Porous Slab Using the One-Dimensional Solution and the Exact Solution (Labeled 2D Model).

analysis of field data.

3.3.1. Basic Model

In formulating the governing equations for the pressures in the fractures and rock matrices, the approach used by Warren and Root lumping the fractures and the rock matrices into two different continua is used. Using this approach the governing equation for the pressure in the fractures can easily be derived, but the geometry of the rock matrix (cubic) causes some problems. For a rigorous treatment of the fluid flow in the rock matrix continuum, a three-dimensional representation is necessary. However, a one-dimensional representation of inter-porosity fluid flow from the rock matrix to the fracture has been justified in section 3.2, that is adequate for the present problem and gives almost identical results for the pressure transients at a well or in fractures to those obtained using a three-dimensional model for inter-porosity fluid flow.

3.3.2. Mathematical Model

In addition to the approximation discussed above, the following assumptions are made:

1. The reservoir is uniform in thickness, with impermeable lower and upper boundaries.

2. The fluid flow from the system into the wellbore is radial and only the fractures feed the well.

3 The initial pressure P_i is uniform throughout the system, but at time $t > 0$, a constant flow rate q at the wellbore is imposed.

4. The pressure in the fractures is assumed to be equal to the pressure in the rock matrix at the contact region ($z = D/2$).

5. All properties such as permeability, porosity, and compressibility, are constants in each continuum.

6. The fluid flow is isothermal and single phase. The fluid is slightly compressible, with constant properties (viscosity and density).

The governing equation describing fluid flow in the fracture system, derived from the conservation law of mass in the fracture (Appendix A), is given by

$$\frac{\partial^2 P_2}{\partial r^2} + \frac{1}{r}\frac{\partial P_2}{\partial r} - \frac{6k_1}{k_2}\frac{1}{D}\frac{\partial P_1}{\partial z}\Big|_{z=D/2} = \frac{\phi_2 c_2 \mu}{k_2}\frac{\partial P_2}{\partial t} \tag{3.22}$$

where P_2 is the pressure in the fracture, and P_1 is the pressure in the rock matrix. Other symbols are defined in the Notation. The governing equation for fluid flow in the rock matrix can be expressed as

$$\frac{\partial^2 P_1}{\partial z^2} + \frac{2}{z}\frac{\partial P_1}{\partial z} = \frac{\phi_1 c_1 \mu}{k_1}\frac{\partial P_1}{\partial t} \tag{3.23}$$

The initial conditions are

$$P_2(r,0) = P_1(r,z,0) = P_i \tag{3.24}$$

The boundary conditions at the well, controlled by the constant flow rate, q, and the effects of wellbore storage, are given by

$$-C_w \frac{\partial P_{wf}}{\partial t} + 2\pi h r_w \frac{k_2}{\mu}\left(\frac{\partial P_2}{\partial r}\right)_{r=r_w} = q\bar{B} \tag{3.25}$$

The effects of an infinitesimal skin region around the wellbore can be expressed as

$$P_{wf} = \left[P_2 - Sr_w \frac{\partial P_2}{\partial r}\right]_{r=r_w} \tag{3.26}$$

The boundary conditions for the rock matrix are

$$\frac{\partial P_1(r,z,t)}{\partial z}\Big|_{z=0} = 0 \tag{3.27}$$

$$P_1(r,z,t)\big|_{z=D/2} = P_2(r,t) \tag{3.28}$$

Three different cases are considered for the outer boundary conditions: (a) the reservoir is infinite in the radial direction, (b) a finite reservoir with a no-flow boundary, and (c) a constant pressure boundary.

Infinite Reservoir

$$\lim_{r\to\infty} P_2(r,t) = P_i \tag{3.29}$$

Finite Reservoir

$$\frac{\partial P_2(r,t)}{\partial r}\Big|_{r=r_e} = 0 \tag{3.30}$$

Constant Pressure

$$P_2(r,t)\big|_{r=r_e} = P_i \tag{3.31}$$

In terms of dimensionless parameters, the governing equations (Eqs. 3.22 to 3.23), the initial conditions (Eq. 3.24), and the boundary conditions (Eqs. 3.25 to 3.31), can be written as

$$\frac{\partial^2 P_{D2}}{\partial r_D^2} + \frac{1}{r_D}\frac{\partial P_{D2}}{\partial r_D} - 3\bar{\lambda}\frac{\partial P_{D1}}{\partial \eta}\Big|_{\eta=1} = \omega\frac{\partial P_{D2}}{\partial t_D} \tag{3.32}$$

$$\frac{\partial^2 P_{D1}}{\partial \eta^2} + \frac{2}{\eta}\frac{\partial P_{D1}}{\partial \eta} = \frac{(1-\omega)}{\bar{\lambda}}\frac{\partial P_{D1}}{\partial t_D} \tag{3.33}$$

$$P_{D2}(r_D,0) = P_{D1}(r_D,\eta,0) = 0 \tag{3.34}$$

$$C_D \frac{\partial P_{Df}}{\partial t_D} + \left(\frac{\partial P_{Df}}{\partial r_D}\right)\Big|_{r_D=1} = 1 \tag{3.35}$$

$$P_{Df} = \left[P_{D2} - S\frac{\partial P_{D2}}{\partial r_D}\right]\Big|_{r_D=1} \tag{3.36}$$

$$\frac{\partial P_{D1}(r_D,\eta,t_D)}{\partial r_D}\Big|_{\eta=0} = 0 \tag{3.37}$$

$$P_{D1}(r_D,\eta,t_D)\big|_{\eta=1} = P_{D2}(r_D,t_D) \tag{3.38}$$

$$\lim_{r_D\to\infty} P_{D2}(r_D,t_D) = 0 \tag{3.39}$$

$$\frac{\partial P_{D2}(r_D,t_D)}{\partial r_D}\Big|_{r_D=r_{eD}} = 0 \tag{3.40}$$

$$P_{D2}(r_D,t_D)\big|_{r_D=r_{eD}} = 0 \tag{3.41}$$

where

$$P_D = \frac{2\pi k_2 h}{q\mu\bar{B}}(P_i - P(r,t)) \tag{3.42}$$

$$r_D = \frac{r}{r_w} \tag{3.43}$$

$$\eta = \frac{2z}{D} \tag{3.44}$$

$$t_D = \frac{k_2 t}{(\phi_1 c_1 + \phi_2 c_2)\mu r_w^2} \tag{3.45}$$

$$\bar{\lambda} = \frac{4k_1 r_w^2}{k_2 D^2} \tag{3.46}$$

$$\omega = \frac{\phi_2 c_2}{(\phi_1 c_1 + \phi_2 c_2)} \tag{3.47}$$

$$C_D = \frac{C_w}{2\pi(\phi_1 c_1 + \phi_2 c_2) h r_w^2} \tag{3.48}$$

The mathematical model is fully defined through Eqs. 3.32 to 3.41. The simultaneous solution of the equations using the Laplace transformation is derived in Appendix B. In the Laplace domain the solutions for the pressure in the flowing well and the fracture are

Infinite Reservoir

$$\bar{P}_{Df} = \frac{K_0(\sqrt{x_2}) + S\sqrt{x_2}K_1(\sqrt{x_2})}{p\,\{\sqrt{x_2}K_1(\sqrt{x_2}) + C_D\,p\,[K_0(\sqrt{x_2}) + S\sqrt{x_2}K_1(\sqrt{x_2})]\}} \tag{3.49}$$

$$\bar{P}_{D2} = \frac{K_0(\sqrt{x_2}r_D)}{p\,\{\sqrt{x_2}K_1(\sqrt{x_2}) + C_D\,p\,[K_0(\sqrt{x_2}) + S\sqrt{x_2}K_1(\sqrt{x_2})]\}} \tag{3.50}$$

$$x_2 = 3\bar{\lambda}x_1\coth(x_1) - 3\bar{\lambda} + \omega p$$

$$= \frac{\lambda}{5}x_1\coth(x_1) - \frac{\lambda}{5} + \omega p \tag{3.51}$$

where $\lambda = \dfrac{60k_1 r_w^2}{k_2 D^2}$ defined by Warren and Root (1963)

$$x_1 = \sqrt{\frac{(1-\omega)p}{\bar{\lambda}}} = \sqrt{\frac{15(1-\omega)p}{\lambda}} \tag{3.52}$$

and p is the Laplace parameter. It should be pointed out that this result without wellbore storage and skin effects is identical to de Swan's result (1976), which was obtained by approximating the behavior of cubical matrix blocks with that of spheres, provided the diameter of the spheres is equal to the side length of the

cubes.

Finite Reservoir

$$\bar{P}_{Df} = \frac{\{I_0(\sqrt{x_2})K_1(\sqrt{x_2}r_{eD}) + I_1(\sqrt{x_2}r_{eD})K_0(\sqrt{x_2})\}}{C_D p^2[Y - S\sqrt{x_2}X] - p\sqrt{x_2}X} - \frac{S\sqrt{x_2}\{I_0(\sqrt{x_2})K_1(\sqrt{x_2}r_{eD}) + I_1(\sqrt{x_2}r_{eD})K_0(\sqrt{x_2})\}}{C_D p^2[Y - S\sqrt{x_2}X] - p\sqrt{x_2}X} \tag{3.53}$$

$$\bar{P}_{D2} = \frac{\{I_0(\sqrt{x_2})K_1(\sqrt{x_2}r_{eD}) + I_1(\sqrt{x_2}r_{eD})K_0(\sqrt{x_2})\}}{C_D p^2[Y - S\sqrt{x_2}X] - p\sqrt{x_2}X} \tag{3.54}$$

where

$$X = I_1(\sqrt{x_2})K_1(\sqrt{x_2}r_{eD}) - I_1(\sqrt{x_2}r_{eD})K_1(\sqrt{x_2}) \tag{3.55}$$

$$Y = I_0(\sqrt{x_2})K_1(\sqrt{x_2}r_{eD}) + I_1(\sqrt{x_2}r_{eD})K_0(\sqrt{x_2}) \tag{3.56}$$

Constant-Pressure Outer Boundary

$$\bar{P}_{Df} = \frac{K_0(\sqrt{x_2})I_0(\sqrt{x_2}r_{eD}) - K_0(\sqrt{x_2}r_{eD})I_0(\sqrt{x_2})}{p\sqrt{x_2}[I_0(\sqrt{x_2}r_{eD})K_1(\sqrt{x_2}) + I_1(\sqrt{x_2})K_0(\sqrt{x_2}r_{eD})]} \tag{3.57}$$

Wellbore storage and skin effects are not considered in the case of a constant-pressure outer boundary. The complex nature of the solutions prohibits analytical inversion from the Laplace domain into real space. Therefore, a numerical inverter by Stehfest (1970) is employed to obtain the solution in real space.

3.3.3. Asymptotic Solutions

In the following discussion, the case of an infinite reservoir without wellbore storage and skin effects is considered, and the asymptotic solutions for the early

and late time behavior are developed (Appendix C).

Early Time Behavior

At early times the pressure response at the well is only governed by the characteristics of the fracture system

$$P_{Df} = \frac{2}{\sqrt{\pi}}\sqrt{\frac{t_D}{\omega}} \tag{3.58}$$

The period for which Eq. 3.58 holds depends on the hydraulic properties of the fractures and the rock matrix. If the fracture storativity (ω) is large and inter-porosity flow factor (λ) small, the early time behavior will last for a long time, and a semilog straight line can be observed. The flowing well pressure is given by

$$P_{Df} = \frac{1}{2}\left[\ln\left(\frac{t_D}{\omega}\right) + 0.80909\right] \tag{3.59}$$

Late Time Behavior

At late time the flow between the rock matrix and the fractures becomes quasi-steady and the pressure response at the well is identical to that of a homogeneous reservoir with a storativity $(\phi c)_T = (\phi_1 c_1 + \phi_2 c_2)$; thus one obtains

$$P_{Df} = \frac{1}{2}\left[\ln t_D + 0.80909\right] \tag{3.60}$$

Comparison of Eqs. 3.59 and 3.60 shows that the early time and late time semilog straight lines will be parallel and offset by $\ln \omega$.

The early and late time behavior described here is identical to that obtained by earlier models, e.g., the Warren and Root model (1963) and layered reservoirs (Streltsova, 1982; Serra et al., 1982). The present model and the earlier models

differ only in the transient pressure response at intermediate times, since the surface interaction area for a given fractured element is different for the present model and the layered model.

3.3.4. Numerical Verification of the Present Model

In order to verify the mathematical model and the accuracy of the numerical inverter, the independent numerical simulation studies are implemented using the simulator PT (Bodvarsson, 1982). Numerical analysis of pressure transients of wells completed in naturally fractured reservoirs were carried out using the multiple interacting continua (MINC) method (Pruess and Narasimhan, 1982). The comparison between the numerical results and the results predicted by the present semi-analytical model is shown in Figure 3-6. The excellent agreement between the methods indicates that the semi-analytical model is appropriate for the analysis of well test data.

3.3.5. Comparison Between Models for Naturally Fractured Reservoirs

The main difference between the present model and that of Warren and Root (1963) is that the transient fluid flow between the rock matrix and the fractures instead of the quasi-steady state fluid flow is employed in the present model. Results from these models for several values of λ are shown in Figure 3-7. As mentioned earlier, the early and late time semilog straight lines are identical for both models. However, significant differences are evident in the transient region at intermediate times. In the present model, significant fluid flow from the rock matrix to the fractures occurs much earlier than in the Warren and Root model (1963); consequently, the pressure deviates earlier from the first semilog

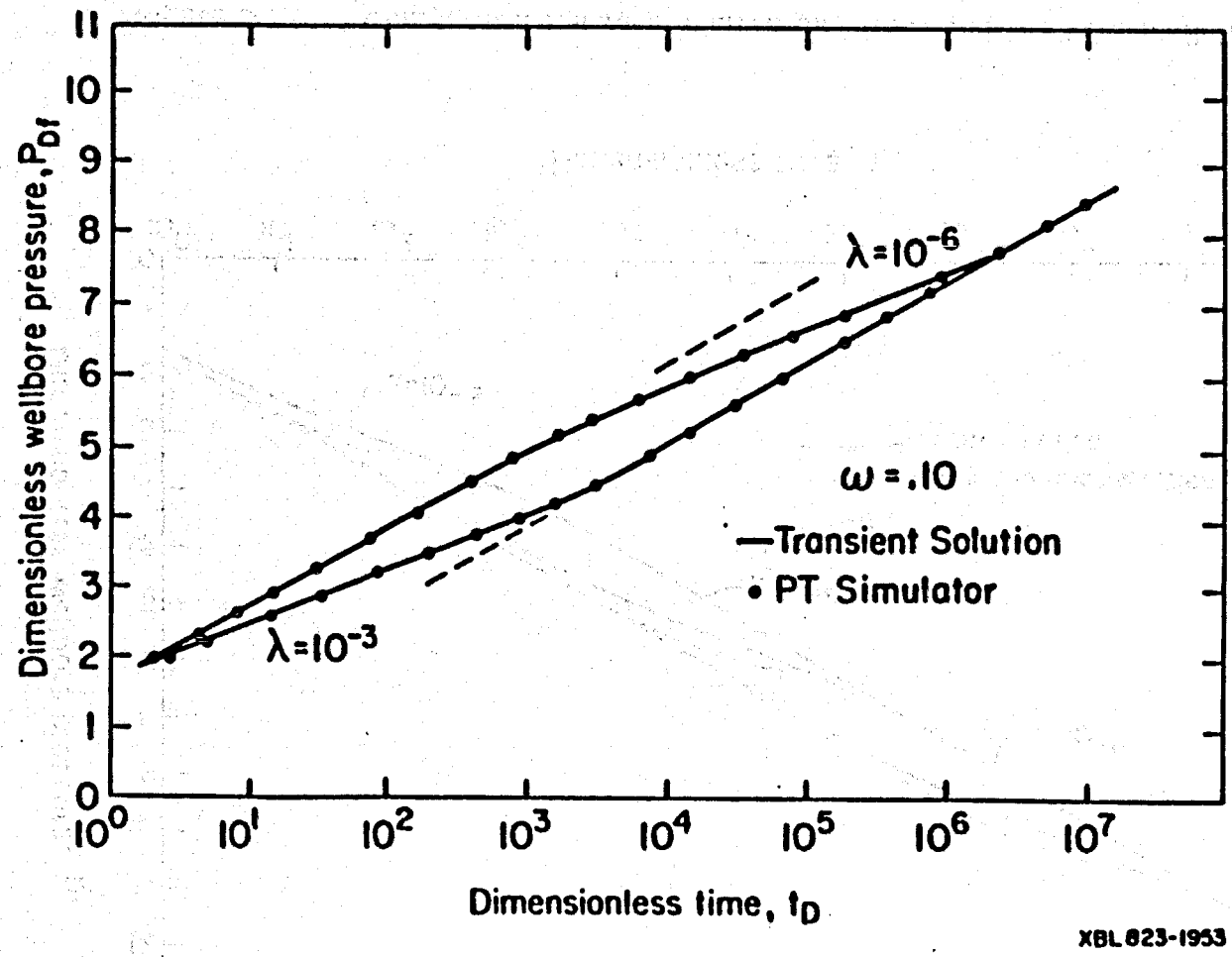

Figure 3-6 Comparison Between Numerical Simulation and Semi-Analytical Solutions.

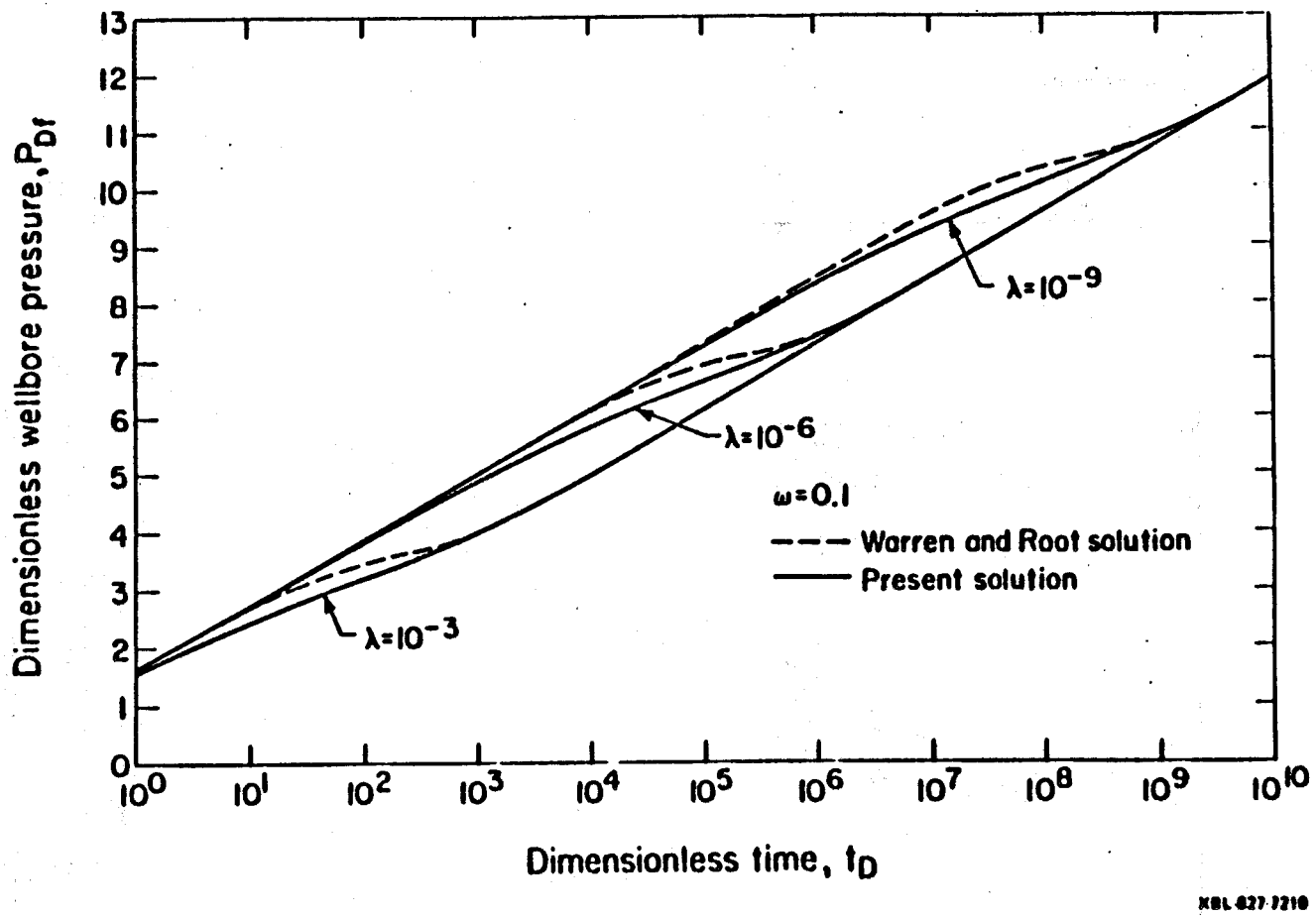

Figure 3-7 Comparison Between Warren and Root and the Present Solution for an Infinite Reservoir.

straight line. Also, the pressure transients in the intermediate time region last considerably longer in the present model than is predicted by the Warren and Root model (1963). As will be shown later, the pressure transient data in the intermediate time region are essential for the determination of the reservoir parameters, since in most cases the early time data (first semilog slope) are marked by wellbore storage effects.

Other models that consider transient fluid flow between the rock matrix and the fractures (Streltsova, 1982; Serra et al., 1982; de Swan, 1976; Najurieta; 1980) show similar in overall transient pressure behavior at the intermediate times. Therefore, depending on the geological conditions that prevail at a given site, the present model for naturally fractured reservoirs may be utilized or, in the case of layered reservoirs, models developed by Streltsova (1982) or Serra et al. (1982) are applicable.

3.4. Pressure Transient Analysis with New Model

The pressure transient behavior for naturally fractured reservoirs is analyzed based on the present model, and the methodology for the analysis of well test data for different boundary conditions is presented.

3.4.1. Well Test Data Analysis for Infinite Reservoirs

Type curves for pressure drawdown tests in naturally fractured reservoirs of infinite areal extent are shown in Figure 3-8 for three different values of λ (10^{-3},10^{-6},10^{-9}) and ω (10^{-1},10^{-2},10^{-3}); these values cover the range of probable values for naturally fractured reservoirs. Not only λ but also ω determines the time of pressure deviation. Figure 3-8 shows that ω controls the shift of the early and late

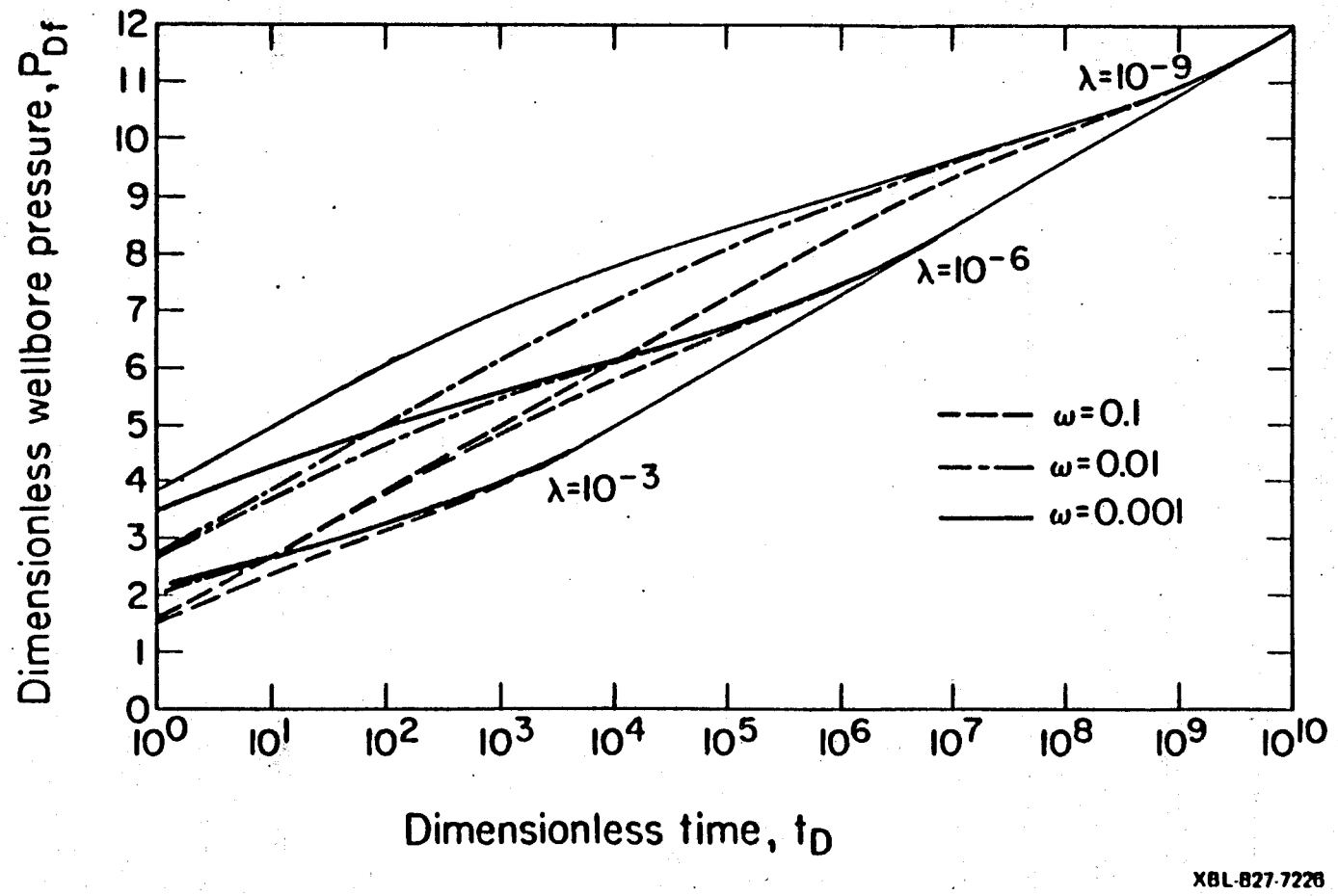

Figure 3-8 Pressure Drawdown Behavior without Wellbore and Skin Effects.

time semilog straight lines, whereas λ determines the time of pressure deviation from the first slope and the time of convergence to the late time curve.

In order to develop methods for analysis of data from naturally fractured reservoirs, an approximate analytical solution is helpful. Applying the improved Schapery technique (1961) to Eq. 3.49 (without wellbore storage and skin effects), one obtains (Appendix D)

$$P_{Df} = -\gamma + \ln 2 - \frac{1}{2} \ln \left[\frac{\lambda}{5} \frac{\sqrt{15(1-\omega)}}{e^{\gamma}\lambda t_D} \coth\left(\frac{\sqrt{15(1-\omega)}}{e^{\gamma}\lambda t_D}\right) - \frac{\lambda}{5} + \frac{\omega}{e^{\gamma} t_D}\right] \qquad (3.61)$$

Eq. 3.61 is valid for dimensionless times greater than $t_D = 10$, which covers times of most practical interest. For this time range Eq. 3.61 is generally accurate within 1%; the maximum deviation from values calculated using the numerical inverter is 2%. At late times the equation is identical to the asymptotic solution. Recently, Ershaghi and Aflaki (1985) double differentiated this equation, and then located the inflection point in the transition period. From the slope of the inflection point, they also developed a method to calculate the reservoir properties of naturally fractured reservoirs including the inter-porosity flow factor, storativity ratio, and fracture permeability. Eq. 3.61 will be used as a basis in the following discussion.

As mentioned earlier, the pressure response of naturally fractured is characterized by three segments, a semilog straight line at early times, a transition period, and a late time semilog straight line. In many cases, regardless of wellbore storage effects, the initial straight line is not present. Only in cases where $(\frac{\lambda}{\omega}) < 7\times10^{-7}$ can the first linear segment be observed. By correlation, the

initial semilog straight line ends at a dimensionless time of

$$t_D = \frac{\omega^2}{10\lambda} \tag{3.62}$$

During the transition period the pressure changes are much less than at early and late times because of the large fluid flow from the rock matrix feeding the fractures. This period lasts for about 7 log cycles of dimensionless time. During the transition period two linear segments on the pressure-log time plot (Figure 3-8) may be identified. The first segment has a slope half that of the initial and final slopes. This half-slope has also been identified by Streltsova (1982) and Serra et. al. (1982) for the case of stratified reservoirs.

The half slope occurs around the dimensionless time, when the two last terms in Eq. 3.61 cancel each other, given by

$$t_D = \frac{5\omega}{e^{\gamma}\lambda} \tag{3.63}$$

At that time the pressure declines can be expressed as

$$P_{Df} = \frac{1}{4}\left[\ln t_D - \ln\lambda(1-\omega) - \ln\frac{3}{80} - 3\gamma\right] \tag{3.64}$$

The time period over which a half slope can be observed depends on ω. For ω=0.001, the half slope occurs for over a log cycle whereas for ω=0.01 it lasts only a half-log cycle. Where ω is larger than 0.1, the half-slope segment can not be easily identified. The intersection between the initial semilog straight line and the half-slope straight line occurs at a dimensionless time of

$$(t_D)_{IH} = \frac{5\omega^2}{3e^{\gamma}\lambda(1-\omega)} \tag{3.65}$$

Similarly, the intersection of the half-slope line with the final linear segment occurs at a dimensionless time of

$$(t_D)_{FH} = \frac{5}{3e^{7}\lambda(1-\omega)} \tag{3.66}$$

At a slightly later time in the transition period, a brief linear segment with a slope two-thirds that of the final slope is apparent. Due to the complex nature of the analytical approximation (Eq. 3.61), it is not possible to mathematically derive the exact time of deviation of this linear segment. It is also of questionable value because of its short duration. However, as is the case with the half-slope, the 2/3 slope increases in duration with decreasing value of ω.

The pressure transients converges on the final slope at a dimensionless time of

$$t_D = \frac{3(1-\omega)}{\lambda} \tag{3.67}$$

However, for accurate determination of the final slope, one should only consider data points at a dimensionless times exceeding

$$t_D \geq \frac{5(1-\omega)}{\lambda} \tag{3.68}$$

Procedures For Analysis

In the above analysis some insight into the pressure transients in naturally fractured reservoirs by using the approximate analytical solution (Eq. 3.61) is gained. However, well test data rarely exhibit all of the theoretical characteristics displayed above. In most cases early data are masked by wellbore storage effects and in some cases the duration of the well test is too short for late time

behavior to be observed. Also, boundary effects may affect the well test data to the extent that the late time behavior predicted by the infinite reservoir model is never observed. The effects of wellbore storage and skin as well as the effects of different outer boundary conditions are discussed in a later section. Analysis procedures are given below for cases when the data are incomplete as well as for the case of a complete data set.

Complete Data Set

in this case the transmissivity k_2h and total storativity $(\phi_1 c_1 + \phi_2 c_2)$ of the reservoir can be determined from the early time or late time slopes using the conventional methods. ω can be determined from the pressure difference between the early and late time slopes using the equation

$$\omega = \exp(-2\Delta P_D) \tag{3.69}$$

Once ω is determined, λ can be calculated from any one Eqs. 3.63, 3.65 to 3.67 by using the appropriate dimensionless time. The fracture storativity $\phi_2 c_2$ can be calculated from ω and the total storativity, k_1/D^2 can be evaluated from the definition of λ and the reservoir transmissivity k_2h. Finally, if the permeability of the rock matrix k_1 is known, e.g., from core data, the fracture spacing D can be determined.

Early Time Data Missing

As mentioned earlier, the initial semilog straight line will not appear if $(\frac{\lambda}{\omega})$ $>10^{-5}$. Also, wellbore storage effects will, in most other cases, mask the initial slope as well as some of the data during the transition period. However, it is still

possible to extract the reservoir parameters from the data. As before, one can determine k_2h and $(\phi_1c_1+\phi_2c_2)$ from the late time slope and intersects using the conventional methods. ω and λ can be determined by solving Eqs. 3.63 and 3.66 or Eqs. 3.66 and 3.67, simultaneously. The fracture storativity and $(\frac{k_1}{D^2})$ can be determined in the same way as before.

Final Slope Missing

If the well test is of short duration and λ is small, the final slope may never be observed in the data. If the initial straight line is present, one can still determine λ, ω, and all reservoir parameters. k_2h and ϕ_2c_2 can be determined from the slope of the initial straight line, λ and ω by solving Eqs 3.63 and 3.65 simultaneously, and other reservoir parameters as discussed above. However, if the initial slope is not observed, λ and ω can not be determined. In this case the use of the pressure transient data to determine the k_2h of the reservoir by the conventional methods will result in estimates that are about twice the actual k_2h of the reservoir.

Wellbore Storage and Skin Effects

At early times during drawdown tests, most of the fluids are produced from the fluids contained in the wellbore. Thus, the surface flow rate greatly exceeds the sandface flow rate. Later on, steady state conditions develop in the wellbore so that the sandface flow rate equals that at the surface. Obviously, during early times the pressure transients are only related to the volume of fluids stored in the wellbore, so that these data can not be used to determine any formation parameters. It is of interest to examine the duration of the wellbore storage effects

depending on the value of the wellbore storage factor C_D.

Figure 3-9 shows the effects of wellbore storage on the pressure transient data for $\lambda=10^{-6}$ and $\omega=0.01$. The figure shows that even for this small value of λ, wellbore storage effects will mask the initial straight line completely. The higher the wellbore storage factor C_D, the more the transition period data will be masked. However, in the case of this low value of λ, the half slope can still be observed even though the wellbore storage factor C_D is as large as $C_D = 10^4$. Consequently, the procedure of analysis discussed in the last section can be applied, and all reservoir parameters determined.

It is obvious that the wellbore storage effects become more critical when the value of λ is higher. In many cases wellbore storage effects will mask all of the data during the transition period so that only the final semilog straight line can be observed. In the overall integrated reservoir parameters k_2h and $(\phi_1 c_1 + \phi_2 c_2)$. Through the analysis, it shows that λ and ω can only be determined if the following constraint holds

$$C_D \leq \frac{5\omega}{4e^7\lambda(60 + 3.5S)} \tag{3.70}$$

The combined effects of wellbore storage and skin are shown in Figure 3-10 for $\lambda=10^{-6}$ and $\omega=0.01$. The skin factor S represents permeability reduction in the near-wellbore region as a result of formation damage (positive skin) or permeability enhancement due to the presence of natural or man-made (hydraulic) fractures. The figure shows that the characteristic unit slope due to wellbore storage at early times (Ramey, 1970), and a steady state pressure drop associated with

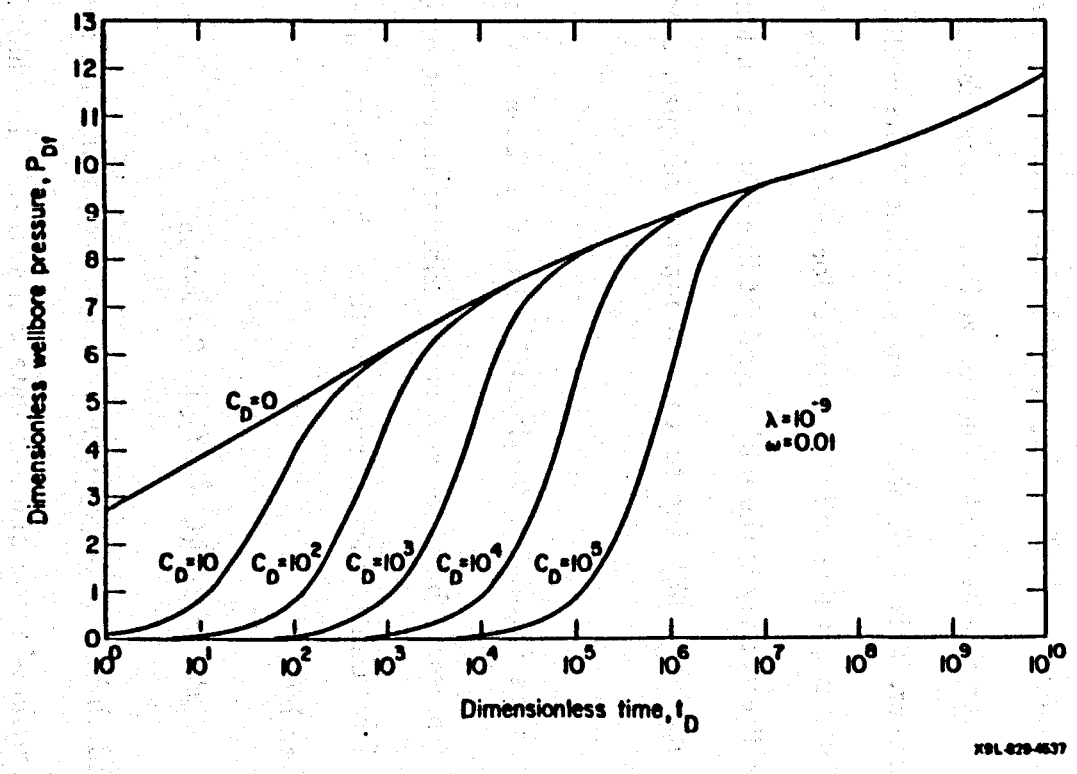

Figure 3-9 Effects of Wellbore Storage on Pressure Drawdown Behavior.

positive skin. The wellbore storage factor C_D can be determined from type curves such as the ones shown in Figure 3-10. The skin factor S is determined by conventional methods by assuming a value for the total storativity.

Mavor and Cinco-Ley (1979) extended the Warren and Root solution (963) to include the effects of wellbore storage and skin. Their results differ considerably from those presented here, mainly because of the quasi steady flow assumption employed by Mavor and Cinco-Ley (1979). For example, these authors develop criteria to determine at what values of wellbore storage factor the initial straight line will appear. This study shows, however, that if the wellbore storage is present, the initial straight line will never appear for realistic values of λ and ω. The reason for this discrepancy is the initial straight line lasts much longer in the Warren and Root model (1963) due to the assumption of quasi steady interporosity flow.

3.4.2. Horner Pressure Build-Up Analysis for Infinite Reservoirs

The analysis of pressure buildup tests is very similar to that of drawdown tests described earlier. Using rules of superposition, the dimensionless shut-in pressure, P_{DS}, is given by

$$P_{DS} = P_{Df}\,[(t_p + \Delta t)_D] - P_{Df}\,[(\Delta t)_D] \tag{3.71}$$

If it is assumed that t_p is large enough that the pressure transients follow the final slope before shut-in, the build-up data will also exhibit a half slope at a dimensionless shut-in time given by Eq. 3.63. At that time the shut-in pressure is given by

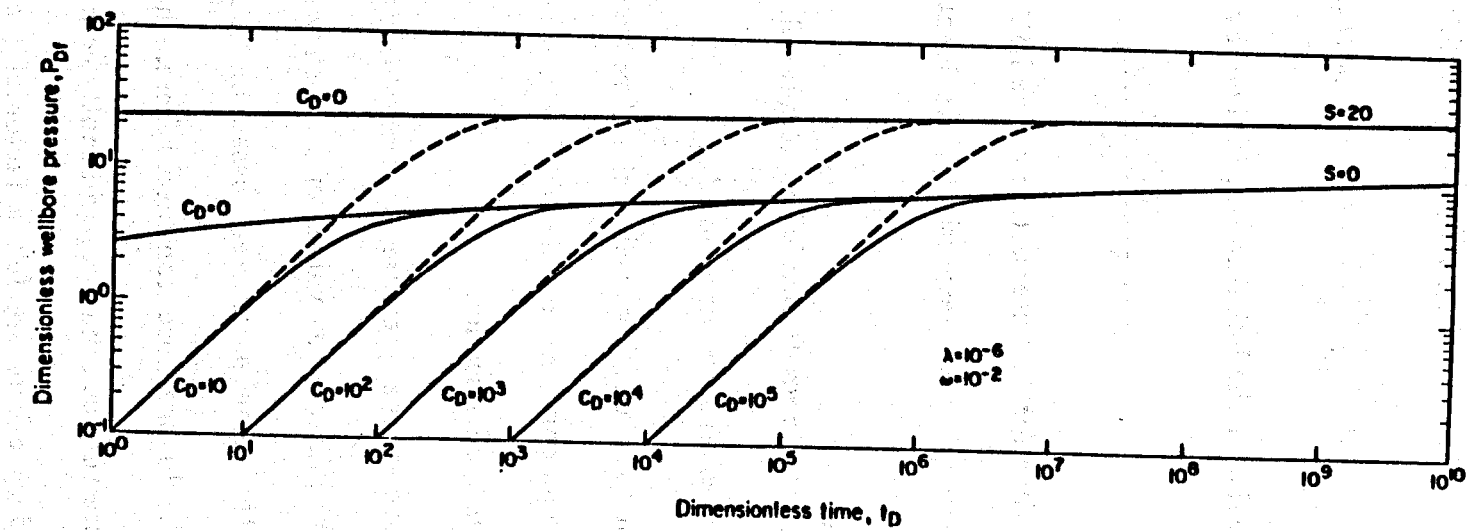

-- XBL 833-8667 --

Figure 3-10 Effects of Wellbore Storage and Skin on Pressure Drawdown Behavior.

$$P_{DS} = \frac{1}{4}\{\ln\frac{(t_p + \Delta t)_D}{(\Delta t)_D} + \ln(t_p + \Delta t)_D + \ln\lambda(1-\omega) + \ln(\frac{3e^7}{5})\} \tag{3.72}$$

Assuming that $\ln(t_p + \Delta t)_D \approx \ln(t_p)_D$, Eq. 3.72 simplifies to

$$P_{DS} = \frac{1}{4}\{\ln\frac{(t_p + \Delta t)_D}{(\Delta t)_D} + \ln(t_p)_D + \ln\lambda(1-\omega) + \ln(\frac{3e^7}{5})\} \tag{3.73}$$

The late time behavior of the build-up test is given by

$$P_{DS} = \frac{1}{2}\ln[\frac{(t_p + \Delta t)_D}{(\Delta t)_D}] \tag{3.74}$$

The dimensionless time for the intersection of the half slope straight line with the initial and final straight lines, respectively, are identical to those presented in Eqs. 3.65 and 3.66.

3.4.3. Pressure Drawdown Behavior in Reservoirs with Closed or Constant Pressure Outer Boundary

In this section the cases involved a closed reservoir and a reservoir with a constant pressure boundary are considered. The mathematical solutions for these cases are given in an earlier section.

Figure 3-11 shows the pressure transient behavior in a closed reservoir (r_{eD}=100) for $\lambda=10^{-6}$ and various values of ω. It shows also for comparison that the solutions for the same parameters based on the Warren and Root quasi steady flow model. In the case considered here, the no-flow outer boundary effects are felt before the rock matrix significantly contributes to the flow. Consequently, the boundary effects are felt a factor of $(1/\omega)$ times earlier than they would be in the case of a homogeneous reservoir (ω=1). Thus, if the conventional methods for homogeneous reservoirs were used to analyze such data, the drainage

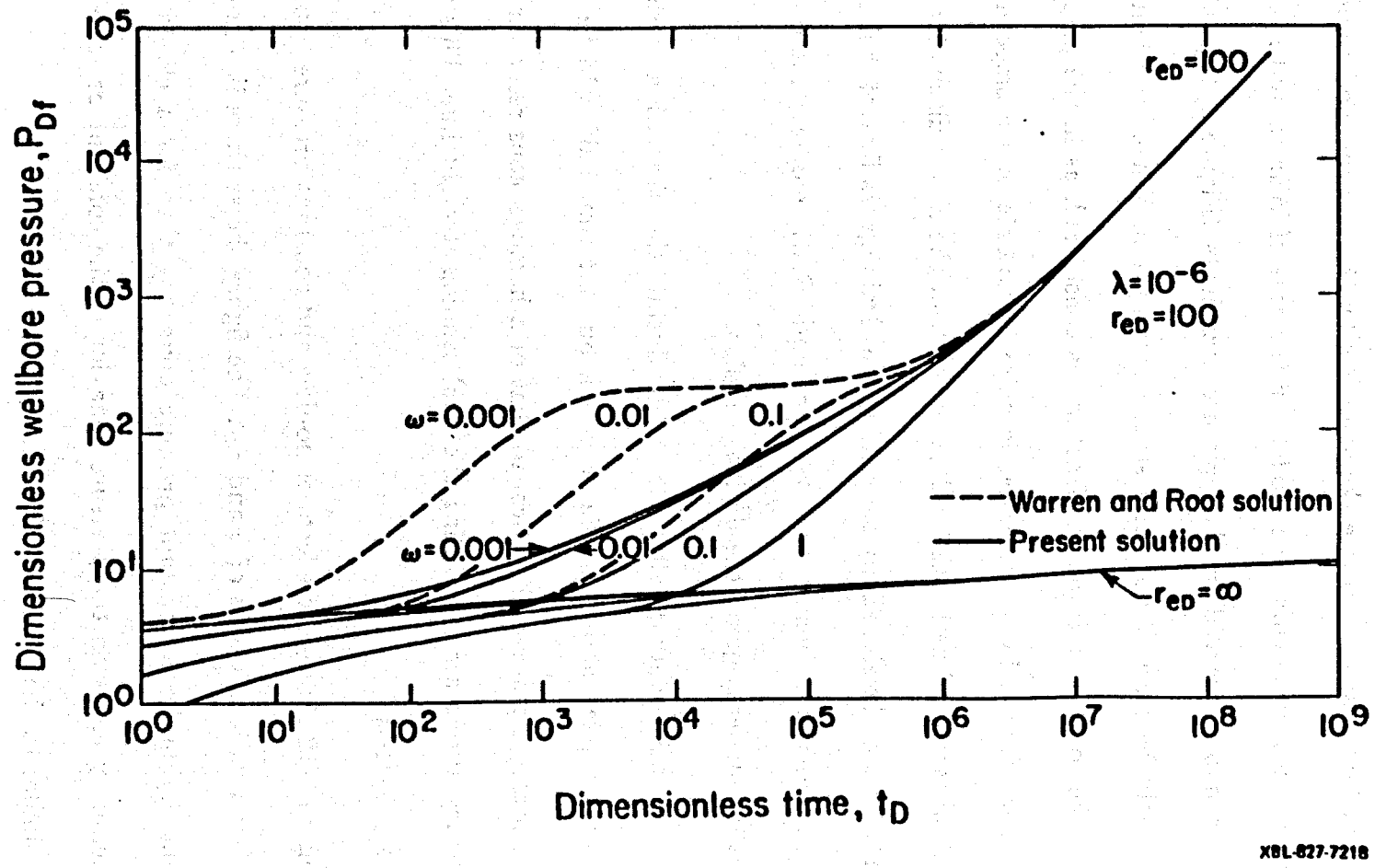

Figure 3-11 Comparison Between Warren and Root and the Present Solutions for a Closed Reservoir.

radius may be underestimated by orders of magnitude. In general, the boundary effects will be felt before significant fluid flow from the matrix occurs if $(\lambda/\omega^2) < (\pi/10 r_{eD}^2)$.

It is of interest to compare the solutions by the present model and the Warren and Root quasi steady type model. In the case of Warren and Root model, a Plateau can be observed in the pressure transients (Figure 3-11). The plateau appears only because of the quasi steady assumption. When transient fluid flow between the rock matrix and the fractures is considered, as in the present model, the pressure decline in the reservoir is more monotonic and a smooth transition to the final straight line is observed. As a result of the above discussions, methods that have been developed to determine the drainage radius of finite naturally fractured reservoirs using the Warren and Root model (1963) may also significantly underestimate the drainage radius.

When the boundary effects are felt during the transition period similar results as discussed above can be observed, but the time shift will be less. Obviously, a pressure response identical to that of a homogeneous reservoir will result if boundary effects are felt during the final semilog straight line. This will be the case if $\lambda > 1/11 r_{eD}^2$.

Figure 3-12 shows the effects of no-flow and constant pressure boundaries for $\lambda = 10^{-6}$ and various values of ω and r_{eD}. The figure shows there is a much shorter transient region for a constant pressure boundary than for a closed boundary. The boundary effect on the pressure behavior in the constant pressure boundary case is similar to that in the no-flow boundary case.

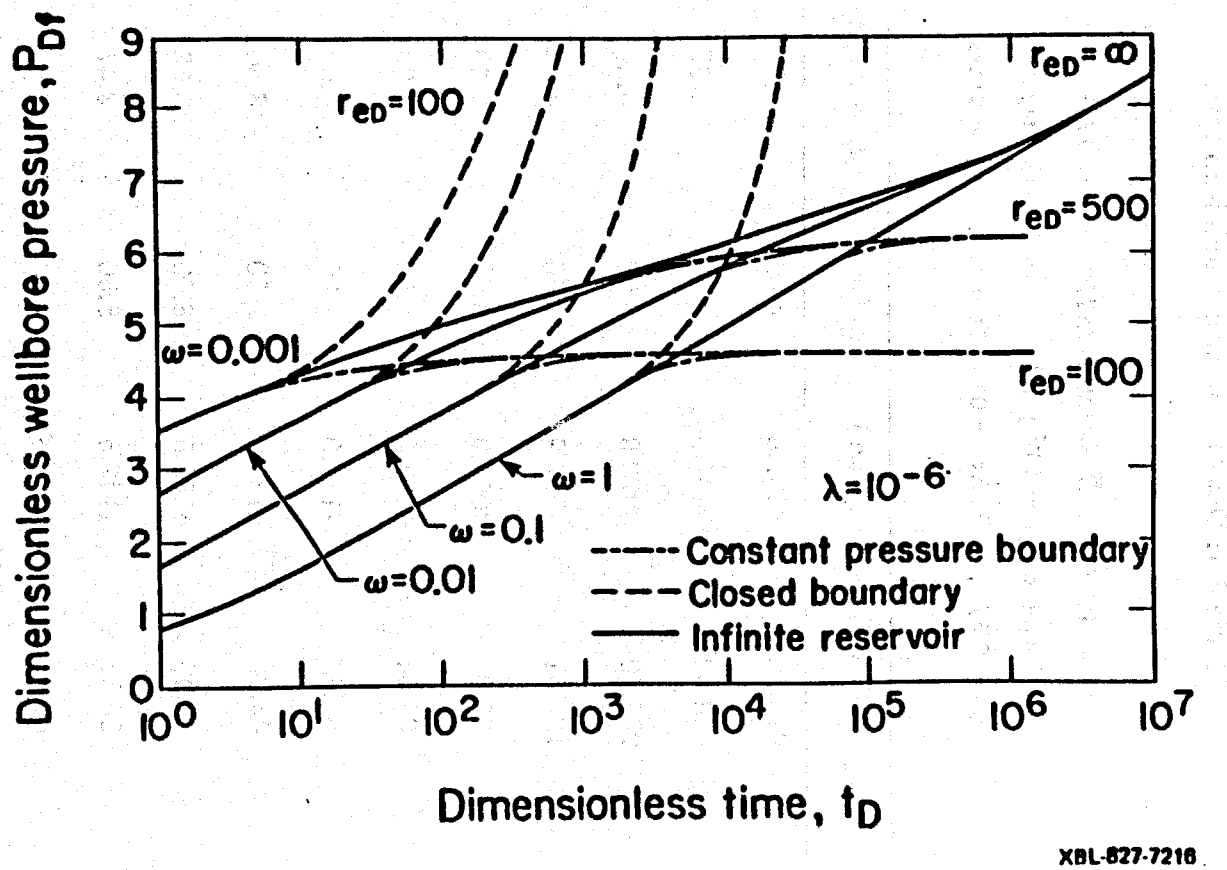

Figure 3-12 Effects of Outer Boundary Conditions on Pressure Behavior.

3.4.4. Application of New Model to Field Data

Bourdet and Gringarten (1980) presented the build-up data from a naturally fractured reservoir shown in Table 3-1.

Table 3-1: Data for pressure build-up test.

$$h = 100ft, \quad \bar{B} = 1.2RB/STB, \quad \mu = 0.5cp,$$
$$(\phi_1 c_1 + \phi_2 c_2) = 10^{-6}\ psi^{-1}, \quad q = 4500bbl/day,$$
$$r_w = 0.3ft, \quad P(\Delta t = 0) = 3420.8psi, \quad t_p = 21hrs$$

$\Delta t\,(hrs)$	$(t_p + \Delta t/\Delta t)$	$P_{wf}\,(psi)$	$\Delta t\,(hrs)$	$(t_p + \Delta t/\Delta t)$	$P_{wf}\,(psi)$
0.0216	973.32	3607.6	4.00	6.25	4211.3
0.0480	438.50	3867.6	4.50	5.67	4216.9
0.0833	253.10	3970.9	5.00	5.20	4220.8
0.1660	127.51	4067.9	5.50	4.82	4225.9
0.250	85.0	4093.9	6.00	4.50	4228.7
0.333	64.64	4108.0	6.50	4.23	4232.1
0.416	51.48	4117.0	7.00	4.00	4233.8
0.500	43.00	4127.2	7.50	3.80	4237.8
0.667	32.48	4138.5	8.00	3.63	4239.5
0.833	26.21	4147.5	8.50	3.47	4242.3
1.0	22.0	4154.8	9.00	3.33	4245.1
1.25	17.8	4162.7	9.50	3.21	4246.8
1.50	15.0	4170.6	10.00	3.10	4248.5
1.75	13.0	4176.8	10.50	3.00	4250.7

$\Delta t\,(hrs)$	$(t_p + \Delta t/\Delta t)$	$P_{wf}\,(psi)$	$\Delta t\,(hrs)$	$(t_p + \Delta t/\Delta t)$	$P_{wf}\,(psi)$
2.00	11.5	4182.5	11.00	2.91	4251.9
2.25	10.33	4187.6	11.50	2.83	4254.1
2.50	9.40	4192.6	12.00	2.75	4256.4
2.75	8.64	4196.6	13.00	2.62	4259.2
3.0	8.0	4199.9	14.00	2.50	4263.2
3.25	7.46	4202.8	15.00	2.40	4264.9
3.50	7.00	4205.6	16.00	2.31	4267.7
3.75	6.60	4208.4	17.00	2.23	4269.4

This data is used to illustrate how the present model can be used to determine important reservoir parameters. The best match obtained between the observed data and the calculated values using the present model is shown in Figure 3-13. An excellent match is obtained. The analysis proceeds as follows: Using the final slope of 141.8 psi/cycle the transmissivity of the reservoir can be calculated as

$$k_2 h = \frac{162.6 q \bar{B} \mu}{m} = \frac{162.6 \times 4500 \times 1.2 \times 0.5}{141.8} = 3088 md-ft$$

For a reservoir thickness of 100 feet, the average reservoir permeability is $k_2 = 30.88 md$.

It is now to calculate ω. As is evident from the data shown in Figure 3-13, wellbore storage effects masks the initial fracture controlled straight line. One must therefore use the methodology developed earlier to determine ω. In the data shown in Figure 3-13 a half slope segment can be observed at Horner time about

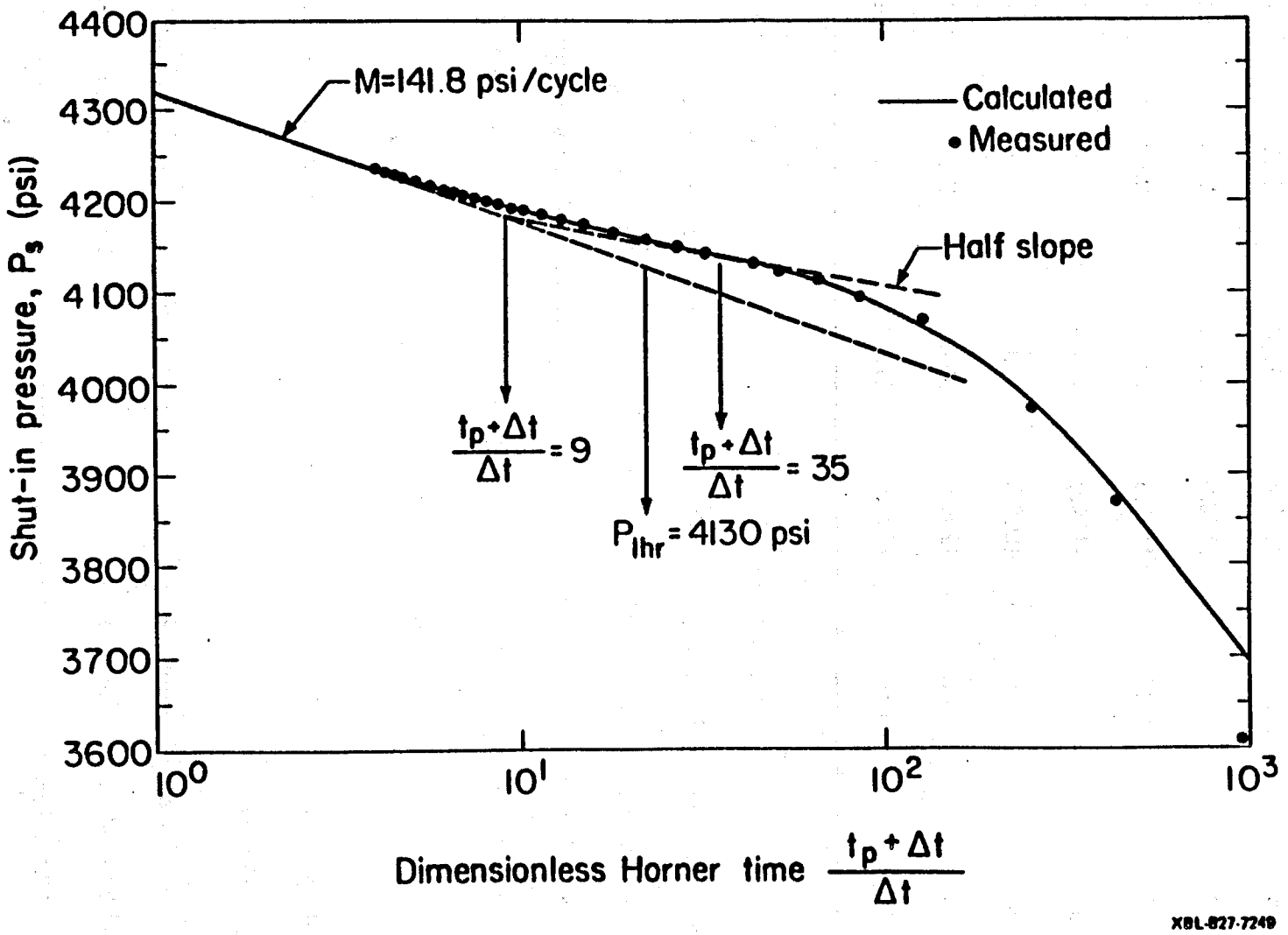

Figure 3-13 Pressure Build-Up Analysis.

$\frac{(t_p + \Delta t)}{\Delta t} = 35$, or $\Delta t = 0.617 hrs$, $(t_p = 21 hrs)$.

The intersection of the half slope line with the final straight line occurs at $(t_p + \Delta t) / \Delta t = 9$, or $\Delta t = 2.625\ hrs$. Dividing Eq. 3.63 by Eq. 3.65, one obtains

$$\frac{(\Delta t_D)_{HF}}{(\Delta t_D)_H} = \frac{1}{3\omega(1-\omega)} \approx \frac{1}{3\omega} \tag{3.75}$$

since $(\Delta t_D)_{HF}/(\Delta t_D)_H = (\Delta t)_{HF}/(\Delta t)_H$, one can determine $\omega = 0.078$. After substituting for λ and ω in Eqs. 3.46 and 3.47, Eq. 3.47 can be used to determine k_1/D^2

$$\frac{1.691\times10^{-2} k_1 (\Delta t)_{HF}}{\mu(\phi c)_T D^2} = 1$$

Solving for k_1/D^2 yields $k_1/D^2 = 1.03\times10^{-5} md/ft^2$.

Unfortunately, there are no core data available on the matrix permeability, k_1. However, if one assumes a reasonable value for the matrix permeability, say, $k_1 = 0.001 md$, the average fracture spacing D equals 10 feet.

One can now proceed to calculate λ based on its definition

$$\lambda = \frac{60 k_1 r_w^2}{k_2 D^2} = 1.82\times10^{-6}$$

The skin factor S can be calculated from

$$S = 1.151 \left[\frac{P_{1hr} - P_{wf}(\Delta t = 0)}{m} - \log \frac{k_2}{(\phi_1 c_1 + \phi_2 c_2)\mu r_w^2} \right] + 3.23 = -0.7$$

The above analysis is based on the approximate solution given by Eq. 3.61. However, if a more accurate analysis is needed, Eq. 3.49 can be employed. The match shown in Figure 3-13 was obtained using Eq. 3.49 $\lambda = 2.63\times10^{-6}$, $\omega = 0.085$, and $S = -0.7$, $C_D = 1200$ and $C_w = 0.012\ bbl/psi$.

Bourdet and Gringarten (1980) analyzed the same data (Figure 3-13) using the Warren and Root model. They do not show the comparison between the calculated and observed pressures, but give values for λ and ω of 2×10^{-6} and 0.25, respectively. Using these parameters and the Warren and Root model, a large discrepancy between the calculated and observed data is found. A much more reasonable match is obtained using $\lambda = 3.5\times10^{-5}$ and $\omega = 0.25$. This value of λ is more than an order of magnitude higher than the value obtained using the present model. The value of λ is also considerably greater than our value.

3.5. Thermal Propagation in Naturally Fractured Reservoirs

In the present study the problem of cold water injection into naturally fractured reservoirs is considered. The basic model used considers the geometric configurations, as proposed by Warren and Root (1963), but transient interporosity heat flow between rock matrix and fractures is employed. Similar work on non-isothermal flow in horizontal fractures have been investigated by Lauwerier (1955), Bodvarsson (1969), and Bodvarsson and Tsang (1982). The objective of the present work is to extend their work to include the effects of vertical fractures and to develop a methodology for the design of the injection schemes for naturally fractured reservoirs.

3.5.1. Basic Model

The model used in this study is shown in Figures 2-1 and 3-1. To simplify the problem of cold water injection into naturally fractured reservoirs, steady state fluid flow is assumed in the fractures, but transient conductive heat transfer between the impermeable rock matrix and the fractures is considered. Thus, the

cold water will flow from the injection well into the fracture network, and as it moves away from the well, it will gradually get heated up due to the heat transfer from adjacent matrix blocks.

The equation for conductive heat transfer between the rock matrix and the fractures is derived based on the basic element shown in Figure 3-1. The basic element represents 1/6 of a single cubic rock matrix, i.e. only one face of the cube is considered. In this approach it is assumed that the thermal gradients are much smaller within the fracture network than in the rock matrix, since the thermal velocity in the fracture network is much larger than that in the rock matrix. Thus, if the temperature in the fractures bounding a rock matrix block is rather uniform, a one-dimensional conduction heat transfer in the rock matrix block is a reasonable approximation.

3.5.2. Mathematical Model

In addition to the approximation discussed above, the following assumptions are made:

1. The reservoir is uniform in thickness, with impermeable lower and upper boundaries, and without heat loss from the reservoir to the boundaries.
2. The mass flow rate is constant and radial, with the well located at $r = 0$.
3. The initial temperature T_0 is uniform throughout the system, but at time $t > 0$, a constant temperature T_i of injected water is maintained.
4. The temperature in the fracture is assumed to be equal to the temperature in the rock matrix at the contact region ($z = D/2$).

5. The system and fluid properties including permeability, porosity, compressibility, fluid density, fluid viscosity, effective thermal conductivity, and thermal capacities are assumed to be constant.

The governing equation describing energy transport in naturally fractured reservoirs can be derived from the conservation law of energy. The procedures are similar to those used in isothermal fluid flow in naturally fractured reservoirs. If one neglects the longitudinal conduction in the fractures, the fluid temperature in the fractures can be expressed as (Bodvarsson and Lai, 1982)

$$q \rho_f c_f \frac{\partial T_2}{\partial r} - \frac{12\pi r h K_k}{D} \frac{\partial T_1}{\partial z}\Big|_{z=D/2} = 6\pi r \bar{b} \frac{h}{D} \rho_f c_f \frac{\partial T_2}{\partial t} = 2\pi r \bar{b} \rho_f c_f \frac{\partial T_2}{\partial t} \quad (3.76)$$

where T_2 is the fluid temperature in the fractures, and T_1 is the temperature in the rock matrix, and $\bar{b}$ $(3bh/D)$ is the effective fracture aperture. The temperature in the rock matrix is governed by the one-dimensional heat conduction equation as Eq. 3.77, whose derivation is similar to that describing pressure transient behavior in the rock matrix of the naturally fractured systems.

$$\frac{\partial^2 T_1}{\partial z^2} + \frac{2}{z}\frac{\partial T_1}{\partial z} = \frac{\rho_r c_r}{K_k}\frac{\partial T_1}{\partial t} \quad (3.77)$$

The initial and boundary conditions can be expressed as

$$T_2(r,0) = T_1(r,z,0) = T_0 \quad (3.78)$$

$$T_2(0,t) = \begin{cases} T_0 & t < 0 \\ T_i & t \geq 0 \end{cases} \quad (3.79)$$

$$T_2(r,t) = T_1(r,0,t) \quad (3.80)$$

$$T_1(r,0,t)|_{z=0} = 0 \quad (3.81)$$

The dimensionless parameters T_D, τ, η, ξ, and θ are defined as

$$T_D = \frac{T - T_0}{T_i - T_0} \tag{3.82}$$

$$\tau = \frac{4K_h t}{\rho_r c_r D^2} \tag{3.83}$$

$$\eta = \frac{2z}{D} \tag{3.84}$$

$$\xi = \frac{\pi r^2 h K_h}{\rho_f c_f q D^2} \tag{3.85}$$

$$\theta = \frac{4\rho_f c_f \bar{b}}{\rho_r c_r h} \tag{3.86}$$

In dimensionless form the governing equations for the temperatures in the fractures (T_2) and the rock matrix (T_1) are

Fractures:

$$-\frac{\partial T_{D2}}{\partial \xi} - 12\frac{\partial T_{D1}}{\partial \eta}\Big|_{\eta=1} = \theta\frac{\partial T_{D2}}{\partial \tau} \tag{3.87}$$

Rock Matrix:

$$\frac{\partial^2 T_{D1}}{\partial \eta^2} + \frac{2}{\eta}\frac{\partial T_{D1}}{\partial \eta}\Big|_{\eta=1} = \frac{\partial T_{D1}}{\partial \tau} \tag{3.88}$$

The initial and boundary conditions are

$$T_{D1}(\xi,\eta,0) = T_{D2}(\xi,0) = 0 \tag{3.89}$$

$$T_{D2}(0,\tau) = \begin{cases} 0 & \tau < 0 \\ 1 & \tau \geq 0 \end{cases} \tag{3.90}$$

$$T_{D1}(\xi,1,\tau) = T_{D2}(\xi,\tau) \tag{3.91}$$

$$T_{D1}(\xi,0,\tau) = finite \tag{3.92}$$

The real parameters in Eqs 3.82-3.86 are defined in the Notation.

The solutions to Eqs. 3.87 and 3.88 for the given initial and boundary conditions in the Laplace domain are given in Appendix E. In the Laplace domain the solutions for the fracture and the rock temperatures are

$$\psi_2 = \frac{1}{p}\exp\{-[\theta p + 12\sqrt{p}\frac{I_{3/2}(\sqrt{p})}{I_{1/2}(\sqrt{p})}]\xi\} \tag{3.93}$$

$$\psi_1 = \frac{\psi_2}{\sqrt{\eta}}\frac{I_{1/2}(\sqrt{p}\,\eta)}{I_{1/2}(\sqrt{p})} \tag{3.94}$$

where p is Laplace parameter. Because the form of Eqs. 3.93 and 3.94 is complicated, it is convenient for one to invert the solutions to real space by numerical methods. In this study Eqs. 3.93 and 3.94 are inverted using a numerical method developed by Stehfest (1970).

3.5.3. Thermal Front Propagation

It is of primary interest in this study to examine the rate with which the cold water front advances away from the injection well during injection. This information is useful in the design of the safe location and rates of injection wells in relation to the production wells. The cold water front is defined as the locus of points with temperature being the average of the initial temperature of the reservoir (T_0), and the temperature of the injected water T_i ($T_{CF} = 1/2[T_0 + T_i]$). In Figure 3-14 the dimensionless radial distance ξ of the cold water front is plotted against dimensionless time τ for various values of θ. The parameter θ represents the ratio of the energy content of the fracture to that of the rock. In

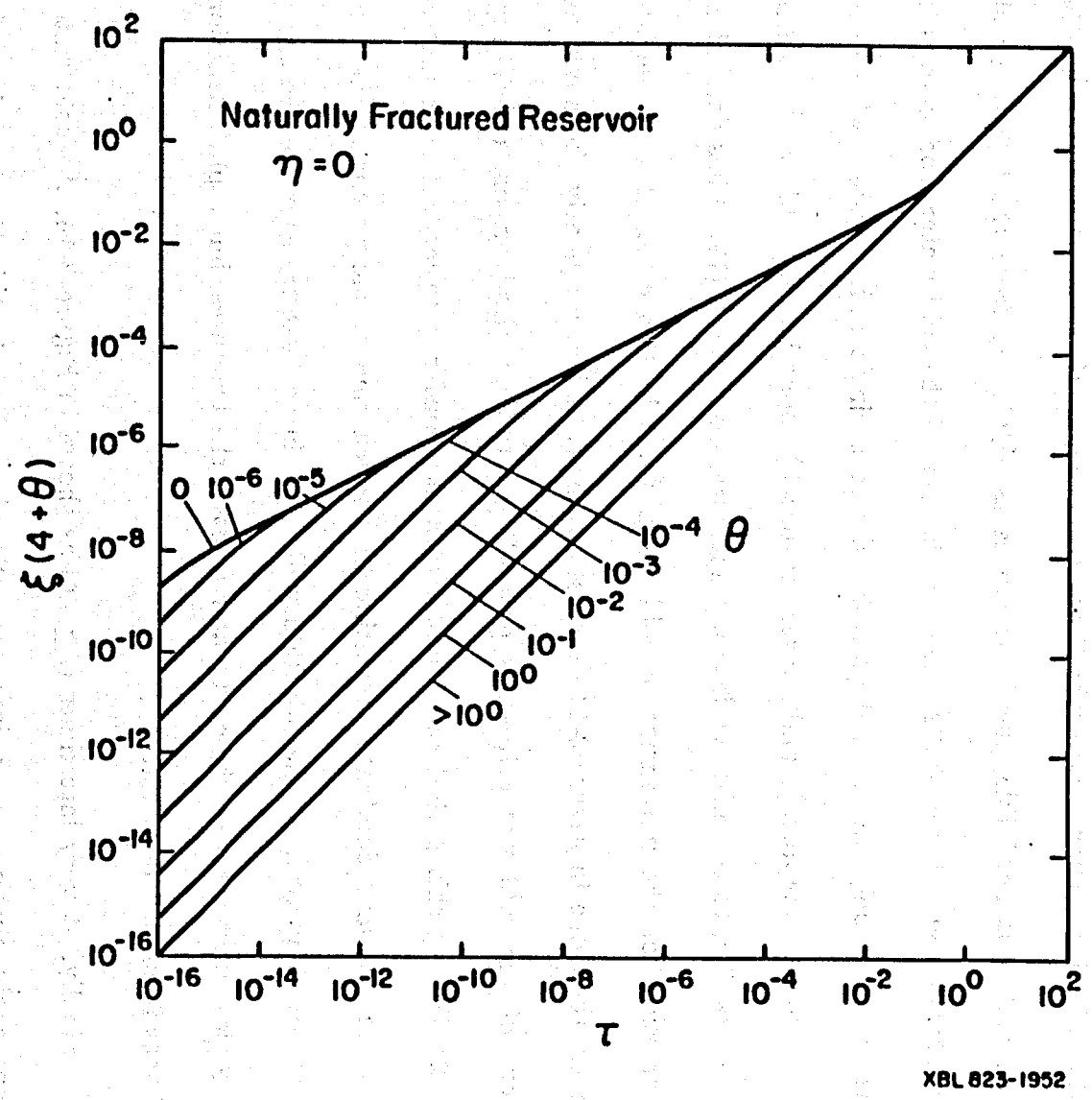

Figure 3-14 Type Curves for Thermal Front Movement in Naturally Fractured Reservoirs.

most cases realistic values of θ range from 10^{-6} to 10^{-8}. The figure actually shows for a given value of θ, the radial location of the cold water front in the fractures away from the injection well, at any given time. If one follows the advancement of the cold water front for one value of θ, say $\theta = 10^{-5}$, one can see three different rates of advancement. At early times when conduction heat transfer from the rock matrix is negligible, the front moves as r^2/t away from the injection well (Bodvarsson and Tsang, 1982). During this period the cold water front moves in the fractures only, in an analogous manner to a single radial system with insulated upper (caprock) and lower (bedrock) boundaries, and a thickness corresponding to the effective fracture aperture. Bodvarsson (1972) has derived as expression for the movement of cold water front in this case. At intermediate times, the slope in Figure 3-14 decreases by half, and consequently the advancement of the cold water front is proportional to r^4/t (Bodvarsson and Tsang, 1982). During this period the conductive heat transfer between the rock matrix and the fractures dominates, resulting in a much smaller movement of the cold water front away from the injection well. The large heat transfer area causes a very slow movement of the cold water front in the fractures, but rapid extraction of heat from the rock matrix.

Finally, at very late times ($r \geq 1.0$) as shown in Figure 3-14, the cold water front again advances at a rate proportional to r^2/t. At this time quasi-steady state heat transfer between the rock matrix and the fractures has been reached, and consequently the cold water front will move as if only a porous medium was present (i.e. independent of the fracture nature of the reservoir). However, in contrast to the early time behavior, the cold water front now moves at the same rate

in the fractures as in the rock matrix.

In order to explain this more thoroughly Figures 3-15 and 3-16 were constructed. Figure 3-15 shows the time sequence of the dimensionless temperature profiles away from the injection wells in the fractures and the rock matrix for a given value of θ. The dimensionless temperature of $T_D = 1.0$ represents the temperature of the injected water, whereas the dimensionless temperature $T_D = 0.$ corresponds to the initial reservoir temperature. Temperature profiles are given for the fractures ($\eta = 1.0$), the center of the cubes ($\eta = 0.0$) and two intermediate values ($\eta = 0.4, 0.7$). The figures show that at early times ($\tau = 0.1$) there is a considerable difference between the temperature profiles in the fractures and rock matrix. At later times the curves start to converge, although the cold water front is constantly moving away from the well. As shown on Figure 3-16, at a dimensionless time of $\tau = 1.0$ the temperature profiles are practically identical in the fractures and the rock matrix. This can be shown analytically by considering an asymptotic solution for the late time behavior of Eqs. 3.93-3.94 (Appendix E).

The reason for this phenomenon is that at early time the cold water shoots rapidly through the fractures, increasing the surface area for conductive heat transfer between the fractures and the rock matrix. The large surface area enhances energy transfer from the rock matrix to the fracture fluids, thus retarding the advancement of the cold water front along the fractures. This in turn, tends to equilibrate the temperatures in the fractures and the rock matrix so that eventually the temperature profiles away from the well are identical for the fractures and the rock matrix.

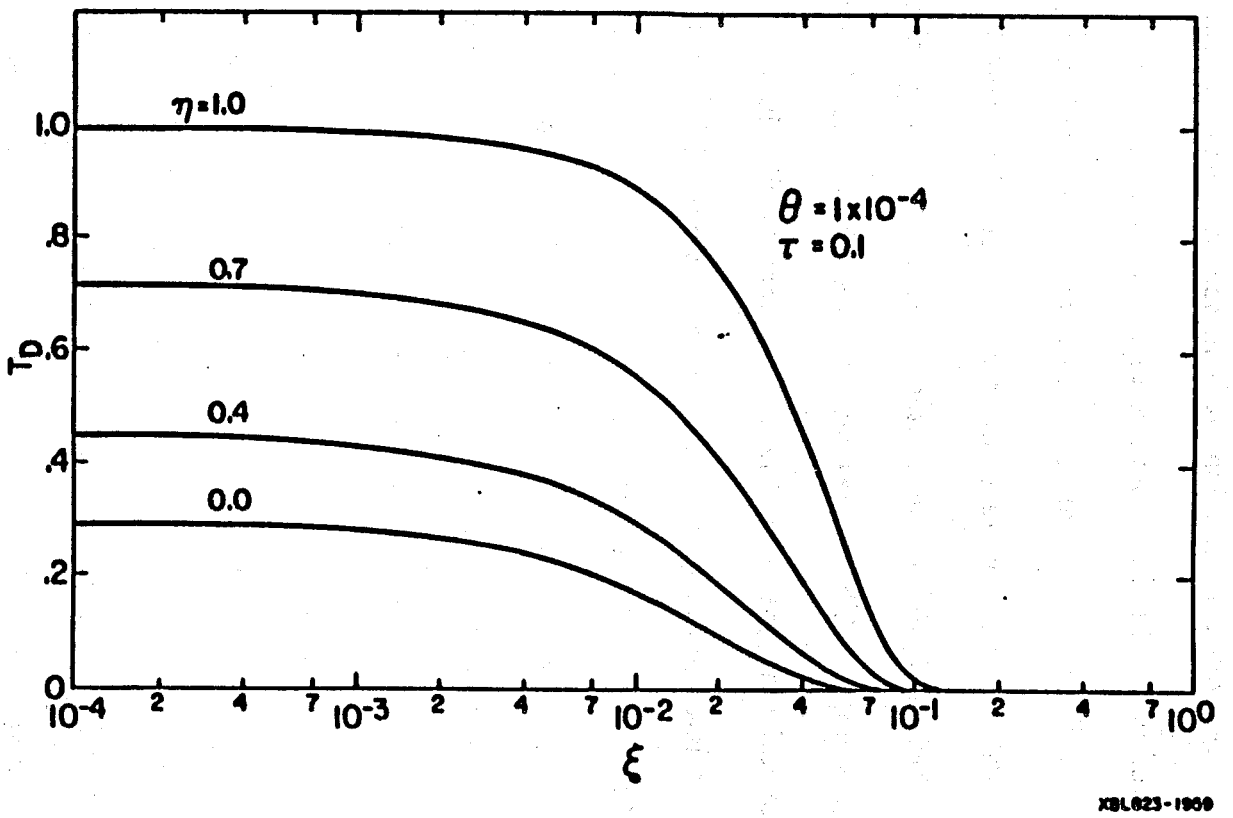

Figure 3-15 Temperature Profiles in Fractures and Rock Matrix; $\tau = 0.1$.

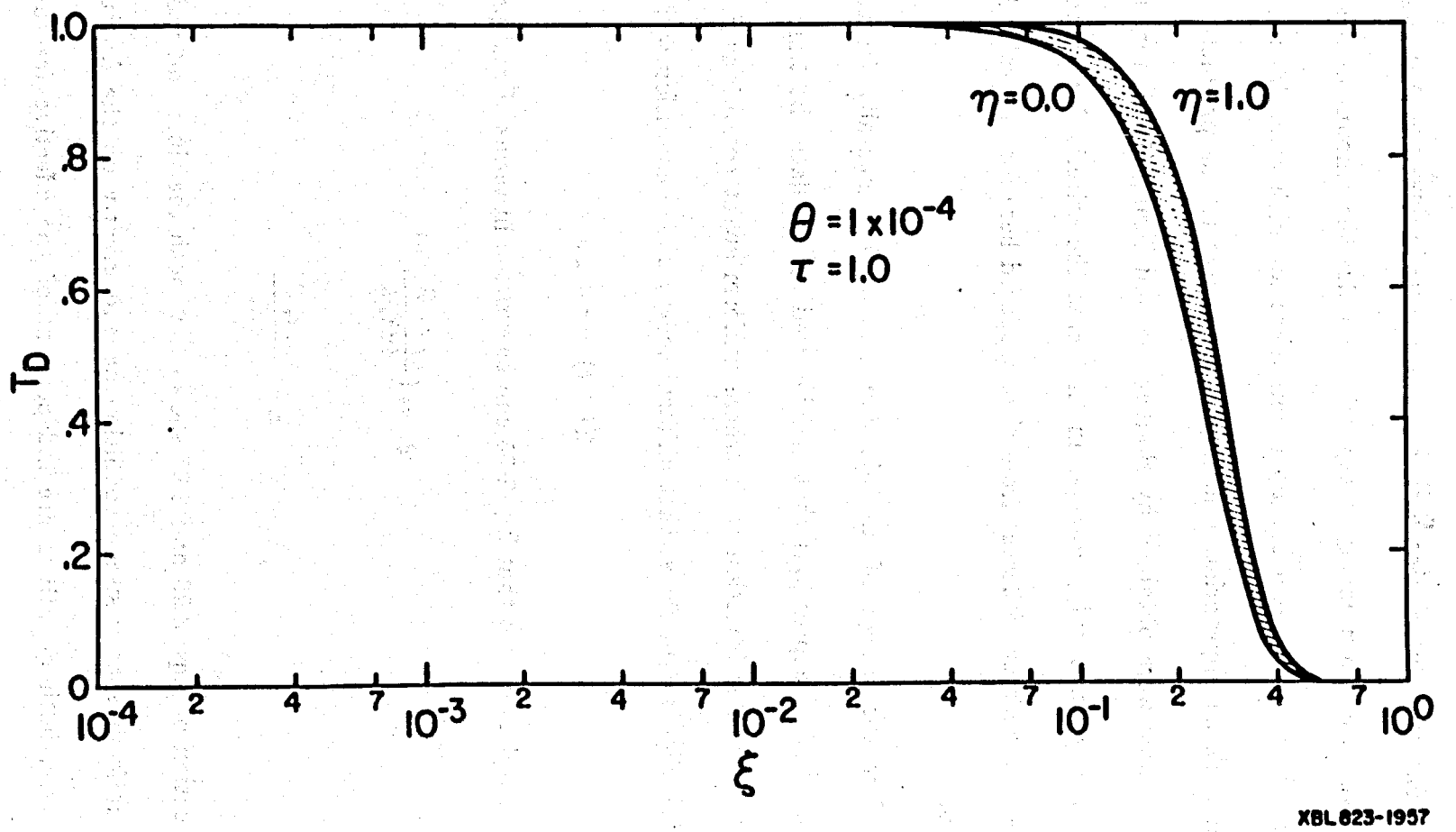

Figure 3-16 Temperature Profiles in Fractures and Rock Matrix; $\tau = 1.0$.

3.5.4. Design of Injection Systems

The most interesting aspect of the results obtained is that even for fractured reservoirs, uniform energy sweep will maximize the amount of recoverable energy from the resource. A necessary requirement for such conditions is that the injection wells be appropriately located with respect to the production wells. Similar conclusions were obtained by Bodvarsson and Tsang (1982) for the case of horizontal fractures only; however in that case the criteria for proper siting of the injection wells are different from that proposed here for naturally fractured reservoirs.

For the design of an injection system for naturally fractured reservoirs mathematical expressions that can be used to calculate the time and radial distance from the injection wells where uniform sweet conditions prevail are quite useful. Figure 3-14 shows that uniform energy sweep condition will prevail when

$$\xi(4 + \theta) = \tau = 1.0 \tag{3.95}$$

In general $4 >> \theta$ so that Eq. 3-95 can be written in terms of real parameters as

$$\xi_c = \left(\frac{\rho_f \, c_f \, D^2}{4\pi K_h \, h}\right)^{1/2} \tag{3.96}$$

$$t_c = \frac{\rho_r \, c_r \, D^2}{4K_h} \tag{3.97}$$

Inspection of Eqs. 3.96 and 3.97 shows that both the time and radial distance of the uniform energy sweep condition depend greatly on the fracture spacing D. However, both quantities are independent of the effective fracture aperture $\bar{b}$. Fractures possessing small apertures will contain very small amounts of fluids, so

that even though fluid velocities are high very little energy is needed to increase the temperature.

A problem involving as injection well in a naturally fractured reservoir using the parameters shown in Table 3-2 is considered. If the average fracture spacing is not known the following expressions can be calculated.

$$\xi = 2.6 \times D \text{ (meters)} \tag{3.98}$$

$$t_e = 0.01 \times D^2 \text{ (years)} \tag{3.99}$$

Thus, for an average fracture spacing of 50 meters, uniform energy sweep condition will prevail 130 m away from the well after 25 years of injection.

Table 3-2: Parameters used for design of injection systems

Injection rate, q_m	$20 kg/s$
Fluid density, ρ_f	$1000 kg/m^3$
Fluid heat capacity, c_f	$4200 J/kg \cdot {}^\circ C$
Thermal conductivity, K_h	$2.0 J/m \cdot s \cdot {}^\circ C$
Reservoir thickness, h	$500 m$
Rock density, ρ_r	$2700 kg/m^3$
Rock heat capacity, c_r	$1000 J/kg \cdot {}^\circ C$

3.6. Conclusions

The MINC approximation, which has been employed to model transport phenomena in double-porosity media, has been verified. The results show that this approximation can accurately represent transient inter-porosity flow in

fractured porous media, and provides the rationale for the development of models to analyze pressure transient behavior and thermal propagation in naturally fractured reservoirs.

Semi-analytical models for the analysis of isothermal and nonisothermal fluid flow in fractured reservoirs have been developed. The models consider the original geometrical configurations proposed by Barenblatt et al. (1960) and Warren and Root (1963), as well as transient inter-porosity flow between rock matrix and fractures. For isothermal fluid flow in naturally fractured reservoirs, a simple approximate analytical solution for transient pressure behavior in an infinite reservoir without wellbore storage and skin effects has been developed. This approximate solution is useful for pressure analysis of intermediate and late times. It shows that the pressure transient data during the transition period for values of ω smaller than 0.1 exhibit a half slope similar to that observed for the layered reservoir case. The half slope is followed by a brief segment with a slope of 2/3. All reservoir parameters can be determined if the half slope segment is observed, even if the early time straight line is not present. The appropriate procedure for analysis is given.

From the present study, it shows that in the case of a finite reservoir, the drainage radius may be significantly underestimated using a Warren and Root model (1963). The model presented here is similar to other transient models, e. g., layered reservoir models. Geologic information must be used to determine which model is appropriate. A field example of pressure build-up tests is given to illustrate the applicability of the present model to naturally fractured reservoirs.

This field example also demonstrates that inter-porosity flow factor λ and storativity ω are significantly overestimated by the Warren and Root model.

For nonisothermal fluid flow, proper locations and flow rates of injection wells in naturally fractured reservoirs have been determined by the model used to study the injection of cold water into hot reservoirs. Type curves have been developed to help in optimizing an injection operation for maximum energy recovery from the resource.

CHAPTER 4

NUMERICAL MODEL FOR THERMAL AND CHEMICAL TRANSPORT

4.1. Introduction

The ability to predict thermal and chemical transport in geologic media is important in such diversified fields as hydrothermal resource development, enhanced oil recovery processes, and waste water purification. Also, in the face of the urgent need for underground disposal of nuclear wastes, the problem of nonisothermal chemical transport in geologic media has become the topic of much interest (Witherspoon et al. 1981). Because of the inhomogeneous nature of geologic formations and nonlinearity of the governing equations, numerical methods must be employed to address these problems.

To model thermal and chemical transport in geologic formations, convection-diffusion type equations that arise from the conservation of energy and chemical species on a macroscopic scale are commonly used. For this work, an accurate numerical method different from conventional finite difference methods for the computation of the solutions of convection-diffusion type equations is developed. The method consists of a novel combination of a second-order Godunov scheme with the monotonized upwind/central differencing method (Van Leer, 1977; Colella, 1984), and the operator splitting technique (Strang, 1968). The accuracy of the present numerical method is investigated and a comprehensive comparison between the method and a conventional method for solving several benchmark problems is given so that one can easily assess the perfor-

mance of the present method.

4.2. Numerical Simulator PTC

The two-dimensional numerical simulator PTC (Lai et al., 1985) was developed to analyze coupled hydrological-thermal-chemical processes encountered in geologic formations. PTC was developed from the code PT (Bodvarsson, 1982), which is capable of modeling three-dimensional, coupled fluid and heat transport processes in fractured porous media. In the code PT, the noniterative Newton's method with a direct matrix solver was employed to solve sparse systems of linearized equations.

In addition to fluid and heat transport, the code PTC can simulate one-component chemical transport processes, including the effects of convection, dispersion, and kinetics of mineral-water reactions. To improve the accuracy of the code, a combination of a second-order Godunov method and the operator splitting technique is introduced to solve convection-diffusion type equations. A set of governing equations describing the transport processes, the numerical method, and a iterative solution procedure employed in the code are presented in the following sections.

4.3. Mathematical Model

In this section, the basic equations of single phase, thermal and chemical transport in geologic space are derived from the conservation laws of mass, energy and chemical species.

4.3.1. Conservation of Mass

As shown in Figure 4-1, let R be a region in two or three-dimensional geologic media that is saturated with a fluid. It is assumed that W is a fixed subregion of R. The rate of change of mass in W is expressed as

$$\frac{d}{dt}m(W,t) = \int_W \frac{\partial(\phi\rho_f)}{\partial t} dV_e + \int_W q_m \, dV_e \tag{4.1}$$

where dV_e is a volume element in a space, $m(W,t)$ is the total mass in W, ϕ is porosity, ρ_f is fluid density, q_m is mass generation rate per unit volume, and t is time. The total mass flow rate across the surrounding boundary of W is the surface integral of mass flux (Figure 4-2) expressed as

$$\int_{S_A} \rho_f \, \bar{v} \cdot \bar{n} \, dS_A \tag{4.2}$$

where $\bar{n}$ denotes the unit outward normal vector, S_A is the surface area of the boundary, and $\bar{v}$ is Darcy's velocity given by

$$\bar{v} = -\frac{k}{\mu}(\nabla P + \rho_f \, g) \tag{4.3}$$

where k is the intrinsic permeability of the medium, μ and ρ_f are fluid viscosity and density, respectively, P is the average pressure, and g is the gravitational acceleration.

From the principle of conservation of mass, the rate of change of mass in W equals the rate at which mass across the boundary in the inward direction add the rate of mass generation. Thus, one obtains

$$\int_W \frac{\partial(\phi\rho_f)}{\partial t} dV_e = -\int_{S_A} \rho_f \, \bar{v} \cdot \bar{n} \, dS_A + \int_W q_m \, dV_e \tag{4.4}$$

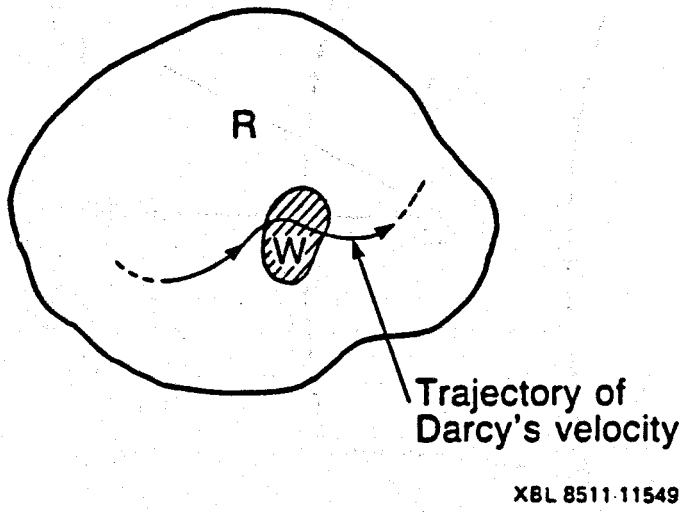

Figure 4-1 Fluid Motion in a Porous Space R (W is a Subregion of R).

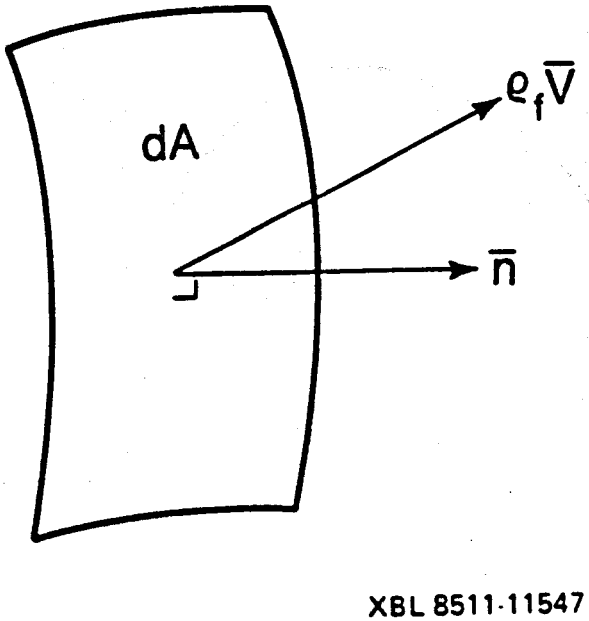

Figure 4-2 The Mass Flow Rate Across the Unit Surface Area.

By the divergence theorem, Eq. 4.4 is equivalent to

$$\int_W \frac{\partial(\phi\rho_f)}{\partial t}\, dV_e = -\int_W \nabla\cdot\rho_f\, \bar{v}\, dV_e + \int_W q_m\, dV_e \tag{4.5}$$

This equation is the integral form of the continuity equation.

4.3.2. Conservation of Energy

The total energy of fluid-saturated geologic media assuming thermodynamic equilibrium between rock and fluid is expressed as

$$E = [\phi\rho_f\, c_f + (1-\phi)\rho_r\, c_r]T \tag{4.6}$$

where c_f is specific heat of fluid, c_r is specific heat of rock, ρ_r is density of rock, and T is temperature. The rate of change of total energy in W is expressed as

$$\frac{d}{dt}E(W,t) = \int_W \frac{\partial}{\partial t}[\phi\rho_f\, c_f + (1-\phi)\rho_r\, c_r]T\, dV_e \tag{4.7}$$

If total energy flow rate across the boundary involves only convection and conduction effects, it can be obtained from the surface integral of energy flux expressed as

$$\int_{S_A} \bar{q}_{cond}\cdot\bar{n}\, dS_A + \int_{S_A} \bar{q}_{conv}\cdot\bar{n}\, dS_A \tag{4.8}$$

According to Fourier's law, the conductive heat flux is expressed as

$$\bar{q}_{cond} = -K_h \nabla T \tag{4.9}$$

where K_h is the effective thermal conductivity of geologic media. The convection heat flux is expressed as

$$\bar{q}_{conv} = \rho_f\, \bar{v} c_f\, T \tag{4.10}$$

Substituting Eqs. 4.9 and 4.10 into Eq. 4.8 and using the principle of conservation of energy, one obtains

$$\int_W \frac{\partial}{\partial t}[\phi\rho_f c_f + (1-\phi)\rho_r c_r]T \, dV_e = \int_{S_A} K_h \nabla T \cdot \bar{n} \, dS_A - \int_{S_A} \rho_f \bar{v} c_f T \cdot \bar{n} \, dS_A + \int_W q_m c_f T_s \, dV_e$$

$$= \int_W \nabla \cdot K_h \nabla T \, dV_e - \int_W \nabla \cdot \rho_f \bar{v} c_f T \, dV_e + \int_W q_m c_f T_s \, dV_e \tag{4.11}$$

where T_s is the temperature of fluid sources. This equation is the integral form of the energy equation.

4.3.3. Conservation of Chemical Species

A material balance for solutes resulting in the chemical species equation in a similar way as energy equation is expressed as

$$\int_W \frac{\partial}{\partial t}(\phi\rho_f C) \, dV_e = \int_W \nabla \cdot \rho_f D_{ij} \nabla C \, dV_e - \int_W \nabla \cdot \rho_f \bar{v} C \, dV_e + \int_W q_m C_s \, dV_e \tag{4.12}$$

where D_{ij} is a dispersion tensor, C_s is the concentration of fluid sources. This equation is the integral form of chemical species equation.

If the variables in the integrand of Eqs. 4.5, 4.11, and 4.12 are smooth enough, the differential form of the conservation laws of mass, energy and chemical species can be directly obtained by removing the integral signs. Otherwise, the integral form will then be the one to use. With recognization of this fact, any physical quantities should be considered as the average values with respect to subregion W, if the differential form is to be used when geologic media are treated as a continuum. To give a complete description of thermal and chemical transport processes, changes in pressure and density affect temperature variations

and the principles of thermodynamics must also be considered. From thermodynamics, one obtains equations of state for water and rock. The properties of liquid water are calculated using polynomial functions of pressure and temperature (Buscheck, 1980; Bodvarsson, 1982). The viscosity is assumed to be only temperature dependent, its dependence on pressure being neglected. The density is a function of pressure as well as temperature. The specific heats of water and rock, and the effective thermal conductivity of geologic media are assumed constant. By definition, the expansivities and compressibilities of water and rock can be expressed as

$$\varsigma = \frac{1}{\rho_l}\frac{\partial \rho_l}{\partial P}\Big|_T \qquad \epsilon = \frac{1}{\phi}\frac{\partial \phi}{\partial P}\Big|_T$$

$$\beta = -\frac{1}{\rho_l}\frac{\partial \rho_l}{\partial T}\Big|_P \qquad \bar{\gamma} = -\frac{1}{\phi}\frac{\partial \phi}{\partial T}\Big|_P \tag{4.13}$$

From the fluid density function, ς and β can be evaluated. The rock compressibility (ϵ) and expansivity ($\bar{\gamma}$) are determined experimentally or estimated using empirical laws. It is assumed that the concentration of the chemical species is low enough so that it does not affect the fluid properties.

4.4. Solution Procedures

In this section, a numerical solution technique for solving the above conservation equations is presented. For hydrologists, the quantities of pressure, temperature and concentration are more important than the fluid and rock properties; thus they are regarded as primary dependent variables and the latter as secondary dependent variables in the mass, energy, and chemical equations for numerical calculations. Once the solutions of primary dependent variables are

obtained, the secondary variables can be updated using the equations of state. Combining Eqs. 4.5 and 4.13, one obtains Eq. 4.14 involving two primary dependent variables, pressure and temperature.

$$\int_W \left\{ (\varsigma + \epsilon)\phi\rho_f \frac{\partial P}{\partial t} - (\beta + \bar{\gamma})\phi\rho_f \frac{\partial T}{\partial t} + \nabla\cdot\bar{v}\rho_f \right\} dV_e = \int_W q_m \, dV_e \tag{4.14}$$

If Eq. 4.5 is multiplied by a factor of $c_f\ T$ and subtracted from Eq. 4.11, one obtains the following energy equation for the numerical formulation

$$\int_W \{\phi\rho_f \frac{\partial(c_f\ T)}{\partial t} + \frac{\partial[(1-\phi)\rho_r\ c_r]T}{\partial t}\} dV_e = \int_W \nabla\cdot K_h \nabla T \ dV_e - \int_{S_A} \rho_f\ \bar{v}c_f\ T\cdot\bar{n}\ dS_A$$

$$+ \int_W c_f\ T\nabla\cdot\rho_f\ \bar{v}\ dV_e + \int_W q_m\ c_f\ (T_e - T)\ dV_e \tag{4.15}$$

Since c_f and c_r are assumed constant, Eq. 4.15 can be further simplified by linearizing porosity, ϕ,

$$\int_W \sigma_T \frac{\partial T}{\partial t}\ dV_e = \int_W \nabla\cdot K_h \nabla T \ dV_e - \int_{S_A} \bar{v}_T\ T\cdot\bar{n}\ dS_A$$

$$+ \int_W T\nabla\cdot\bar{v}_T + \int_W q_m\ c_f\ (T_e - T)\ dV_e \tag{4.16}$$

where $\sigma_T = \phi\rho_f\ c_f + (1-\phi)\rho_r\ c_r$ and $\bar{v}_T = \bar{v}\rho_f\ c_f$

Similarly, the equation for conservation of chemical species can be expressed as

$$\int_W \sigma_c \frac{\partial C}{\partial t} dV_e = \int_W \nabla\cdot\rho_f\ D_{ij}\nabla C \ dV_e - \int_{S_A} \bar{v}_c\ C\cdot\bar{n}\ dS_A$$

$$+ \int_W C\nabla\cdot\bar{v}_c\ dV_e + \int_W q_m (C_e - C)\ dV_e \tag{4.17}$$

where $\sigma_c = \phi\rho_f$ and $\bar{v}_c = \bar{v}\rho_f$

As a first step, Eqs. 4.3 and 4.14 are combined to solve for the pressure field neglecting temperature effects (β and $\bar{\gamma}$ assumed equal zero), resulting in a diffusion type equation. There is no difficulty to solve this equation by the implicit central finite difference method. The detailed procedure can be found in PT (Bodvarsson, 1982). After obtaining the pressure field, Darcy's law, Eq. 4.4, can then be applied to obtain the velocity field, which is used to solve the energy and chemical species equations, Eqs. 4.16 and 4.17. The method used to solve Eqs. 4.16 and 4.17 consists of a combination of the explicit, monotonized upwind/central differencing and operator splitting. By means of operator splitting, the first fractional step omits the diffusion and sources terms in Eqs. 4.16 and 4.17. Thus, the following equations are solved

$$\int_W \sigma_T \frac{\partial T}{\partial t} dV_e + \int_{S_A} \bar{v}_T T \cdot \bar{n} \; dS_A - \int_W T \nabla \cdot \bar{v}_T \; dV_e = 0 \tag{4.18}$$

and

$$\int_W \sigma_c \frac{\partial C}{\partial t} dV_e + \int_{S_A} \bar{v}_c C \cdot \bar{n} \; dS_A - \int_W C \nabla \cdot \bar{v}_c \; dV_e = 0 \tag{4.19}$$

The method used to solve Eqs. 4.18 and 4.19 is the explicit, monotonized upwind/central differencing method, proposed by Van Leer (1977) and further developed for multidimensional, nonlinear hyperbolic systems by Colella (1984). A description of the method is given in the following section. The second fractional step considers the diffusion type equations that arise when the convection term is neglected. This leads to the following two equations

$$\int_W \sigma_T \frac{\partial T}{\partial t} dV_e = \int_W \nabla \cdot K_h \nabla T \; dV_e + \int_W q_m c_f (T_e - T) \, dV_e \tag{4.20}$$

and

$$\int_W \sigma_e \frac{\partial C}{\partial t} dV_e = \int_W \nabla \cdot \rho_f D_{ij} \nabla C \; dV_e + \int_W q_m (C_e - C) \, dV_e \tag{4.21}$$

Eqs. 4.20 and 4.21 are solved using the implicit central difference method. After pressure, temperature and concentration are obtained, the fluid and rock properties are updated, and the procedure repeated until the solution has converged. The criterion set for convergence is

$$\left(\frac{\lambda_{new} - \lambda_{old}}{\lambda_{old}}\right)_{max} \leq \tau_\lambda \tag{4.22}$$

where λ refers to P, T or C; τ_λ is a specified residue constant; and the subscript "max" denotes the maximum value over all grid blocks.

4.5. Method For Controlling Numerical Diffusion Errors And Grid Orientation Effects

As the forms of Eqs. 4.18 and 4.19 are identical, it will be sufficient to describe the application of a second-order Godunov method with the explicit, monotonized upwind/central differencing to Eq. 4.18. The basic idea behind the method is to approximate the solution at the new time level, $t^{n+1} = t^n + \Delta t$, by integrating the energy flux across the grid boundaries and considering the mixing effects due to compressible fluids (Eq. 4.23). In order to obtain second-order accuracy in time, the primary variables at the grid boundaries are evaluated at the intermediate time level, $t^{n+1/2} = t^n + 1/2\Delta t$, for each time interval by tracing characteristics, and solving difference approximations to the characteristic equations (Eq. 4.24). The second-order accuracy in space for the difference

approximations to the characteristic equations can be obtained by constructing a piecewise, linear distributions of primary dependent variables at each grid rather than a piecewise constant (first-order Godunov method). Furthermore, the linear distribution is obtained calculating the slope at each grid center by a suitable difference formula, which includes a "limiting" process to guarantee solution possessing monotonicity properties (Eq. 4.25). The detailed procedure is given as follows: In two dimensions (Figure 4-3), Eq. 4.18 can be expressed in conservation form by finite difference method as

$$T_{i,j}^{n+1} = T_{i,j}^{n} + \frac{\Delta t}{(\sigma_T \Delta x)_{i,j}} \Big\{ (\overline{v}_{Tx} T^{n+1/2})_{i-1/2,j} - (\overline{v}_{Tx} T^{n+1/2})_{i+1/2,j}$$

$$+ \frac{(T_{i+1/2,j}^{n+1/2} + T_{i-1/2,j}^{n+1/2})}{2} [(\overline{v}_{Tx})_{i+1/2,j} - (\overline{v}_{Tx})_{i-1/2,j}] \Big\}$$

$$+ \frac{\Delta t}{(\sigma_T \Delta y)_{i,j}} \Big\{ (\overline{v}_{Ty} T^{n+1/2})_{i,j-1/2} - (\overline{v}_{Ty} T^{n+1/2})_{i,j+1/2}$$

$$+ \frac{(T_{i,j+1/2}^{n+1/2} + T_{i,j-1/2}^{n+1/2})}{2} [(\overline{v}_{Ty})_{i,j+1/2} - (\overline{v}_{Ty})_{i,j-1/2}] \Big\} \tag{4.23}$$

where the subscripts (i,j), and $(i \pm 1/2, j)$ or $(i, j \pm 1/2)$ denote grid center and grid boundaries, respectively; the superscripts n, $n+1/2$, and $n+1$, denote the time level; and $T_{i+1/2,j}^{n+1/2}$ represents the average temperature at time $t^{n+1/2} = t^n + 1/2\Delta t$ in the computational grid boundary at $x = (i+1/2)\Delta x$ and $y = j\Delta y$. With $\overline{v}_{Tx} > 0$ at $(i+1/2, j)$, $T_{i+1/2,j}^{n+1/2}$ can be expressed by a first-order Taylor series expansion as

$$T_{i+1/2,j}^{n+1/2} = T_{i,j}^{n} + \frac{\Delta x}{2} \frac{\partial T}{\partial x}\Big|_{i,j} + \frac{\Delta t}{2} \frac{\partial T}{\partial t}\Big|_{i,j}$$

$$= T_{i,j}^{n} + \frac{\Delta x}{2} \frac{\partial T}{\partial x}\Big|_{i,j} + \frac{\Delta t}{2(\sigma_T)_{i,j}} \Big\{ - \frac{\partial(\overline{v}_{Tx} T)}{\partial x} + T \frac{\partial \overline{v}_{Tx}}{\partial x}$$

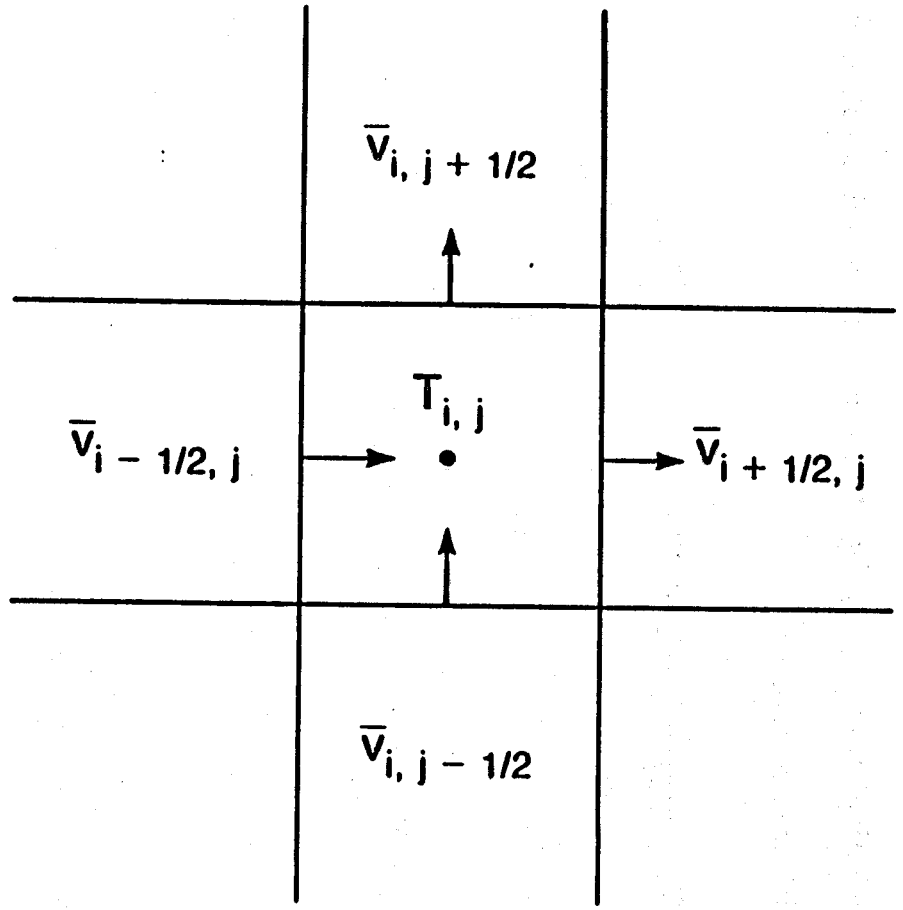

XBL 8511-11552

Figure 4-3 The Symbols of Numerical Computations in Two Dimensions.

$$-\frac{\partial(\overline{v}_{Ty}\,T)}{\partial y}+T\frac{\partial\overline{v}_{Ty}}{\partial y}\Big\}_{i,j}$$

$$=T^n_{i,j}+(\frac{\Delta x}{2}-\frac{\Delta t\overline{v}_{Tx}}{2\sigma_T})_{i,j}\frac{\partial T}{\partial x}\Big|_{i,j}-\frac{\Delta t}{2(\sigma_T)_{i,j}}\Big\{\frac{\partial(\overline{v}_{Ty}\,T)}{\partial y}-T\frac{\partial\overline{v}_{Ty}}{\partial y}\Big\}_{i,j}$$

$$=T^n_{i,j}+(\frac{\Delta x}{2}-\frac{\Delta t\overline{v}_{Tx}}{2\sigma_T})_{i,j}(\frac{\Delta^x T}{\Delta x})_{i,j}-\frac{\Delta t}{2(\sigma_T\,\Delta y)_{i,j}}$$

$$\Big\{(\overline{v}_{Ty})_{i,j+1/2}(T^n_{i,j+1/2}-T^n_{i,j})-(\overline{v}_{Ty})_{i,j-1/2}(T^n_{i,j-1/2}-T^n_{i,j})\Big\}$$

$$=T^n_{i,j}+(\frac{1}{2}-\frac{\Delta t\overline{v}_{Tx}}{2\sigma_T\,\Delta x})_{i,j}\,\Delta^x T_{i,j}-\frac{\Delta t}{2(\sigma_T\,\Delta y)_{i,j}}$$

$$\Big\{(\overline{v}_{Ty})_{i,j+1/2}(T^n_{i,j+1/2}-T^n_{i,j})-(\overline{v}_{Ty})_{i,j-1/2}(T^n_{i,j-1/2}-T^n_{i,j})\Big\} \tag{4.24}$$

In Eq. 4.24, $(\frac{\Delta^x T}{\Delta x})_{i,j}$ represents the temperature gradient at the node (i,j). In order to obtain second-order accuracy in space, a central differencing formula is employed. However, to avoid numerical oscillations near fronts, the limiter $\Delta^x T_{i,j}$ is constrained by the monotonicity principle expressed as (Van Leer, 1977)

$$\Delta^x T_{i,j}=\min\{\delta T^n_{i,j}\,,\ 2\,|T^n_{i+1,j}-T^n_{i,j}|\,,\ 2\,|T^n_{i,j}-T^n_{i-1,j}|\}$$

$$\times sgn\,(T^n_{i+1,j}-T^n_{i-1,j})\,,\ \text{if}\ (T^n_{i+1,j}-T^n_{i,j})(T^n_{i,j}-T^n_{i-1,j})>0;$$

$$=0\,,\ \textit{otherwise}. \tag{4.25}$$

where $\delta T^n_{i,j}$ is $1/2|T^n_{i+1,j}-T^n_{i-1,j}|$ for equally spaced grids. The central differencing formula for unequally spaced grids can be obtained in a similar way. Similarly, with $\overline{v}_{Ty}>0$ at $(i,j+1/2)$, $T^{n+1/2}_{i,j+1/2}$ can be defined as

$$T^{n+1/2}_{i,j+1/2} = T^{n}_{i,j} + \left(\frac{1}{2} - \frac{\Delta t \bar{v}_{Ty}}{2\sigma_T \Delta y}\right)_{i,j} \Delta^y T_{i,j} - \frac{\Delta t}{2(\sigma_T \Delta x)_{i,j}}$$

$$\left\{(\bar{v}_{Tx})_{i+1/2,j}(T^{n}_{i+1/2,j} - T^{n}_{i,j}) - (\bar{v}_{Tx})_{i-1/2,j}(T^{n}_{i-1/2,j} - T^{n}_{i,j})\right\} \qquad (4.26)$$

where $\Delta^y T_{i,j}$ is defined as in Eq. 4.24 but with the roles of i and j reversed. The primary function of the limiters $\Delta^x T_{i,j}$ and $\Delta^y T_{i,j}$ is to track fronts and select the proper temperature gradients for the nodes at the fronts. The first-order differencing of Eq. 4.25 is employed at discontinuities in the solution, allowing a small amount of numerical dissipation to avoid oscillations. Thus, a sharp front will be smeared to some extent. Then the second-order differencing is employed in the smooth region of the front, as shown in Figure 4-4. By adjusting the limiters (Colella, 1985), one can obtain steeper gradients at fronts than those obtained using Eq. 4.25. However, such refined limiters require information from two more grid points, and this makes the computation more complicated, especially for the treatment of boundary conditions.

If $\Delta^x T_{i,j}$ or $\Delta^y T_{i,j}$ is equal to zero, this numerical scheme reduces to a first-order upwind differencing method. It should be noted that the third terms on the right hand side of Eqs. 4.24 and 4.26 must also be approximated using the first-order Godunov scheme (ie., the first-order upwind differencing scheme) (Colella, 1984). The role of these terms is to take into account the effects of fluid flow in the direction tangential to the grid boundaries.

Because this numerical scheme is explicit, time steps must be controlled to avoid numerical instabilities. The magnitude of chemical velocity, $\frac{|\bar{v}_c|}{\sigma_c}$, is always

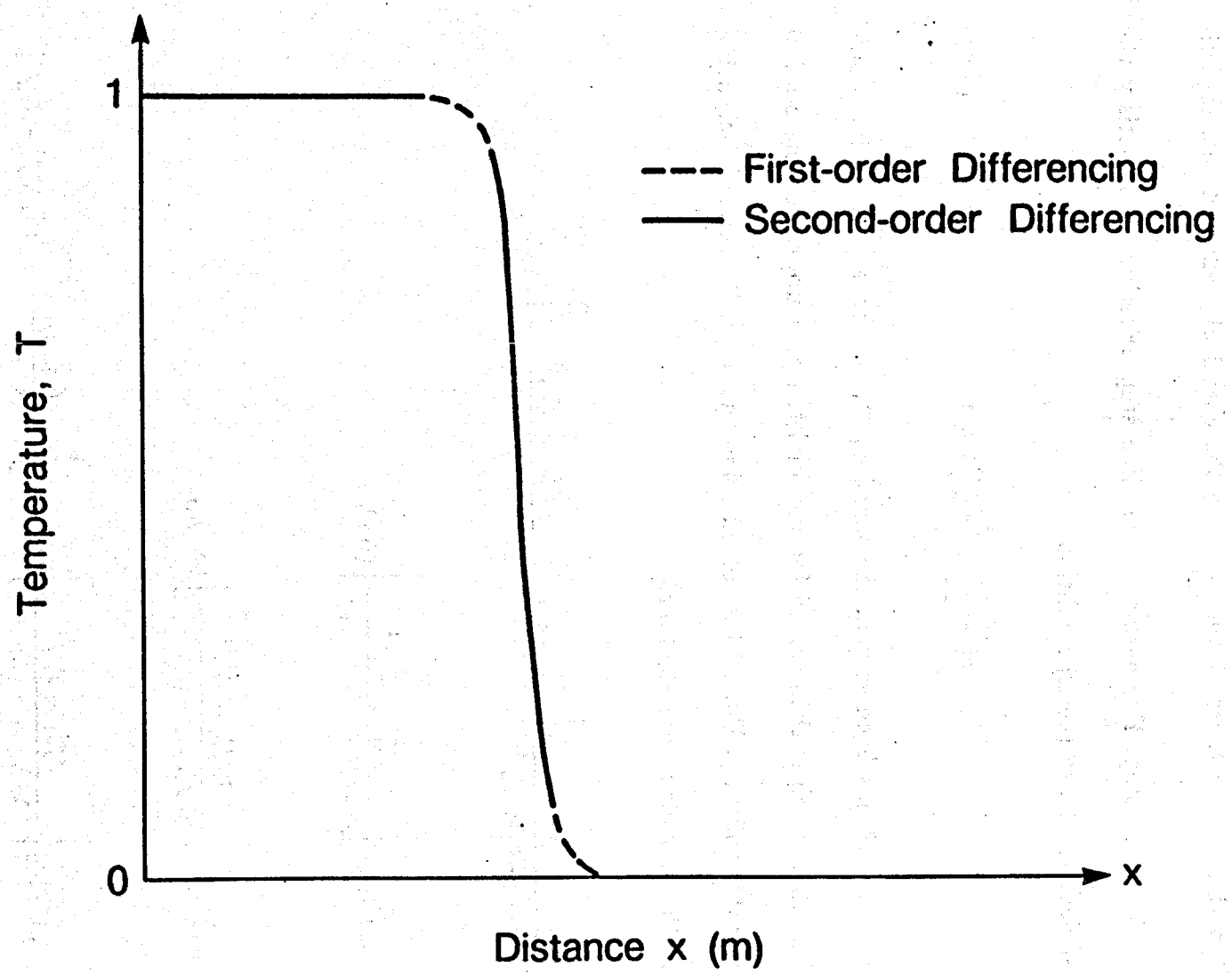

XBL 856-10536

Figure 4-4 Solutions at the Front Where First-Order or Second-Order Differencing (the Limiter $\Delta^2 T_{i,j}$) is Used.

larger than that of the thermal one, $\frac{|\bar{v}_T|}{\sigma_T}$, so the chemical transport sets the criterion for the time step. Furthermore, the time step criterion must satisfy the Courant-Friedrichs-Lewy (CFL) condition

$$\max\left(\frac{|\bar{v}_{cx}|\Delta t}{\sigma_c \Delta x}, \frac{|\bar{v}_{cy}|\Delta t}{\sigma_c \Delta y}\right) \leq 1 \tag{4.27}$$

Once Eq. 4.23 has been solved, the solution, $\hat{T}$, is used as the initial condition in Eq. 4.25, which is then solved for the final temperature to complete a full step of operator splitting. Eq. 4.25 is solved using the implicit central differencing method in the following numerical form

$$\begin{aligned}
T_{i,j}^{n+1} = \hat{T}_{i,j} + \frac{\Delta t}{(\sigma_T \Delta x \Delta y)_{i,j}^{n+1}} \Bigg\{ & 2(K_h)_{i-1/2,j}^{n+1} \left[\frac{T_{i-1,j}^{n+1} - T_{i,j}^{n+1}}{(\Delta x)_{i-1,j} + (\Delta x)_{i,j}} \right] (\Delta y)_{i,j} \\
& + 2(K_h)_{i+1/2,j}^{n+1} \left[\frac{T_{i+1,j}^{n+1} - T_{i,j}^{n+1}}{(\Delta x)_{i,j} + (\Delta x)_{i+1,j}} \right] (\Delta y)_{i,j} \\
& + 2(K_h)_{i,j-1/2}^{n+1} \left[\frac{T_{i,j-1}^{n+1} - T_{i,j}^{n+1}}{(\Delta y)_{i,j-1} + (\Delta y)_{i,j}} \right] (\Delta x)_{i,j} \\
& + 2(K_h)_{i,j+1/2}^{n+1} \left[\frac{T_{i,j+1}^{n+1} - T_{i,j}^{n+1}}{(\Delta y)_{i,j+1} + (\Delta y)_{i,j}} \right] (\Delta x)_{i,j} \Bigg\} + \left(\frac{q_m c_f}{\sigma_T} \right)_{i,j}^{n+1} \left[(T_s)_{i,j}^{n+1} - T_{i,j}^{n+1} \right]
\end{aligned} \tag{4.28}$$

The above procedure is repeated for each time step. Eq. 4.28 is solved by a sparse matrix solver SPARSPAK (George et al., 1980). It should be noted that SPARSPAK provides a variety of options for solving sparse systems of linear

equations, however, there are only two options, ORDRA2 and ORDRB4, available for solving mass and energy equations simultaneously. By comparison of the efficiency of SPARSPAK and that of the matrix solver MA28 (Duff, 1977), it was found that the memory storage required by SPARSPAK is about 1/3 less than MA28, but the computational speed is about 1/4 slower, if a 980×980 asymmetric sparse matrix resulting from PT's formulation is solved.

4.6. Validation of the Numerical Scheme

The validity of this numerical scheme has been tested with various problems for which exact or approximate solutions (analytical or numerical) are available. The following four cases are considered to illustrate the accuracy of this numerical method and some areas of application.

4.6.1. One-Dimensional Convection-Diffusion Problem

The test case considered is a one-dimensional, isothermal, chemical transport problem in a semi-infinite, isotropic porous medium. A constant concentration, C_0, is maintained at the inlet ($x=0$), and an initial concentration of zero is assumed everywhere. The fluid velocity ($\frac{\bar{v}}{\phi}$), rock and fluid properties, and the longitudinal dispersion coefficient, D_l, are assumed constant. The analytical solution to Eq. 4.22 without the source term for the given boundary and initial conditions is given by Carslaw and Jaeger (1959) as

$$\frac{C}{C_0} = \frac{1}{2}\left\{erfc\left(\frac{x - \frac{\bar{v}t}{\phi}}{2\sqrt{D_l t}}\right) + \exp\left(\frac{\bar{v}x}{\phi D_l}\right) erfc\left(\frac{x + \frac{\bar{v}t}{\phi}}{2\sqrt{D_l t}}\right)\right\} \tag{4.29}$$

In the numerical calculations, the computational domain is divided into

equal volume elements with a nodal point spacing of $0.5m$. To obtain accurate results, the CFL condition (Eq. 4.27) used in this test case was set at 0.5. Calculations were made over a wide range of Peclet numbers, $\frac{\bar{v}\Delta x}{\phi D_l}$, to thoroughly test the performance of the numerical scheme. The results are shown in Figure 4-5. The comparison between the numerical and analytical solutions shows excellent agreement for Peclet numbers 0.1 and 1. This shows that the approximate solution using the present numerical scheme converges toward the exact solution of the differential equation; the numerical scheme with the operator splitting procedures is consistent. When the Peclet number is 10 or 100, the numerical diffusion errors are still small and there is no oscillation near the front. The numerical solution for a Peclet number of ∞ is very close to that for a Peclet number of 100.

It is of interest to compare the results from the present numerical scheme with those of the conventional first-order upwind scheme. Figure 4-6 compares the two schemes for Peclet numbers 10 and 100, and shows clearly that for these Peclet numbers the conventional first-order upwind scheme can lead to greater numerical diffusion errors than those produced by the present scheme. When the Peclet number is below 2, the conventional central differencing scheme can be employed to model the convection term with no oscillation, generating identical results to the present scheme.

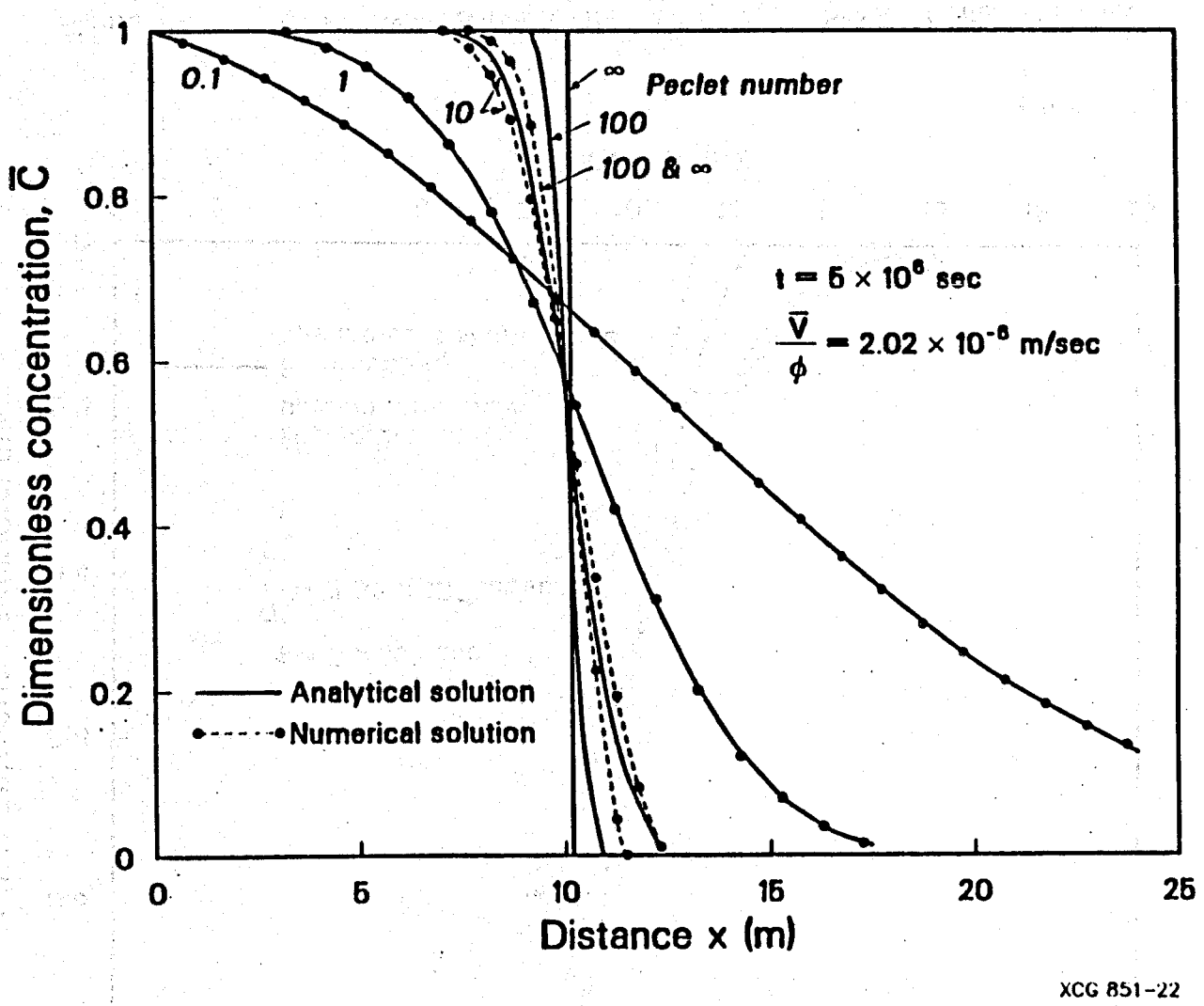

Figure 4-5 Comparison Between Analytical and Numerical Solutions Using a Second-Order Godunov Method.

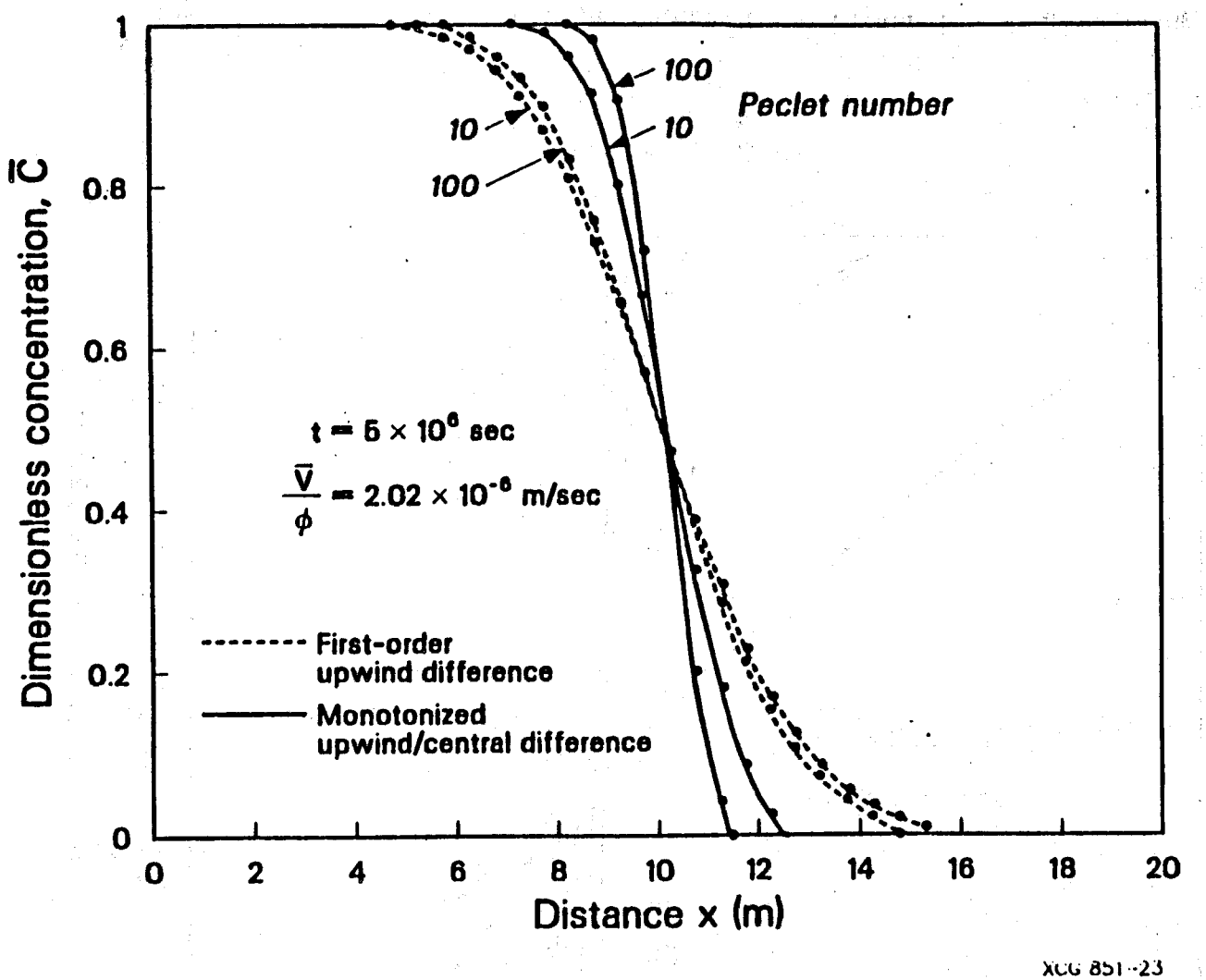

Figure 4-6 Comparison Between Results Using a Second-Order Godunov Method (Monotonized Upwind/Central Differencing Method) and a Conventional First-Order Upwind Difference Method.

4.6.2. Two-Dimensional Convection with Longitudinal and Transverse Dispersion

For this case, we consider a rectangular, homogeneous and isotropic porous medium with constant concentration, C_0, maintained over a portion of the boundary ($0 \leq y \leq b$), zero concentration maintained over rest of the boundary ($b < y \leq l$), and uniform initial concentration of zero (Figure 4-7). The isothermal fluid velocity ($\frac{\bar{v}}{\phi}$), longitudinal dispersion coefficient, D_l, and transverse dispersion coefficient, D_t, are assumed constant. Under these conditions, the chemical transport equation simplifies to

$$\frac{\partial C}{\partial t} = D_l \frac{\partial^2 C}{\partial x^2} + D_t \frac{\partial^2 C}{\partial y^2} - \frac{\bar{v}}{\phi}\frac{\partial C}{\partial x} \tag{4.30}$$

When the input concentration is maintained at the boundary for a long enough time, the concentration distribution approaches a quasi-steady condition. Harleman and Rumer (1963) obtained an approximate steady-state solution for this problem by neglecting longitudinal dispersion. Their solution can be expressed as

$$\frac{C}{C_0} = \frac{1}{2} erfc\left(\frac{y-b}{2\sqrt{D_t x \phi/\bar{v}}}\right) \tag{4.31}$$

In this test case, the computational domain is divided into equal volume elements with a nodal point spacing of $1m$ in both x and y directions. Comparison of the numerical results with the approximate analytical solution is shown in Figure 4-8. Good agreement is obtained except in the region near $x = 0$. The observed differences between analytical and numerical results are expected,

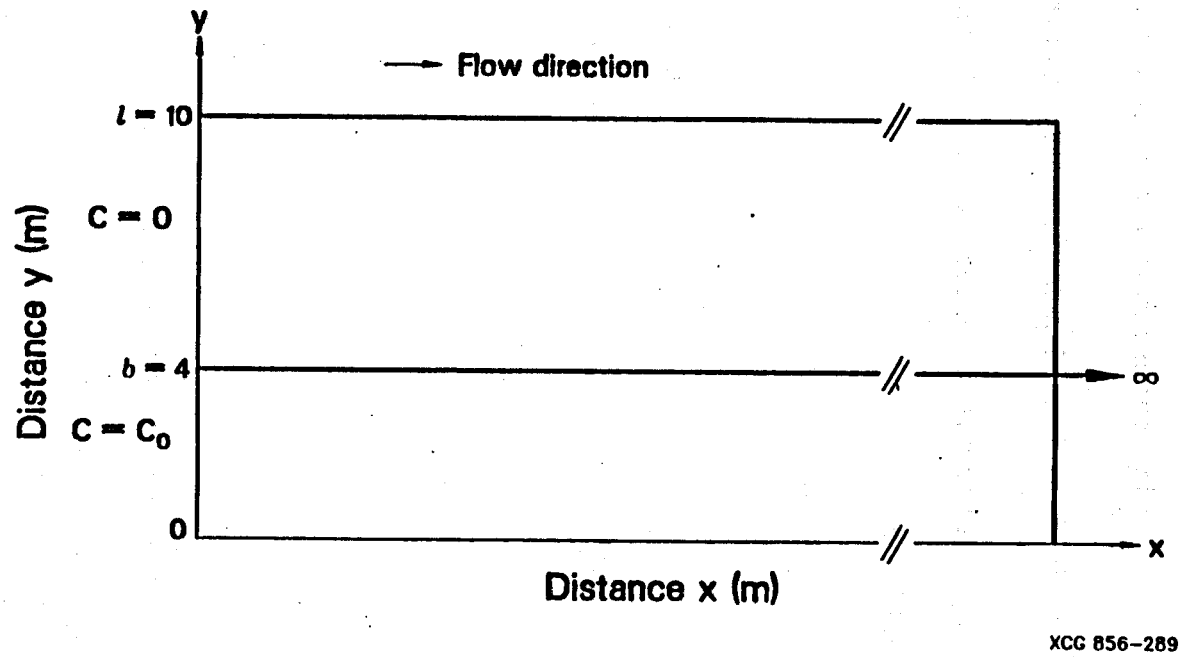

Figure 4-7 Schematic Illustration of a Convection-Diffusion Problem with Longitudinal and Transverse Dispersion.

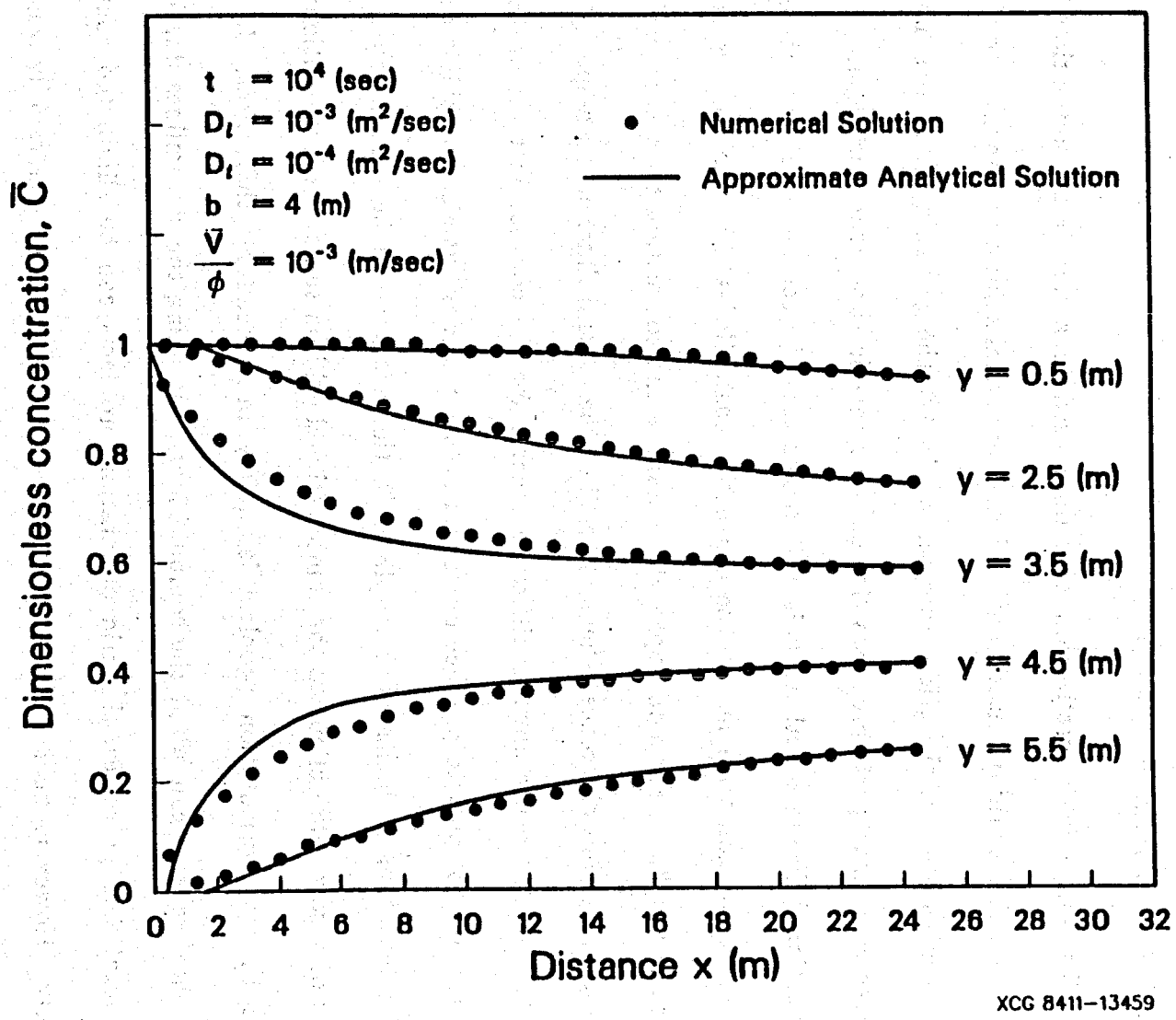

Figure 4-8 Comparison Between Numerical and Approximate Analytical Solutions for a Convection-Diffusion Problem with Longitudinal and Transverse Dispersion.

because the approximate analytical solution assumes $\frac{\partial^2 C}{\partial x^2} = 0$. These differences are largest for the curves for $y = 3.5$ and $4.5m$ where the largest concentration gradients exists; hence, $\frac{\partial^2 C}{\partial x^2} \neq 0$.

4.7. Grid Orientation Effects

The numerical discretization procedure used in a numerical simulation is said to exhibit a grid orientation effect if the numerical solution is sensitive to the spatial orientation of the grid. As described in 4.3, the governing equations used to describe transport processes in geologic media are transport-dominated convection-diffusion equations. It is well known that the central difference scheme for the convection term may cause convection instabilities if the solution is not smooth enough. A common approach to stablize the convection term is to use a first-order upwind difference scheme instead of the central difference scheme. The effects of a first-order upwind difference scheme for the convection term on the solution are not only to produce numerical diffusion errors but also to exhibit the grid orientation problems. The emphasis in this section will be focused on the effect of a flow field oblique to the computational grid on the numerical solutions, since the grid orientation problem is mainly introduced by this effect. If a numerical scheme can adapt the computational grid along the streamlines during computational processes, the grid orientation problems can be eliminated completely. However, fluid streamlines in the realistic processes can rapidly vary with time, and the adaptive grid technique is not easy to implement, especially for a complicated flow field. Therefore, numerical techniques with stationary grid are usually employed.

From simple Taylor series truncation analysis, one can show that if the conventional central difference scheme is considered as a standard formula for the convection term, the five-point method (in two-dimensions) with a first-order upwind difference scheme will introduce numerical truncation errors (De Vahl Davis and Mallinson, 1976).

$$E_{err} = \frac{|v_x|\Delta x}{2}\frac{\partial^2 S_i}{\partial x^2} + \frac{|v_y|\Delta y}{2}\frac{\partial^2 S_i}{\partial y^2} \qquad (4.32)$$

where v_x and v_y are thermal and chemical velocities in the x and y directions, respectively. S_i represents the temperature or chemical concentration. The form of Eq. 4.32 is identical to diffusion equation. It produces a contribution to the diffusion of heat or chemical concentration analogous to the physical diffusion of heat transport in an anisotropic media, or the physical dispersion of chemical transport in an isotropic porous media. The coordinate axes of the mesh coincide with the principal axes of diffusion and the principal coefficients are

$$D_x = 0.5|v_x|\Delta x \qquad (4.33)$$

and

$$D_y = 0.5|v_y|\Delta y \qquad (4.34)$$

For uniform mesh size $\Delta x = \Delta y = \Delta$, one can express the numerical diffusion constant in tensor form as

$$D_{num} = 0.5\,\Delta \begin{bmatrix} |v_x| & 0 \\ 0 & |v_y| \end{bmatrix} \qquad (4.35)$$

If the flow field is oblique to the computational grid, the value of numerical diffusion constant in the direction normal to the total velocity is given by (De

Vahl Davis and Mallinson, 1976)

$$D_{num} = \frac{|\overline{V}|\Delta x \ \Delta y \ \sin 2\theta}{\{4(\Delta y \ \sin^3\theta + \Delta x \ \cos^3\theta)\}} \tag{4.36}$$

where $|\overline{V}|$ is the magnitude of total velocity, Δx and Δy are grid block sizes in the x and y directions, respectively, and θ is the angle between the x-axis and the vector of total flow velocity $\overline{V}$.

For $\Delta x = \Delta y = \Delta$, one can obtain

$$D_{num} \approx \frac{\Delta|\overline{V}|\sin 2\theta}{4(\sin^3\theta + \cos^3\theta)} \tag{4.37}$$

When the direction of the fluid velocity is diagonal to the grid ($\theta = 45^0$), $D_{num} \approx 0.354\Delta|\overline{V}|$, and the numerical diffusion reaches a maximum value. On the other hand, $D_{num} = 0$, if the fluid velocity is parallel or perpendicular to the computational grid.

In petroleum engineering, Watts and Silliman (1980) used a physical dispersion model to gain insight into the effects of numerical diffusion errors on the grid orientation problems. For an isotropic porous medium, a physical dispersion model can be expressed as

$$D_{ij} = \alpha_l \ |\overline{V}| \begin{bmatrix} \cos^2\theta & \cos\theta \sin\theta \\ \cos\theta \sin\theta & \sin^2\theta \end{bmatrix} + \alpha_t \ |\overline{V}| \begin{bmatrix} \sin^2\theta & -\cos\theta \sin\theta \\ -\cos\theta \sin\theta & \cos^2\theta \end{bmatrix} \tag{4.38}$$

For uniform grid block size and specific values of θ, one can find α_l and α_t such that $D_{num} = D_{ij}$ (equate Eq. 4.35 to Eq. 4.38), and the results are given

$$\theta = 0, \frac{\pi}{2}, \cdots \alpha_l = 0.5\Delta, \alpha_t = 0,$$

$$\theta = \frac{\pi}{4}, \frac{3\pi}{4}, \cdots \alpha_l = \alpha_t \approx 0.354\Delta$$

Eq. 4.37 also indicates that the thermal or chemical transport processes along the stream line will be impeded by the transverse numerical dispersion, if the computational grid is not aligned with the streamline.

The methods used to reduce the grid orientation effects encountered in modeling multiphase/multicomponent transport processes with high mobility ratios are very extensive. The strategy employed by most methods is to generate more flow channels in the computational domain than those generated by the conventional method (five-point method) such that the accuracy of the calculated flow field (controlled by the parabolic equation) is increased. For example, with a first-order upwind difference scheme, the nine-point method (Yanosik and McCracken, 1978; Coats and Modine, 1983; Potempa, 1985) and the seven-point method (Pruess and Bodvarsson, 1983) were used to reduce the grid orientation effects in enhanced oil recovery processes. However, these methods are not able to reduce numerical diffusion errors (front smearing), which are introduced by the first-order upwind method for hyperbolic equations. Because a mathematical model of transport processes in underground formations becomes more complicated, an appropriate numerical scheme, which can accurately simulate real transport processes without losing physical significance, should be able to avoid both numerical diffusion errors and grid orientation effects.

Recently, Bell and Shubin (1985) have employed a technique consisting of a second-order Godunov method and a nine-point scheme to study miscible displacement with high mobility ratio 41 in porous medium. Their results show

that the numerical diffusion errors and grid orientation effects can be effectively reduced by this numerical scheme. For most of transport processes encountered in hydrothermal reservoir simulations, the mobility ratio usually is very low. Thus, a second-order Godunov method with the five-point scheme employed in this study may be sufficient to overcome those difficulties inherent in the numerical simulations. To demonstrate the capability of the present numerical scheme, the following problems, which are prone to numerical diffusion errors and grid orientation effects, are considered.

4.7.1. Convection with Flow Field Oblique to Computational Grid

To test the present numerical scheme used in this study, the most severe case of numerical diffusion is considered; a computational grid is aligned with streamlines at 45^0. A benchmark problem, that has been extensively used in the literature to test alternative numerical methods, is employed. A schematic illustration of the problem is shown in Figure 4-9. The computational domain is a square with side length of $10m$, which is divided into a 10×10 grid with equal spacing. A steady velocity field is first generated, and the chemical species equation is solved without the diffusion and source terms. Two different constant concentrations, one and zero, are imposed on the left and bottom boundaries, respectively. Since physical diffusion is not considered, a sharp discontinuity should exist along the diagonal line with a concentration of one everywhere above the line, zero everywhere below the line, and the concentration at the line assumed to be 0.5 by averaging the concentrations at the boundaries. However, the use of conventional numerical methods will generate numerical diffusion errors, leading

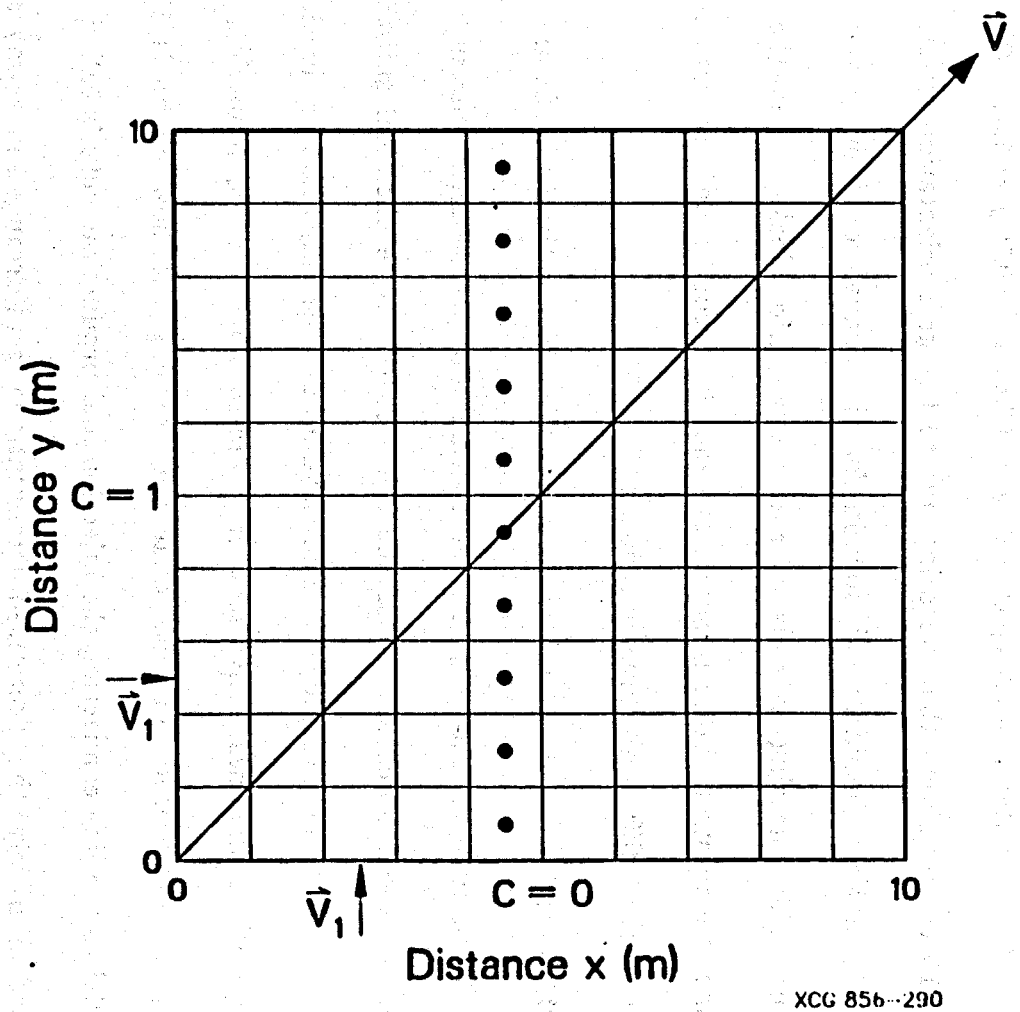

Figure 4-9 Schematic Illustration of a Benchmark Problem for a Flow Field Oblique to the Computational Grid at 45^0.

to a smeared zone along the diagonal line. The extent of this smearing is a measure of the numerical diffusion. The variation of concentration with y at $x = 4.5m$ is presented in Figure 4-10. Due to the finite grid size, one can at best get a linear concentration profile (the solid line in Figure 4-10) defined by the following three points: $y = 3.5m$, $C = 0$; $y = 4.5m$, $C = 0.5$; $y = 5.5m$, $C = 1$. Figure 4-10 clearly shows that smearing due to the grid orientation effects extends over the entire computational domain for the conventional first-order upwind scheme. The smearing extends over only two grid blocks, when the present scheme is employed. Since it possesses generally second-order accuracy in space, the numerical diffusion is greatly reduced.

4.7.2. Chemical Transport Processes in Five-Spot Well Configurations

To improve the recovery of hydrothermal and petroleum resources, the reinjection of spent fluids as well as the injection of active chemical substances or steam are usually employed. The layout of the injection-production well configurations includes a five-spot or seven-spot pattern. In numerical simulations, the discretized computational grid forming the flow channels that are parallel to the line connecting the injection and production wells is called a parallel grid. Similarly, the discretized computational grid arranged in a way that the flow channels are diagonal to the line connecting the injection and production wells is called a diagonal grid. It is known that in reservoir simulations the numerical solutions for miscible displacement with high mobility ratios are strongly dependent on the choice of the grid discretization type, if the five-point method with first-order upwind scheme is used. By comparing the performance

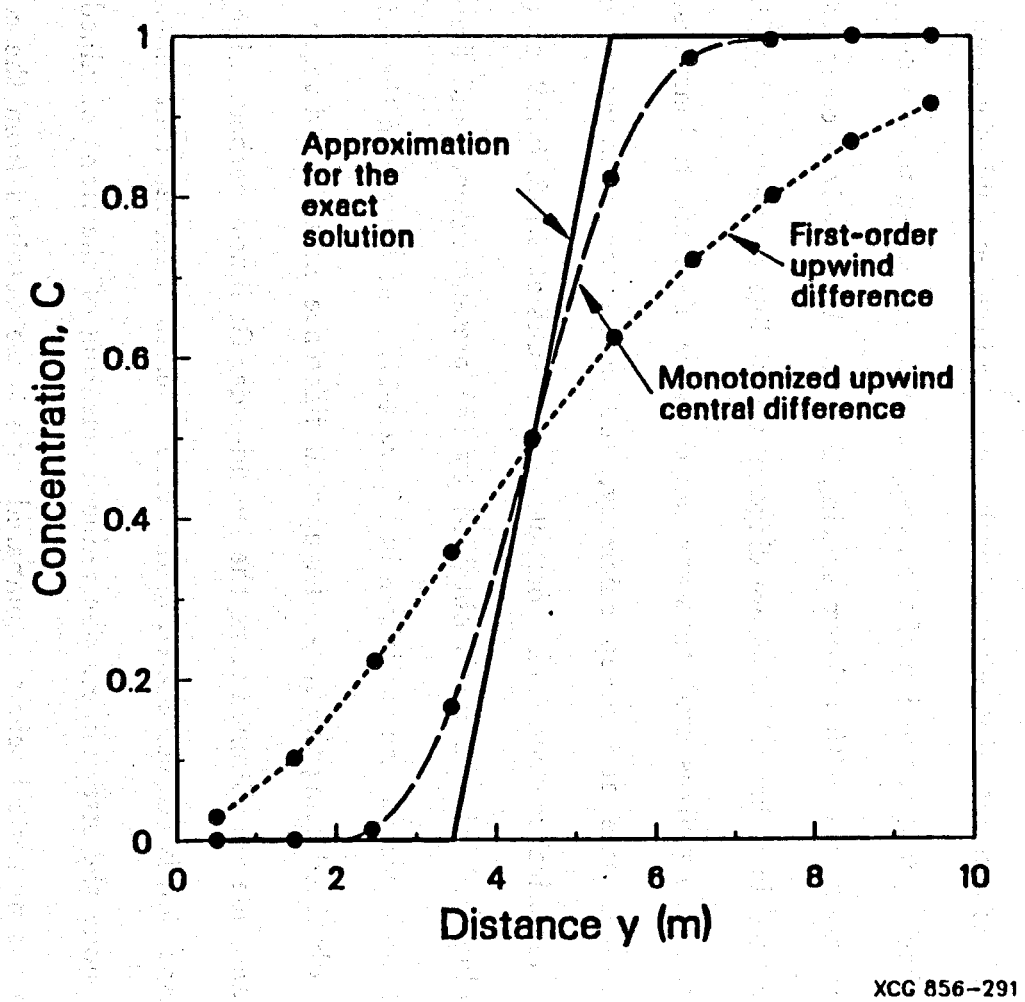

Figure 4-10 Comparison of Numerical Solutions and the Approximate Solution for the Grid Orientation Problem.

between parallel and the diagonal grids, it was found that in general the parallel grid will predict earlier breakthrough of the injected fluid at the production wells while the diagonal grid will indicate greater sweep efficiency in the system.

To verify the present numerical scheme, a problem of the injection-production in a five-spot pattern is considered. The reservoir is initially filled with fluids of concentration equal to unity, and the injected fluid of concentration zero. A basic symmetry region of the five-spot pattern is taken to be $400m \times 400m$, in which 20×20 grid with uniform spacing is used. A discretized computational grid forming flow channels that are diagonal to the line connecting the injection and production wells is used; thus one can compare the computational results of breakthrough time and sweep efficiency, and assess the performance of the present numerical method. The computational results at 0.143, 0.428, and 0.713 pore volume of injected fluids obtained by the present scheme and first-order upwind difference scheme are shown in Figure 4-11. The figures on the left-hand side are obtained using the first-order upwind difference method, and those on the right-hand side are obtained using the second-order Godunov method. Since physical dispersion is not considered in this case, a sharp chemical front should propagate along the streamlines. The reduced smearing of the front obtained from the present numerical scheme, compared with those obtained from the conventional method, is very pronounced.

For comparison purposes, the same problem is solved by the computer code RESSQ (Javandel et al., 1984), which is available to study solute transport in homogeneous porous media under a steady state two-dimensional flow field. The

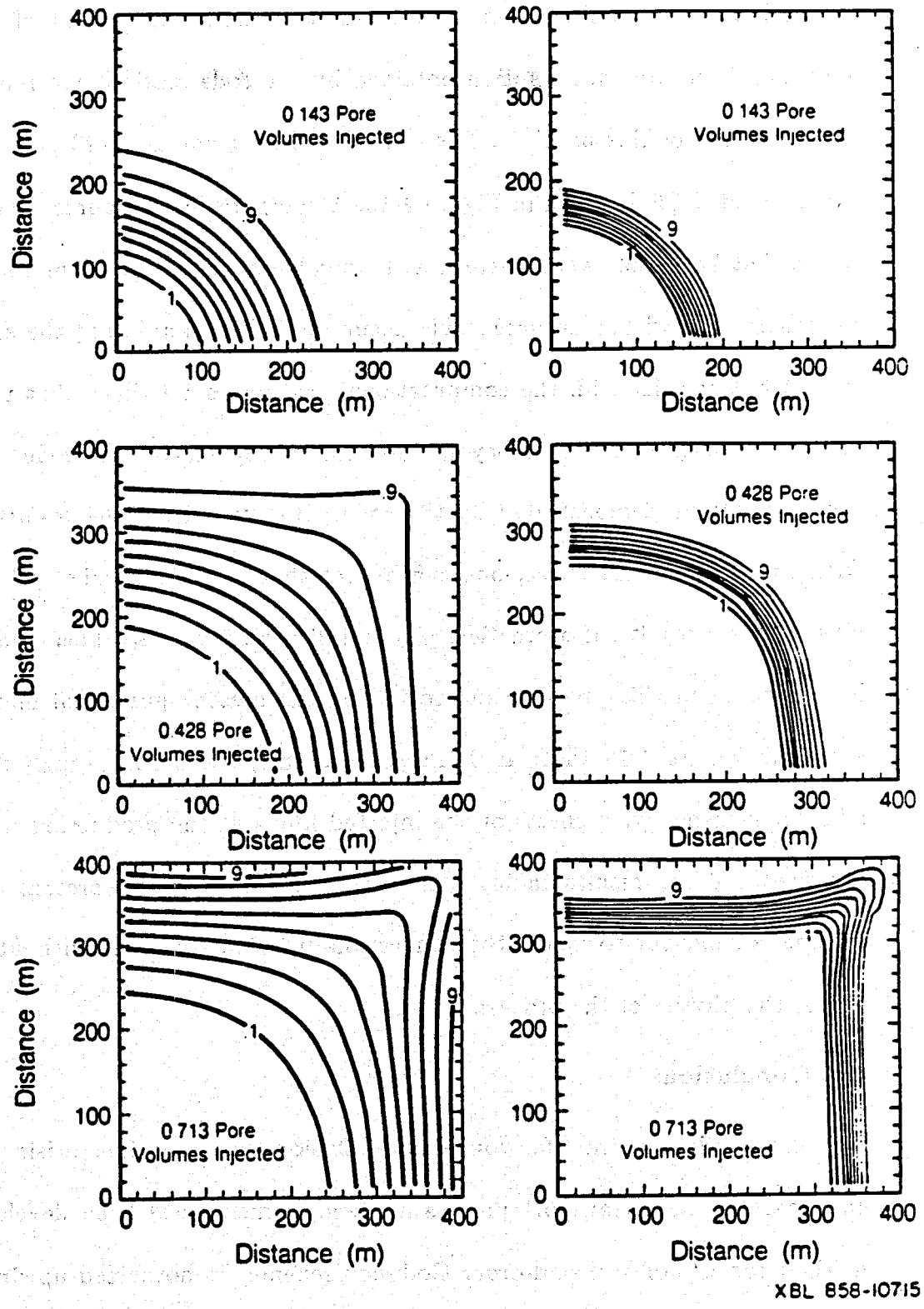

Figure 4-11 Comparison Between Numerical Solutions for Chemical Transport in Injection-Production Wells with a Five-Spot Pattern.

code RESSQ is capable of tracing the concentration of a given solute based on the arrival of streamlines, and gives result without the errors of numerical diffusion. Therefore, the solution obtained by the code RESSQ can represent the exact solution of this problem. The exact chemical front at 0.713 pore volume of the injected fluids is given in Figure 4-12. A comparison of Figures 4-11 and 4-12 shows that both the sweep pattern and front locations using the present numerical scheme are within an acceptable accuracy. When simulating the same problem with a parallel grid, the computational grid needs 1.4 times that used in the diagonal grid case, and it is beyond the storage capacity of the code. Thus, this case can not be demonstrated by the code. However, from the results obtained with the diagonal grid case, one can expect that using a parallel grid will also give accurate results. If a practical physical dispersivity of $\alpha_l = 1.0m$ and $\alpha_t = 0.1m$ is considered in this problem and solved by the present numerical method, it is shown in Figure 4-13 that, at 0.713 pore volume, the breakthrough due to the additional dispersivity effects of the injected fluids at the production well can be observed. These results indicate that the accuracy of the present numerical scheme is sufficient to model the convection-diffusion processes without omitting any of the physics of the process.

4.8. Conclusions

A numerical method for convection-diffusion type equations arising from the chemical and heat transport process in geologic media has been developed. The method consists of a second-order Godunov scheme, monotonized upwind/central differencing, and the operator splitting technique. This numerical method has

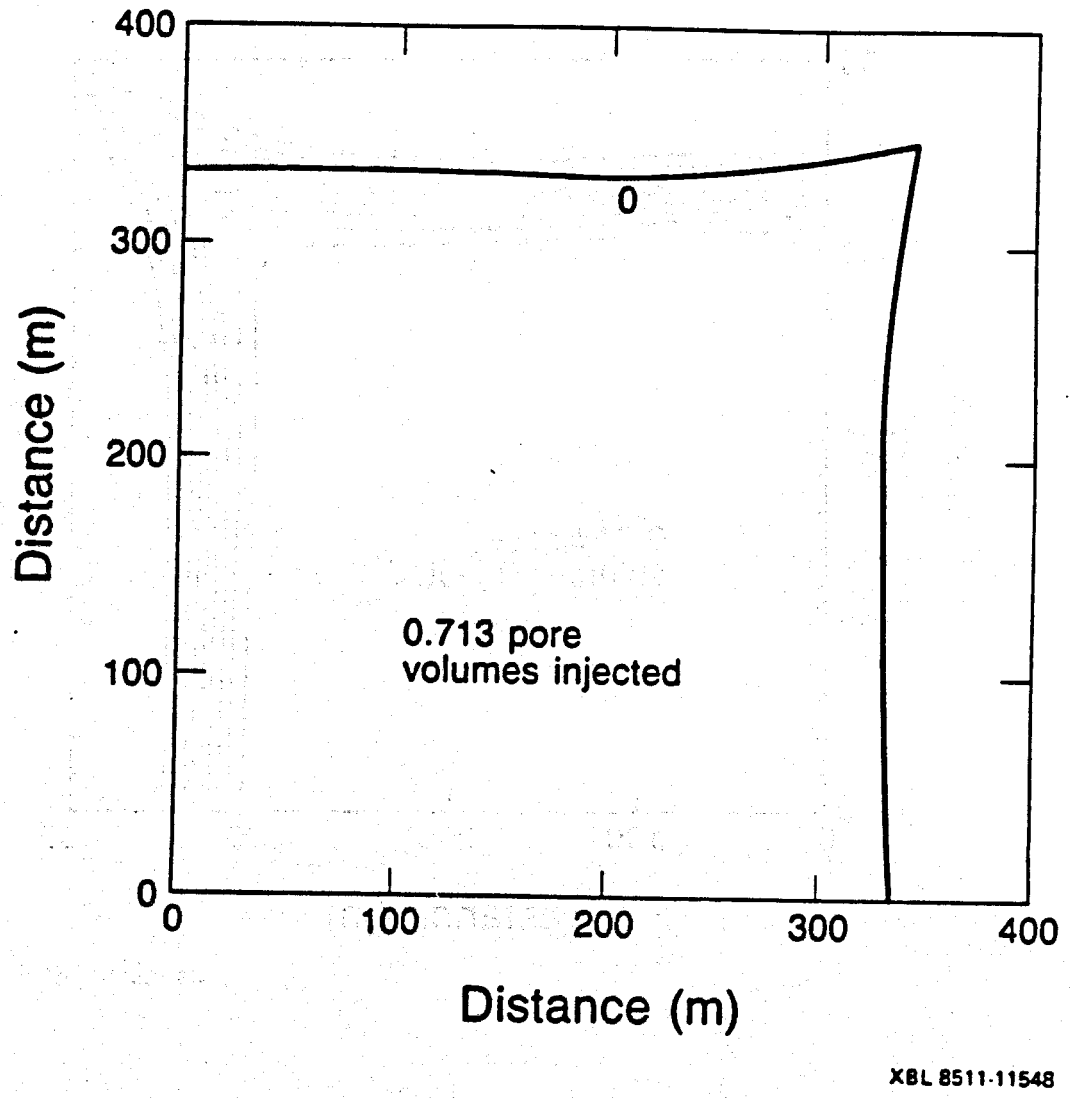

Figure 4-12 Solutions for Chemical Transport in Injection-Production Wells with a Five-Spot Pattern Using the Code RESSQ.

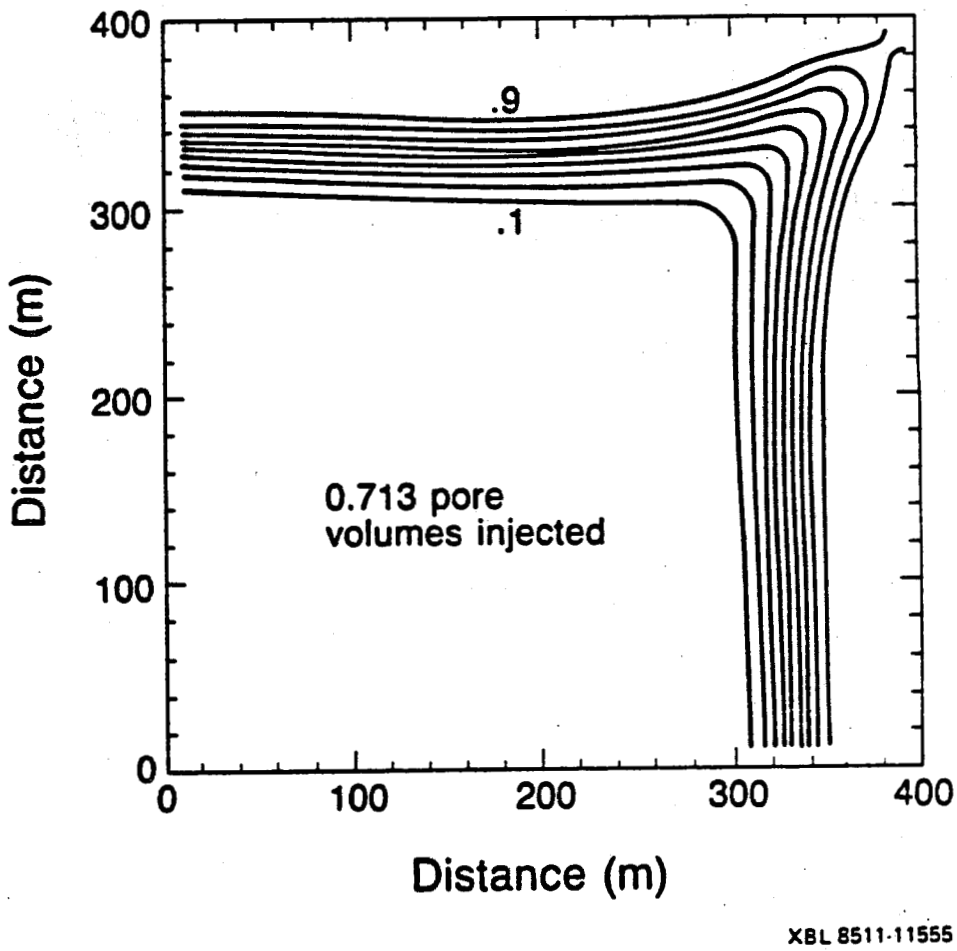

Figure 4-13 Solutions for Chemical Transport in Injection-Production Wells with a Five-Spot Pattern Using a Second-Order Godunov Method (with Physical Dispersions).

been incorporated into a two-dimensional code that is capable of modeling thermal and chemical transport in geologic media. Various test cases have been studied to illustrate the accuracy of the numerical scheme, and the applicability of the code. In contrast to the conventional finite difference method, the present method greatly reduces numerical diffusion errors and gives no oscillations near fronts for high Peclet numbers. In particular, the method significantly reduces grid orientation effects. The results show that the present numerical method is potentially applicable for modeling convection-diffusion transport processes without dramatic loss of the physics of the processes.

CHAPTER 5

APPLICATIONS

5.1. Introduction

As fossil resources are gradually depleted, geothermal energy is being increaingly considered as an important alternative energy source for electrical generation or space heating. For any geothermal reservoir, assessment of the total recoverable energy prior to development and prediction of productivity of the field under exploitation are among the fundamental problems to be considered. In order to facilitate such assessments and predictions, an adequate mathematical model of a geothermal reservoir is needed. Complicated transport phenomena in geothermal reservoirs can be considered as coupled mass and heat transport processes only in a first approximation. Many geothermal fluids, particularly those from liquid-dominated reservoirs, may undergo severe disequilibrium due to temperature and/or pressure changes during the energy extraction processes. As the fluids regain equilibrium, dissolution or precipitation may occur, resulting in significant variations in reservoir properties. Thus, a more appropriate mathematical model of a geothermal reservoir would include coupled mass, heat, and chemical transport processes.

In this chapter, the capability of the computer code PTC (Lai et al., 1985) is demonstrated by applying the code to the following fundamental and practical problems encountered in geothermal reservoirs: (1) natural convection in a porous slab subjected to horizontal temperature differences, (2) coupling effects between

silica precipitation/dissolution and transient flow behavior in a single fracture, and (3) the multicomponent modeling of the Ellidaar geothermal field in Iceland.

Natural convection in porous media has been of some interest to both hydrologists and heat transfer engineers, although for different reasons. The hydrologist is concerned with detailed information about fluid motion and temperature distributions in the system rather than the overall heat transfer behavior which is the concern of the heat transfer engineer. When calculating the rate of heat transfer, the Boussinesq and/or boundary layer approximations are usually employed by the heat transfer engineer to simplify the problem. However, these approximations may not be valid, if details of fluid motion and temperature distributions are needed. Studies of the effects of these simplified approximations on fluid motion, temperature distributions, and overall heat transfer behavior in a natural convection problem in a porous slab subjected to horizontal temperature differences are presented in section 5.2.

Since silica is a common constituent in the earth's crust, and is frequently found in geothermal brines at concentrations sufficient to form scaling or precipitates upon cooling, many hydrothermal exploitation models must consider reactive silica transport. For example, Truesdell et al. (1984) pointed out that localized aquifer boiling causes quartz precipitation near wells at the Cerro Prieto geothermal field, Mexico. Boiling causes a temperature decline, and a consequent decrease in quartz solubility. Also, separation of steam from the produced fluids can increase quartz concentration in the residual fluids. Under such circumstances, quartz will precipitate after a concentration reaches a high degree of

supersaturation, which results in reductions of the permeability and mass flow rate. Another example is silica scaling during reinjection operations. Reinjection is often employed to enhance the total energy from the system and to prevent chemical contamination of the environment by surface disposal. However, the spent brine is often cooled below the saturation temperature, causing silica deposition in the surface pipelines, the disposal well or within the reservoir rock itself. If scaling occurs around the wellbore, permeabilities will be reduced and the injectivity of the well will decrease.

To investigate these adverse effects of silica reactions on geothermal systems, Keith et al. (1983) conducted an experiment involving nonisothermal flow of supersaturated silica fluid through Westerly and Barre granite. Their experimental results confirm that silica precipitation is responsible for reductions in permeability, porosity and flow rate. Itoi et al. (1984) also performed an experimental study involving near-isothermal flow of geothermal fluid with supersaturated silica through a porous medium column. Their experimental results show that the silica is deposited mainly in the region near the entry of the fluid in the column, resulting in drastic permeability reduction. Lai et al. (1985) conducted numerical simulations of silica precipitation to study the effects of silica deposition on permeability and flow rate variations in a single fracture system. They also applied a reactive silica transport model to the Ellidaar geothermal field in Iceland to evaluate properties of the reservoir and its connection with adjacent geologic formations. The results will be presented in sections 5.3 and 5.4.

5.2. Natural Convection in a Porous Slab

In this section, two-dimensional free convection in a porous slab is considered. A schematic illustration of the problem is shown in Figure 5-1. The porous slab is bounded by adiabatic horizontal walls and isothermal vertical walls at different temperatures, T_H and T_C, respectively. All boundaries are assumed impermeable to the fluids. The problem is to determine the flow and temperature fields, and overall heat transfer behavior in the system at steady state. For natural convection problems, the exact governing equations are very difficult to solve by exact analytical means. Some approximations are needed, the simplest one is the Boussinesq approximation which assumes all fluid properties are constant, except that fluid density varies linearly with temperature in the buoyancy force term (Eqs. 5.3 and 5.5). Under this approximation, the governing equations for the problem can be simplified as

$$\frac{\partial v_x}{\partial x} + \frac{\partial v_y}{\partial y} = 0 \tag{5.1}$$

$$v_x = -\frac{k}{\mu}\frac{\partial P}{\partial x} \tag{5.2}$$

$$v_y = -\frac{k}{\mu}\left(\frac{\partial P}{\partial y} + \rho_f\, g\right) \tag{5.3}$$

$$v_x \frac{\partial T}{\partial x} + v_y \frac{\partial T}{\partial y} = \frac{K_h}{\rho_f\, c_f}\left(\frac{\partial^2 T}{\partial x^2} + \frac{\partial^2 T}{\partial y^2}\right) \tag{5.4}$$

and

$$\rho_f = \rho_{ref}\,[\,1 - \beta\,(T - T_{ref})\,] \tag{5.5}$$

where T_{ref} is the referenced temperature, and ρ_{ref} is the fluid density at T_{ref}.

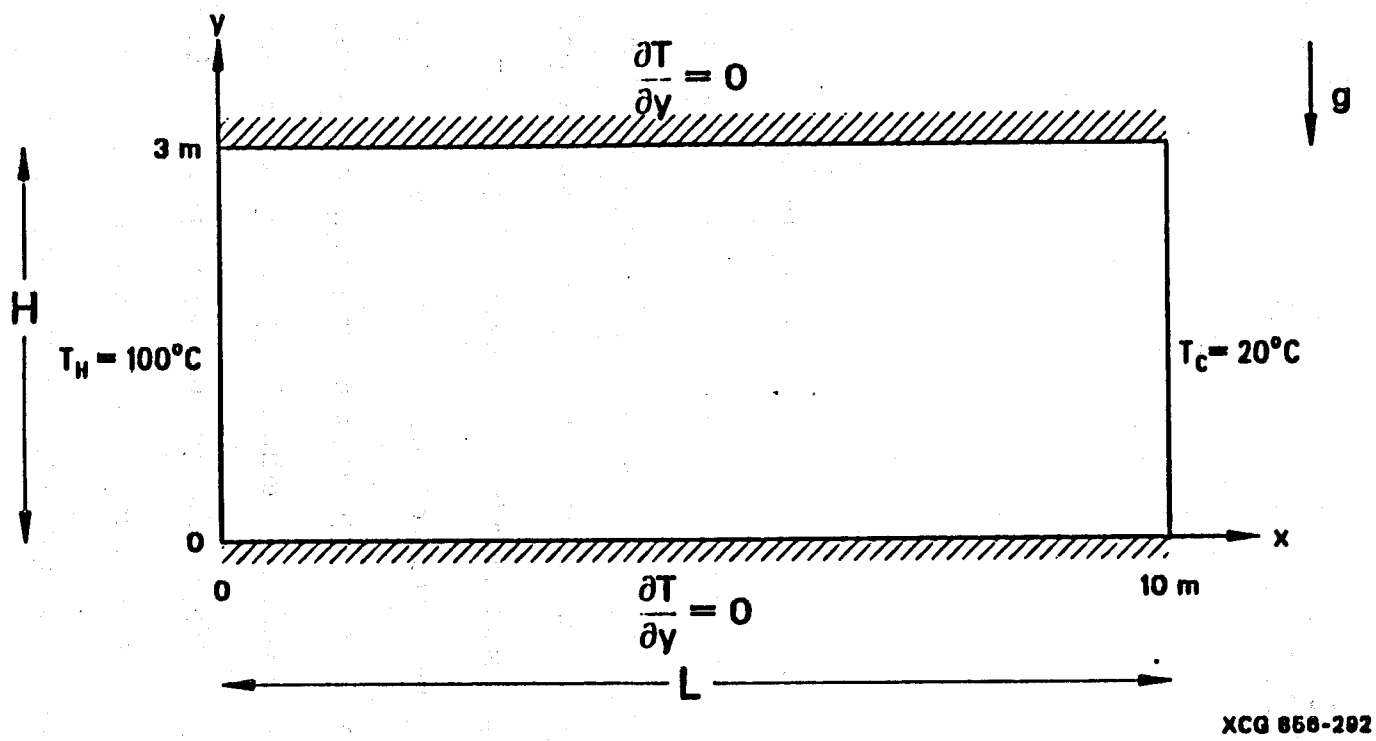

Figure 5-1 The Rectangular Porous Slab Considered for the Natural Convection Problem.

It should be noted that the Boussinesq approximation is valid if the temperature difference $\Delta T = T_H - T_C$ is sufficiently small; however, this is often violated in practice because the variation of fluid viscosity with temperature is very rapid.

Gray and Giorgini (1976) developed a method allowing the specification of the conditions under which the Boussinesq approximation applies to a given Newtonian fluid. To consider the effects of a temperature dependent viscosity on free convection in a porous slab, Weber (1975) used an averaged value of the viscosity for the hot and cold wall boundary layers, respectively. Blythe and Simpkins (1981) developed a method to take into account any variations of the viscosity with temperature, and the results are given for the case of a linear viscosity-temperature relation since complicated viscosity-temperature relations make the computational procedure complicated. The errors introduced by their method are those associated with the choice of velocity profiles in the boundary layers. This same problem, including the effects of temperature and pressure on fluid properties (density, viscosity, expansivity, and compressibility) are investigated; that is, the full governing equations 3.10, 3.16, and 3.18 are solved without the Boussinesq and boundary layer approximations.

With the Boussinesq approximation, numerical solutions for this type of problem have been obtained by Bankvall (1974), Burns et al. (1977), Hickox and Gartling (1981), and Dawson and McTigue (1985). Bejan and Tien (1978) developed an analytical technique to obtain the approximate solutions. To verify the numerical code, Hickox and Gartling compared their numerical results with those obtained by using the approximate analytical solutions. Both numerical and

approximate analytical solutions agree well. All of these workers have shown that the solutions of this problem depend on the aspect ratio and the Rayleigh number.

Without the Boussinesq approximation, the solution will also depend on the temperature range considered, and in some cases on pressure as well. The emphasis in the present study is to further test the numerical code for this non-linear problem under a complicated flow field rather than to make an extensive investigation of heat transfer. Therefore, only a single value of the aspect ratio, $H/L = 0.3$, and constant temperatures of $100\,^{\circ}C$ and $20\,^{\circ}C$ on the vertical walls are used. This aspect ratio was chosen to compare our results with those obtained by Hickox and Gartling (1981) and Dawson and McTigue (1985). The large temperature difference between the vertical walls allows one to test the effect of the Boussinesq approximation on the heat transport process in the system. Values of the parameters used in this problem are given in Table 5-1.

Table 5-1: Input parameters for natural convection problem

Slab height:	3 m
Slab length:	10 m
Effective thermal conductivity:	2 $W/(m \cdot {}^{\circ}K)$
Porosity:	0.1
Specific heat of water:	4184 $J/(kg \cdot {}^{\circ}K)$
Specific heat of rock:	1000 $J/(kg \cdot {}^{\circ}K)$
Rock expansivity:	0 ${}^{\circ}K^{-1}$
Rock compressibility:	0 Pa^{-1}

The computational domain is divided into a 20×12 grid. In order to obtain accurate results, a finer mesh is used near the vertical walls where temperature gradients are steep (Figure 5-2). Calculations have been made for a wide range of Rayleigh numbers, which are calculated using the fluid properties evaluated at the mean temperature (60 ${}^{\circ}C$) and 1 atmosphere pressure from

$$Ra = \left(\frac{\beta c_f \rho_f^2}{\mu}\right)_m \frac{gHk}{K_h}(T_H - T_C) \tag{5.6}$$

Different values of Rayleigh numbers are calculated by changing the permeability in Eq. 5.6; all other parameters are unchanged. For example, for a Rayleigh number of 25, the values of β, ρ_f, c_f, and μ are provided (Batchelor, 1979), and then a permeability of $4.81 \times 10^{-12} m^2$ is obtained. Figures 5-3a to 5-4d show the mass flux and the temperature distributions, respectively, for different Rayleigh numbers. The general pattern of circulation due to the buoyancy forces

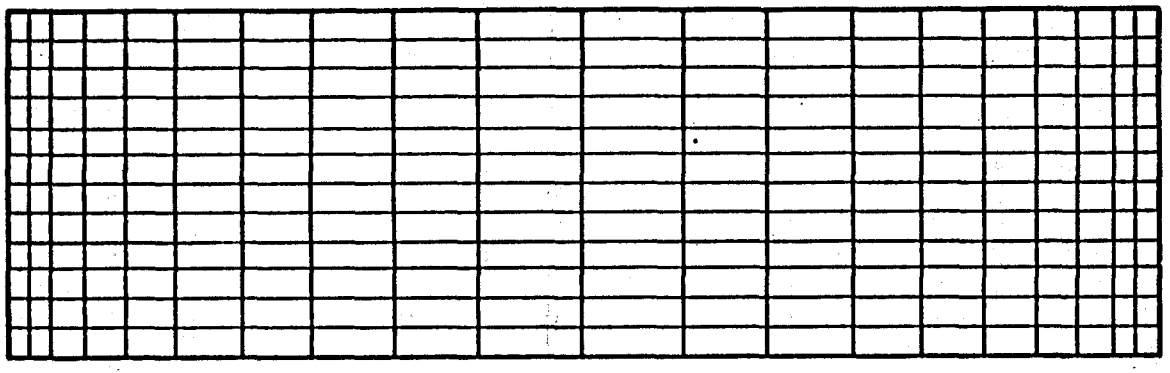

XBL 856-10537

Figure 5-2 The Computational Mesh Used in the Natural Convection Problem.

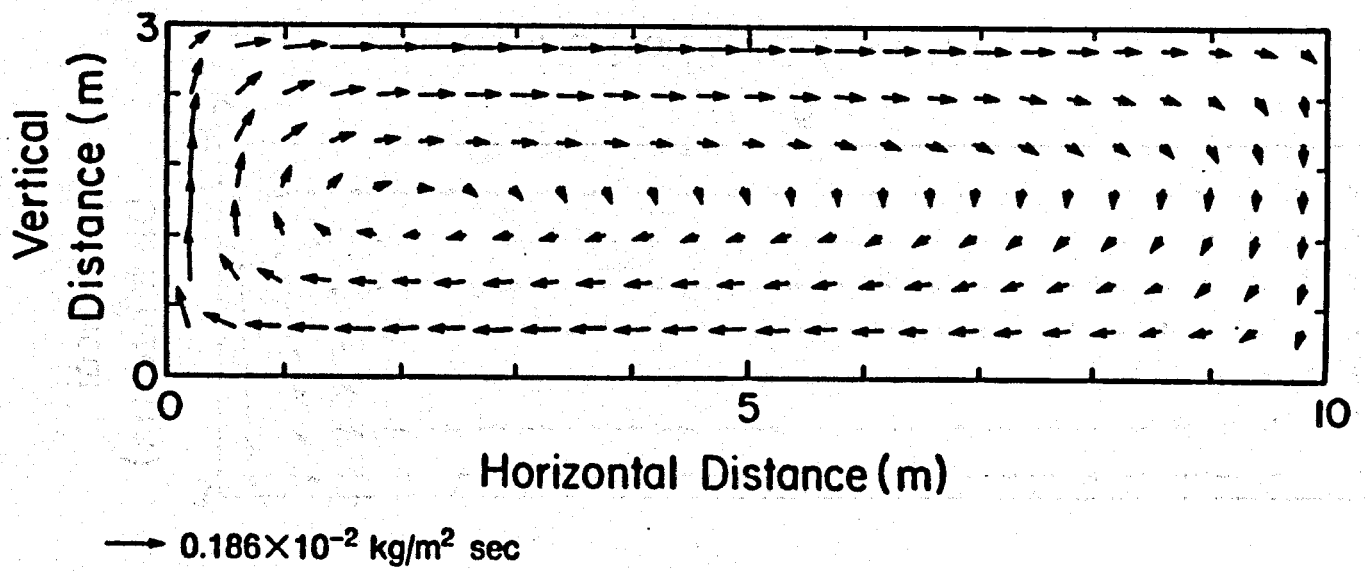

XBL 856-10531

Figure 5-3a The Distribution of Mass Flux in the Porous Slab for Rayleigh Number of 25.

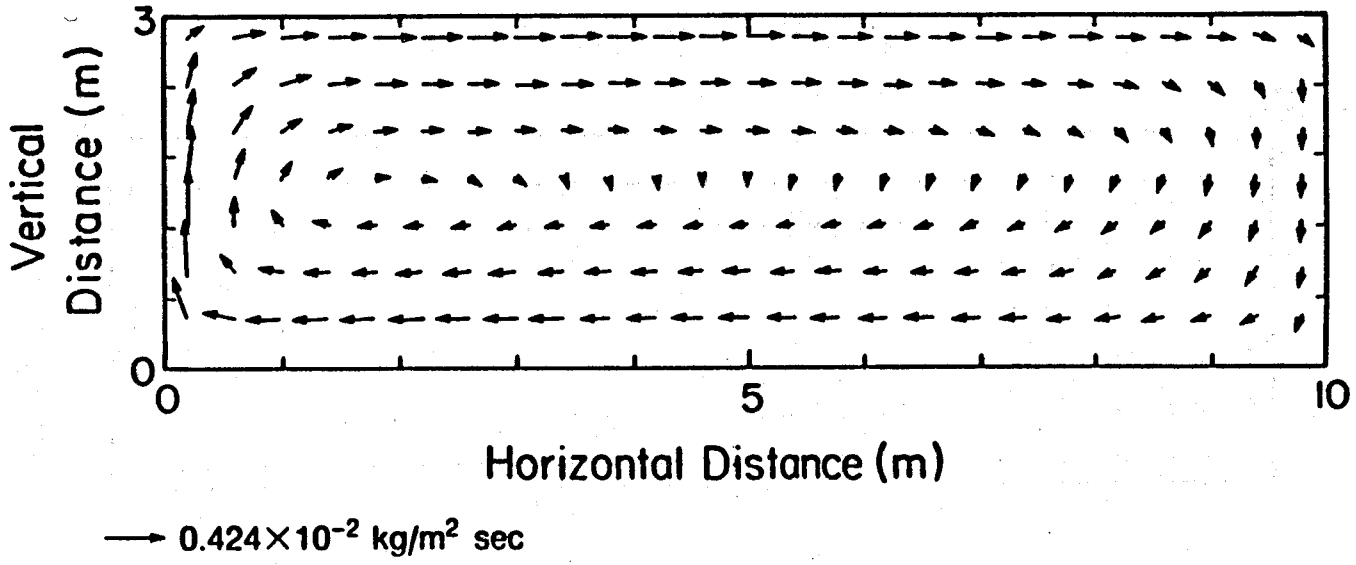

XBL 856-10532

Figure 5-3b The Distribution of Mass Flux in the Porous Slab for Rayleigh Number of 50.

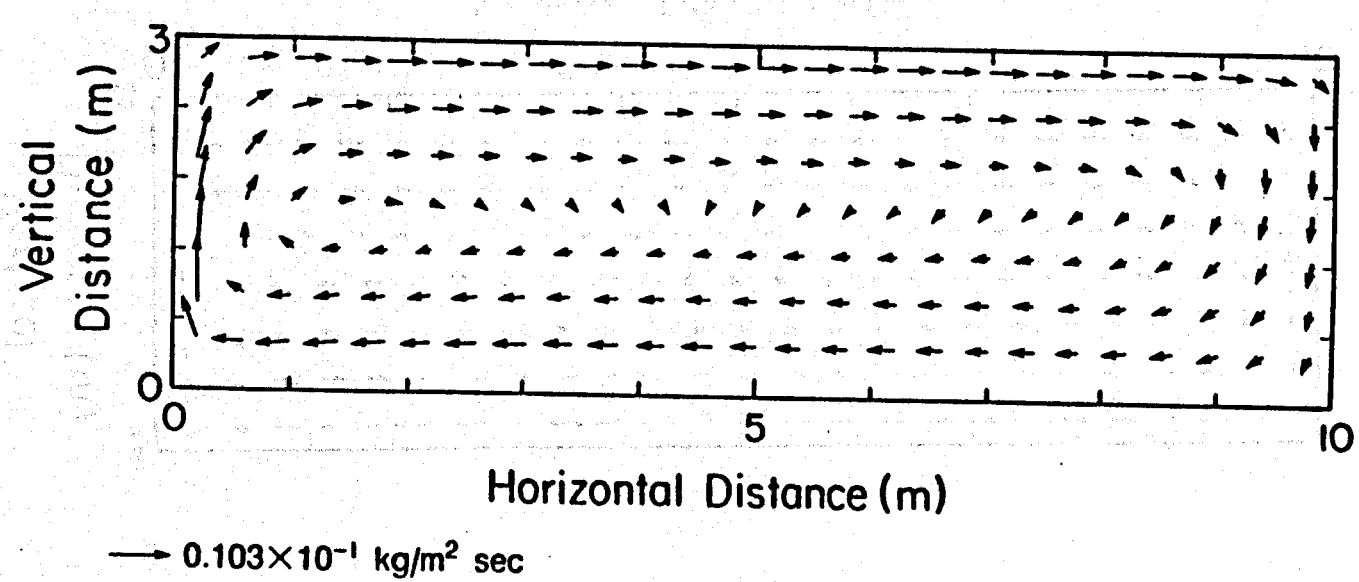

Figure 5-3c The Distribution of Mass Flux in the Porous Slab for Rayleigh Number of 100.

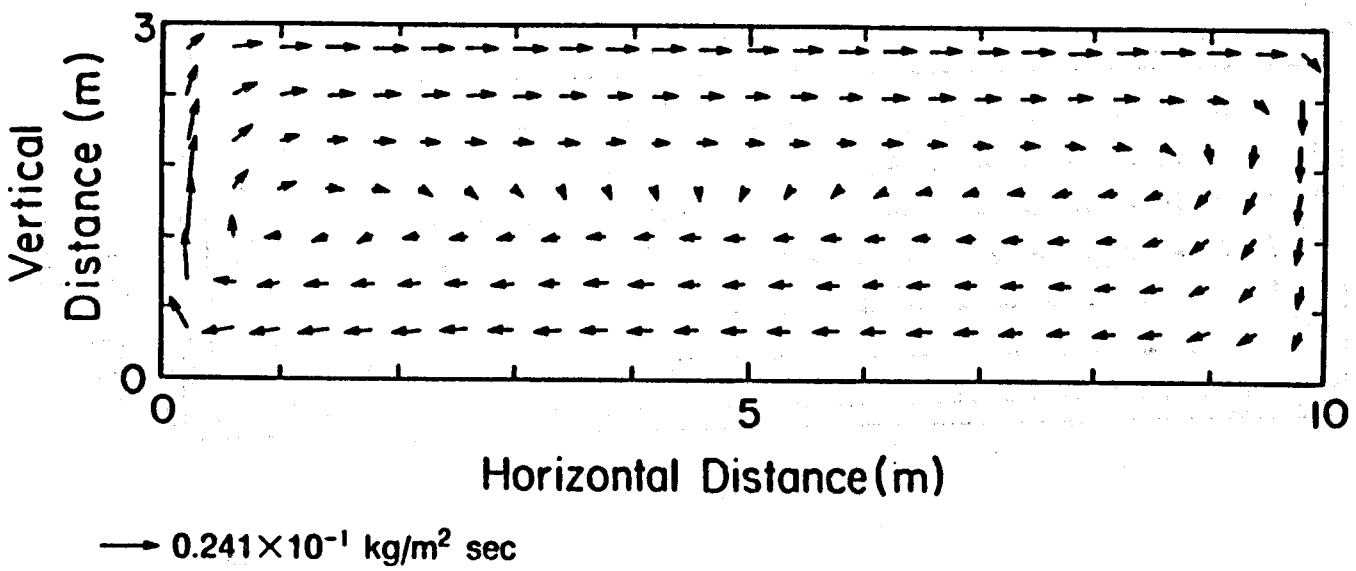

XBL 856-10533

Figure 5-3d The Distribution of Mass Flux in the Porous Slab for Rayleigh Number of 200.

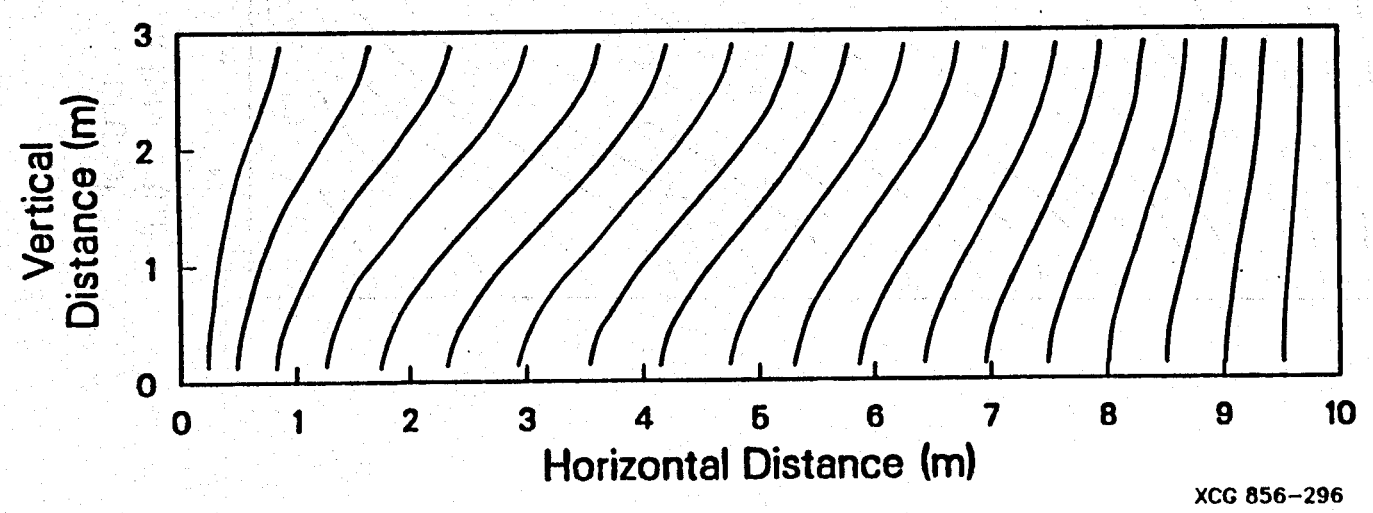

Figure 5-4a The Distribution of Isotherm Contours in the Porous Slab for Rayleigh Number of 25.

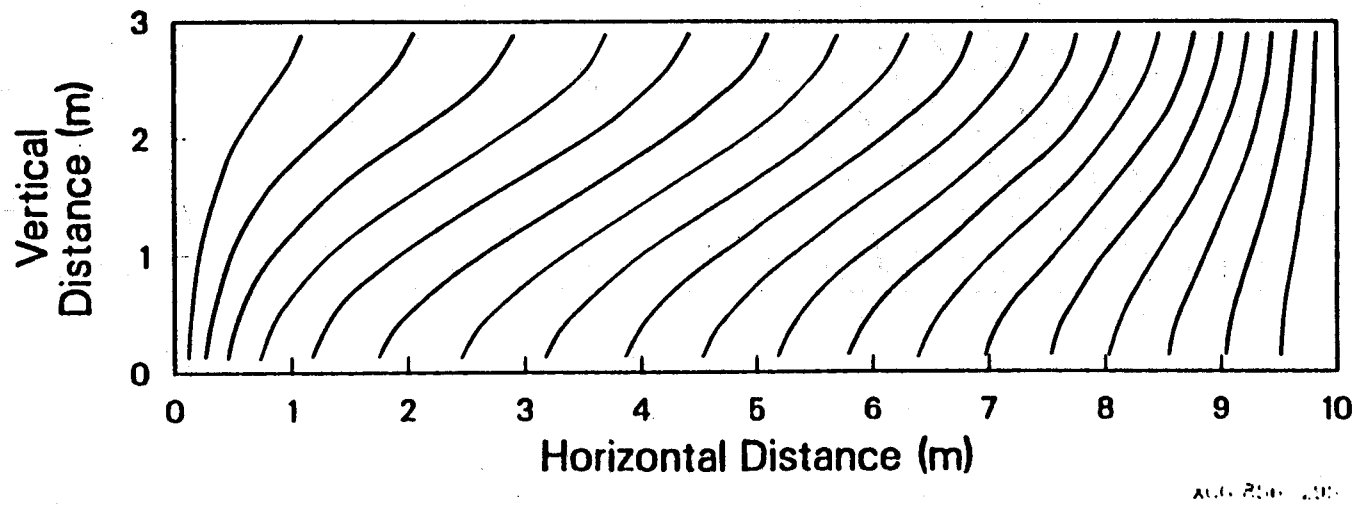

Figure 5-4b The Distribution of Isotherm Contours in the Porous Slab for Rayleigh Number of 50.

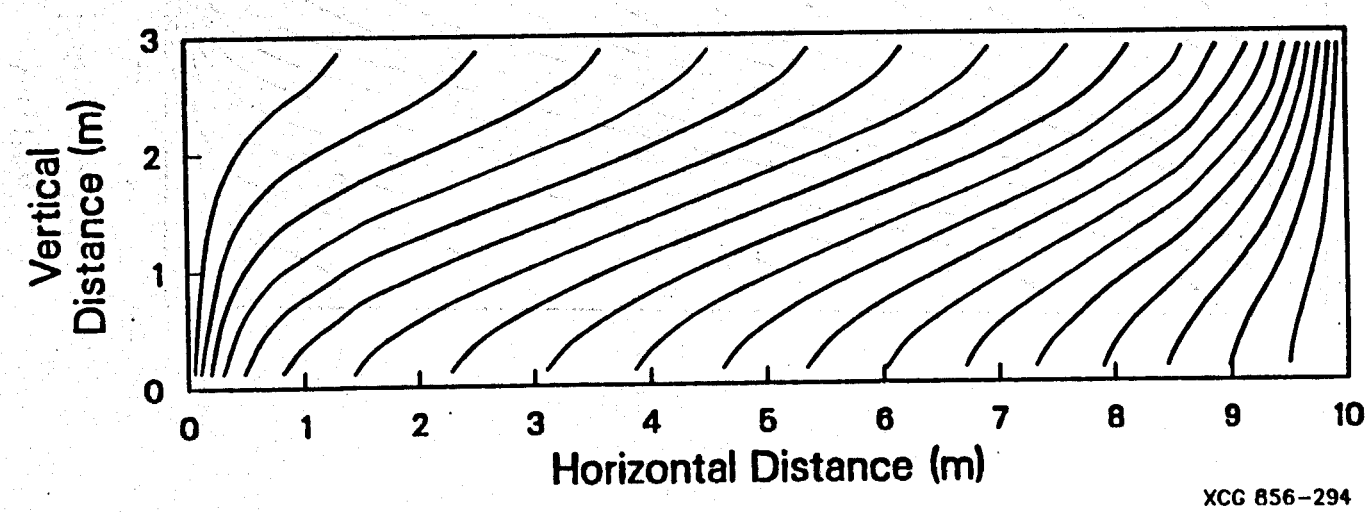

Figure 5-4c The Distribution of Isotherm Contours in the Porous Slab for Rayleigh Number of 100.

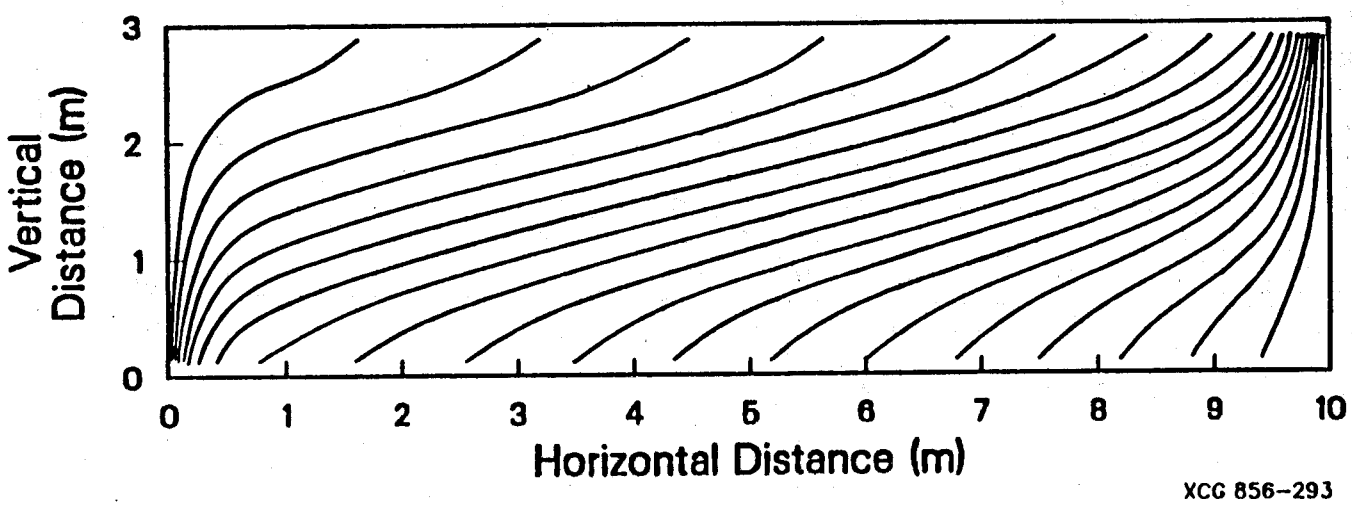

Figure 5-4d The Distribution of Isotherm Contours in the Porous Slab for Rayleigh Number of 200.

that develop is as expected, but it is interesting to observe the flow field as fluid properties change with temperature and pressure. Because the fluid viscosity is about four times lower while the fluid thermal expansivity is three times higher near the hot wall than near the cold wall, the Raleigh number near the hot wall is about twelve times that near the cold wall. The combined effects of the fluid viscosity and thermal expansivity can strongly enhance the buoyancy forces, and thus the mass flux near the hot wall. Figures 5-3a to 5-3d show that the mass flux is always the highest near the hot wall, lowest near the cold wall and has intermediate values near the upper horizontal wall when the Rayleigh number is 100 or less. However, the mass flux is the lowest near the lower horizontal wall when the Rayleigh number is equal to 200. This result also indicates that the driving force of the convection cell is more dominated by the hot wall. Note also how the isotherms in Figures 5-4a to 5-4d are farther away from the hot wall than from the cold wall. These asymmetric distributions would not be predicted by methods that use the Boussinesq approximation. As the Rayleigh numbers increase, the asymmetry becomes even more pronounced. This implies that the effects of temperature and pressure dependent fluid properties on the transport process are significant, so that they must be considered in transport process with high Rayleigh numbers.

To evaluate the rate of heat transfer, one must calculate the Nusselt numbers given by

$$Nu = \frac{Q_A L}{K_A H (T_H - T_C)} \tag{5.7}$$

where Q_A is the total heat flow rate per unit thickness of the slab. The Nusselt

numbers obtained from this study are very close to those obtained by Hickox and Gartling (1981) and Dawson and McTigue (1985), as shown in Table 5-2.

Table 5-2: Nusselt number as a function of Rayleigh number for aspect ratio of 0.3

Source	Rayleigh Number			
	25	50	100	200
Hickox and Gartling (1981)	1.26	1.84	3.45	7.17
Dawson and McTigue (1985)	1.27	1.87	3.46	6.64
This work	1.28	1.85	3.29	6.43

For Rayleigh numbers below 50, the difference is less than 2%, which is expected because convection is not strong at low Rayleigh numbers. Consequently, for these cases the Nusselt number for the overall heat transfer behavior of the system is not strongly affected by the Boussinesq approximation. At higher Rayleigh numbers, the difference between our results and those obtained by the earlier investigators is more pronounced; the largest difference is 11% for a Rayleigh number of 200.

5.3. Reactive Silica Transport in a Single Fracture

Current experience with geothermal injection indicates that silica scaling is a widespread concern. Since silica is slow to respond to physical or chemical variations of geothermal fluids, the processes of its precipitation/dissolution rates are controlled by reaction rates so that they can only be understood in terms of a

kinetics model rather than an equilibrium one.

5.3.1. Kinetic Model of Silica-Water Reactions

The kinetics of quartz dissolution in water has long been investigated, and Robinson (1982) provides a survey of this subject. The experimental results have shown that in general the kinetic rate obeys the following relation

$$\frac{dC}{dt} = \underline{k}\,\frac{A_r}{M_r}(C_{eq} - C) \tag{5.8}$$

where $\underline{k}$ is a kinetic rate constant, $\frac{A_r}{M_r}$ is the ratio of quartz surface area to fluid mass, C_{eq} is the equilibrium concentration of dissolved silica. Rimstidt and Barnes (1980) derived this equation from absolute theory, however, Robinson (1982) pointed out that it is best to consider the rate law to be semi-empirical. To model the coupling effects between silica precipitation and transient flow behavior, the kinetics of silica-water reactions proposed by Rimstidt and Barnes (1980) is employed in the simulator PTC. To calculate the silica-water reactions, one can evaluate $\underline{k}$ and C_{eq} from the data compiled by Rimstidt and Barnes (1980). Table 5-3 shows their results for the solubility of different silica phases as a function of temperature.

Table 5-3: The Equilibrium Constants for Silica-Water Reactions

$$SiO_2(s) + 2H_2O(l) = H_4SiO_4(aq)$$

$$\log \underline{K} = a + bT + c/T \quad (T \text{ in } {}^{\circ}K)$$

Silica Phase	a	b	c
Quartz	1.881	-2.028×10^{-3}	-1560.0
α -Cristobalite	-0.032	0	-988.2
β -Cristobalite	-0.256	0	-793.6
Amorphous Silica	0.338	-7.889×10^{-4}	-840.1

Table 5-4 shows the best fits for the rate constants for silica-water reactions as a function of temperature that were obtained by Rimstidt and Barnes (1980). The rate constants for silica precipitation and dissolution are given by

$$\log \underline{k} = a + bT + c/T \tag{5.9}$$

Table 5-4: The Rate Constants for Silica-Water Reactions

Silica Phase	a	b	c	Processes
All Silica Phases	-0.707	0	- 2598	Precipitation
Quartz	1.174	-2.028×10^{-3}	-4158	Dissolution
α -Cristobalite	-0.739	0	-3586	Dissolution
β -Cristobalite	-0.963	0	- 3392	Dissolution
Amorphous Silica	-0.369	-7.89×10^{-4}	3438	Dissolution

For single fractures, the value of reaction parameters (A_r/M_r) can easily be obtained from fracture geometry as

$$\frac{A_r}{M_r} = \frac{2}{b\,\rho_f} \tag{5.10}$$

where b is the fracture aperture and ρ_f is fluid density.

The permeability of a single fracture is assumed to be governed by the cubic law (Witherspoon et al., 1980). In numerical calculations, Eq.5.8 is treated as the source term, which is needed in the second step of the splitting scheme.

5.3.2. Effects of Silica Deposition on Transient Flow Behavior

The problem considered is that of a 50 m long fracture with an initial aperture of 10^{-4} m. Initially, the fracture contains 100 $^{\circ}C$ fluid, with an equilibrium concentration of 142 ppm. In the numerical work, the computational domain is divided into constant volume grid blocks, with a nodal spacing of 0.5 m.

The isothermal problem of the injection of 100^0 C water supersaturated with 522 ppm of α-cristobalite is considered. The results of numerical calculations are

shown in Figures 5-5 through 5-7. Figure 5-5 shows that the concentration front moves at a rate of approximately 0.3 m/day, with silica scaling occurring behind the front. The silica deposition causes reduction in the permeability, with the most severe reduction close to the inlet. We approximate the permeability changes from the aperture reduction and cubic law (Witherspoon et al., 1980). The rate of silica deposition increases with time because the surface area to fluid mass factor ($\frac{A_r}{M_r}$) increases as the aperture decreases. This causes rapid permeability reduction close the inlet at later times, and results in a small decrease in the concentration profile along the fracture.

Figure 5-6 shows a similar case, but with twice the initial flow rate. As expected, the speed of the concentration front is approximately double that of the first case, resulting in a more rapid permeability decline close to the inlet.

Figure 5-7 shows the flow rate decline for both cases. The mass flow rate at the entrance is represented by the dimensionless variable Q/Q_i, where Q_i is the initial mass flow rate at the entrance. Figure 5-7 shows that the higher the initial flow rate at the inlet, the faster the dimensionless mass flow rate will decline because of greater silica precipitation. Qualitatively speaking, the effects of silica deposition on the transient flow behavior demonstrated by the numerical results are similar to those observed in the experimental study of Itoi et al (1984).

In order to investigate the coupling between mass and heat flow and silica transport processes, we next consider a problem with non-isothermal effects. For this case, the fracture fluid initially contains 150 $^\circ C$ water with a silica concentration of 257 ppm (equilibrium value for α-cristobalite). Then 100 $^\circ C$ water

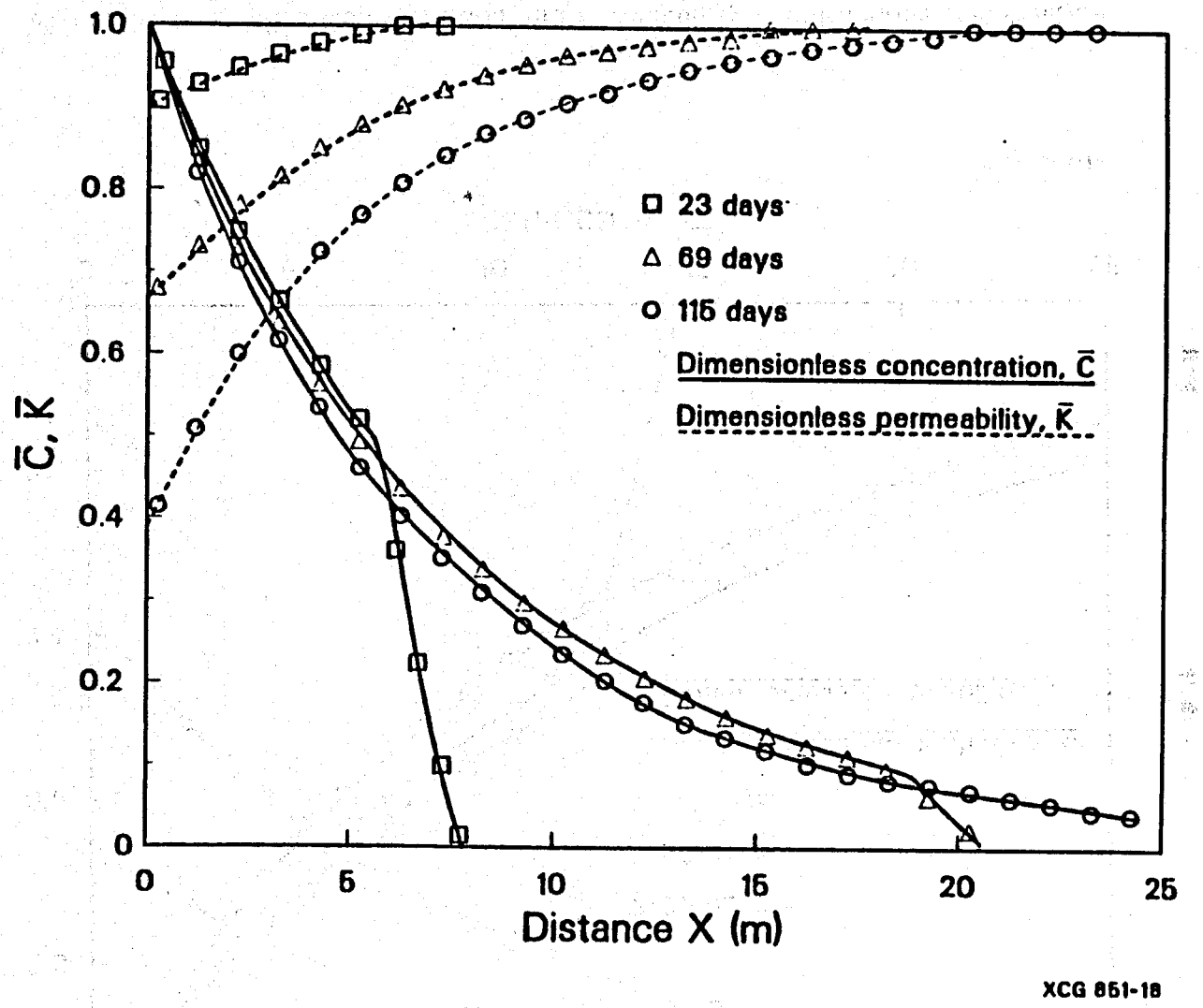

Figure 5-5 Silica Concentration and Permeability Profiles along the Fracture for the Low Pressure Drop Case.

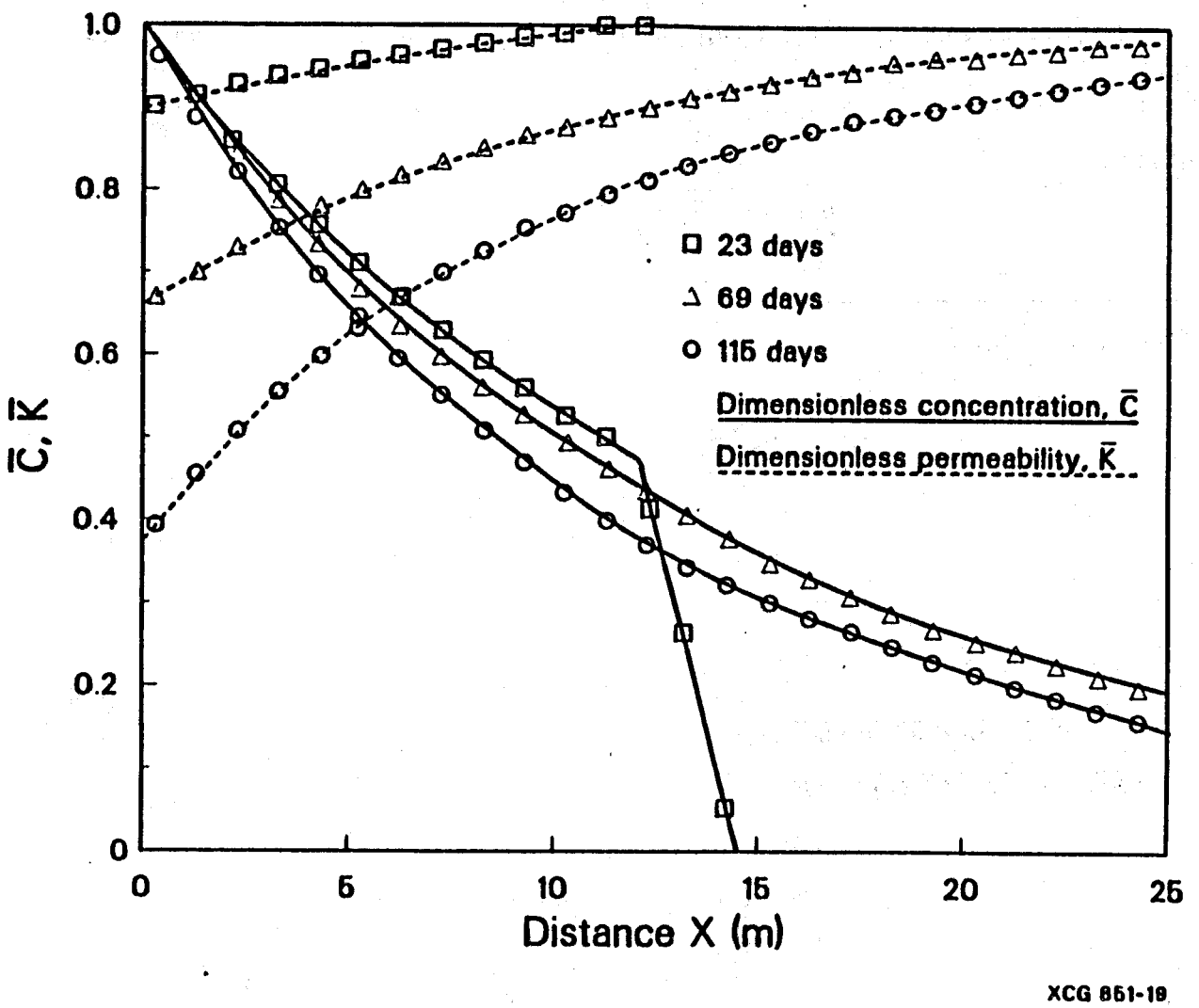

Figure 5-6 Silica Concentration and Permeability Profiles along the Fracture for the High Pressure Drop Case.

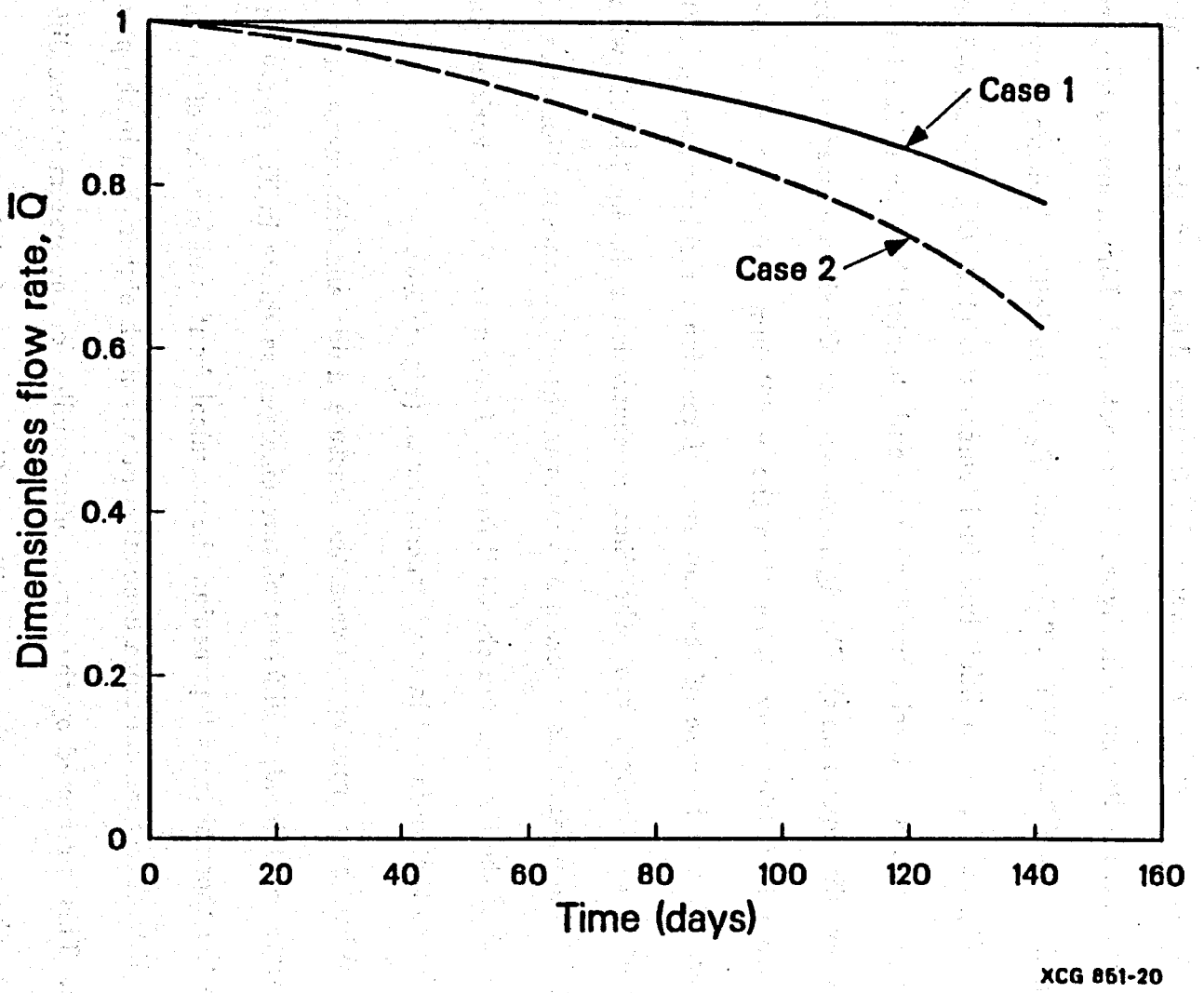

Figure 5-7 Flow Rate Declines along the Fracture under Isotherm Conditions for Low Pressure Drop (Case 1) and High Pressure Drop (Case 2).

supersaturated with silica (522 ppm) enters the fracture at the inlet. Two cases are considered: (i) no heat losses to surroundings, and (ii) conductive heat transfer from the rock matrix to the fracture.

When heat transfer between the fracture fluids and the rock matrix is ignored, the results shown in Figure 5-8 are obtained. Dimensionless temperature is defined as $(T-T_0)/(T_b-T_0)$, where T_0 is the initial fracture temperature (150 $^\circ C$) and T_b is the inlet fluid fluid temperature (100 $^\circ C$). Figure 5-8 shows, as expected, that the velocities of thermal and chemical fronts are identical (fracture porosity equals unit). The figure shows that the silica concentration behind the front is considerably higher than the equilibrium concentration for 100 $^\circ C$ water. This is because of the slow rate of reaction for silica-water at 100 $^\circ C$. Ahead of the thermal front, the silica concentration is in equilibrium with the 150 $^\circ C$ water, and this causes a minimum in the silica concentration close to the location of the thermal and chemical fronts. The permeability at various times is similar to that obtained in the isothermal case (Figure 5-5).

When heat transfer between the fracture fluids and the surrounding rock matrix is considered, a different picture emerges, as shown in Figure 5-9. In this case the thermal front lags behind the chemical front, and because of the higher overall temperature, the silica deposition rate is much higher than in the previous case. This is reflected by the permeability profiles for the system at two different times. The plateau in the permeability profiles close to the inlet is due to the coupling between the temperature and the silica reaction rate. Although the deposition rate reaches a maximum value at different times depending on the distance

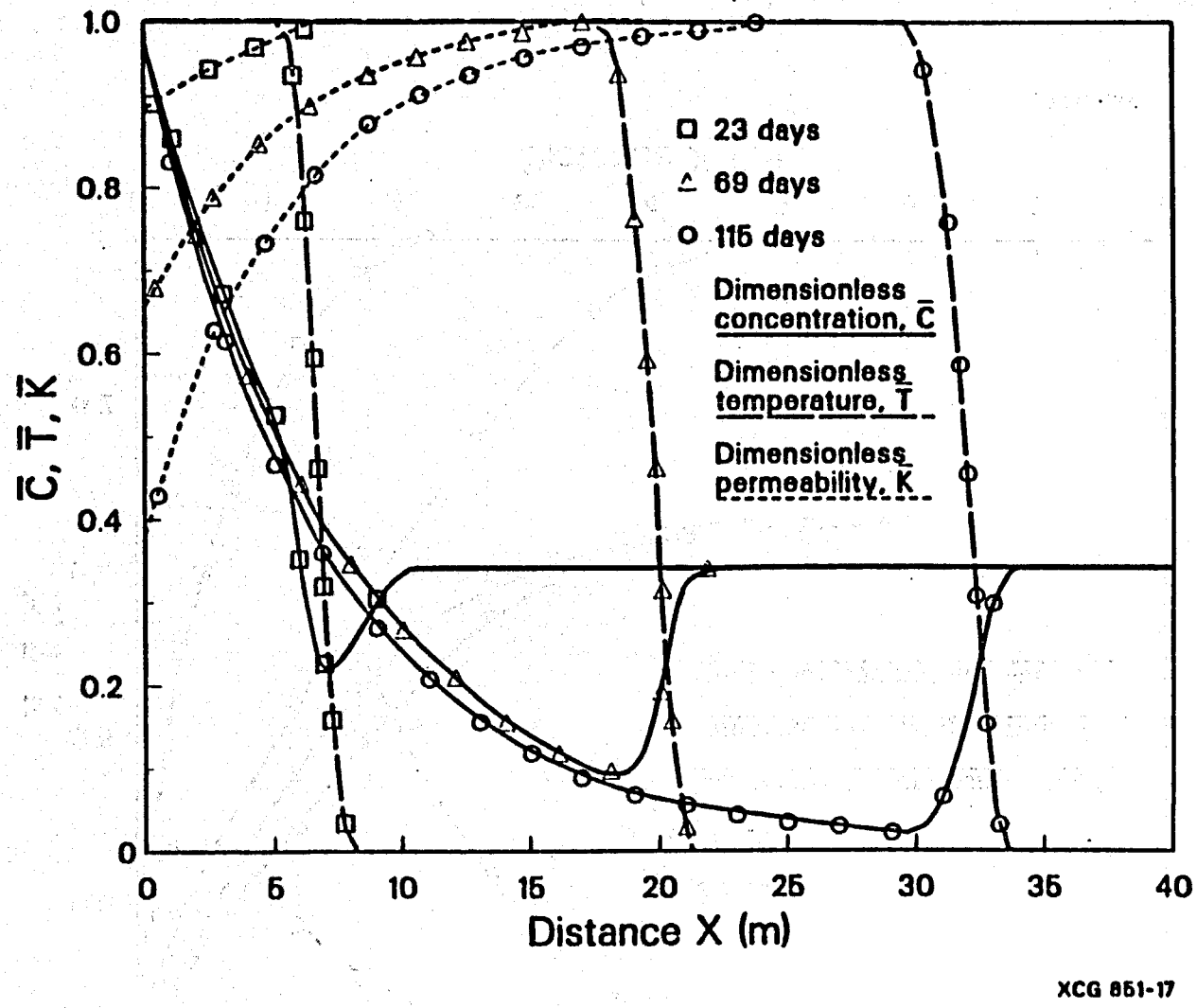

Figure 5-8 Silica Concentrations Compared with Temperature and Permeability Profiles along the Fracture without Heat Transfer from the Rock Matrix.

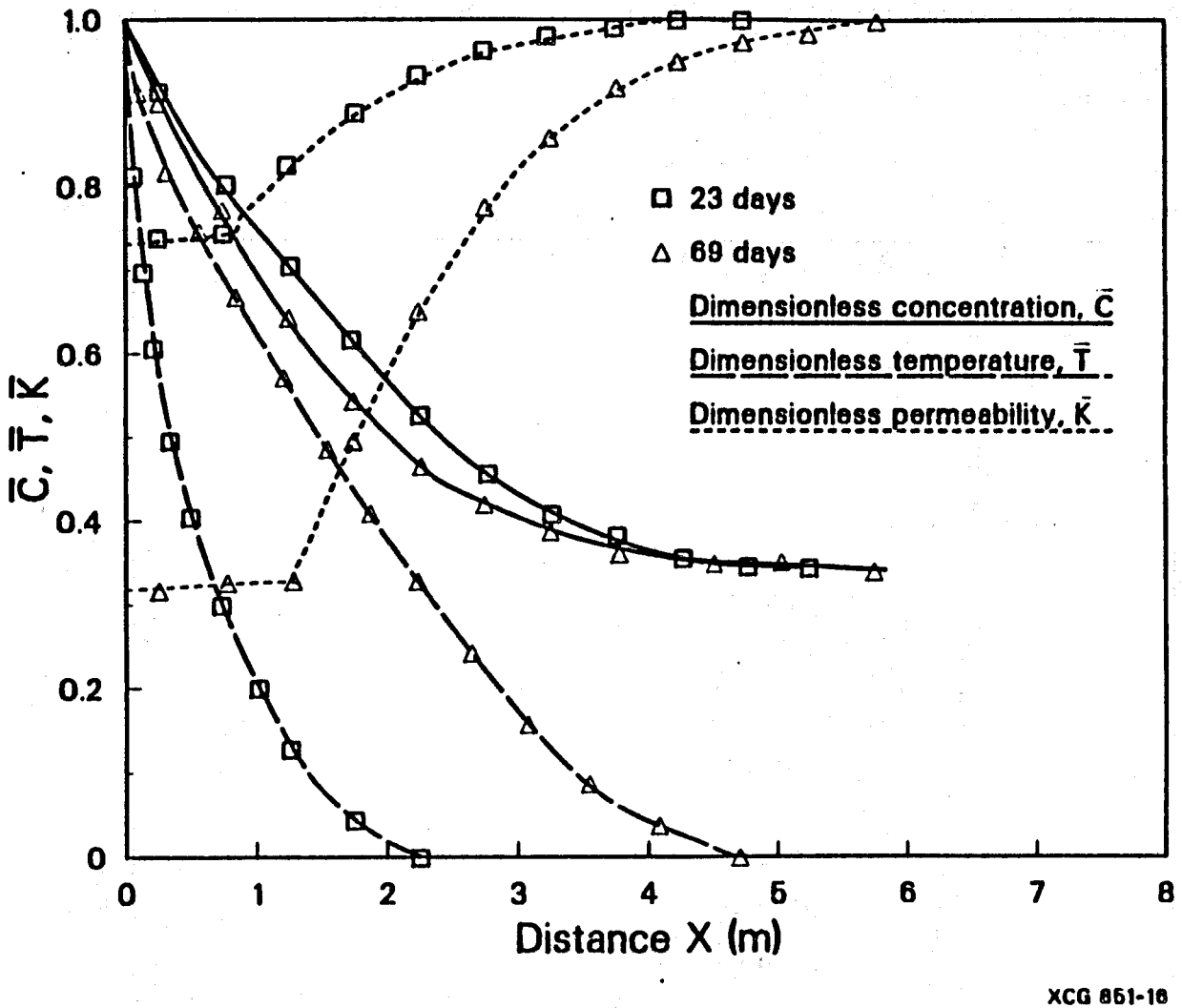

Figure 5-9 Silica Concentrations Compared with Temperature and Permeability Profiles along Fractures with Heat Transfer form Rock Matrix.

from the inlet, essentially the same cumulative amount of silica is deposited in the plateau region. Note that the silica concentration never gives below the equilibrium value for 150 $^{\circ}C$.

5.4. Multiple-Component Modeling of Geothermal Systems

One of the most important uses of numerical simulators in geothermics is to assess the generating capacity of geothermal systems for power production or space heating. At present, the state of the art is to consider only the primary fluid component (water). If concentrations of dissolved solids or noncondensible gases are to be considered, one must modify the equation of state for the fluid and correlate the variations of reservoir properties with chemical concentrations. A major problem in the assessment of geothermal reservoirs is the lack of unique solutions. It is believed that multi-component modeling, i.e., including a method of handling the chemical variations that are observed, can yield more satisfactory solutions to geothermal problems.

In this section a simple model of the Ellidaar geothermal field in Iceland is described. The temperature and pressure behavior in the reservoir as well as silica transients are investigated. All the data used in the analysis are taken from reports by Vatnaskil (1982,1983). The conceptual model we use is shown in Figure 5-10. The reservoir consists of 110 $^{\circ}C$ water with a silica concentration of about 150 ppm. During the 16-year exploitation of the field for space heating, considerable temperature decline has been observed and this has been associated with a drop in silica concentrations of silica in the produced fluids. One possible explanation of these transients is leakage of lower temperature, less concentrated

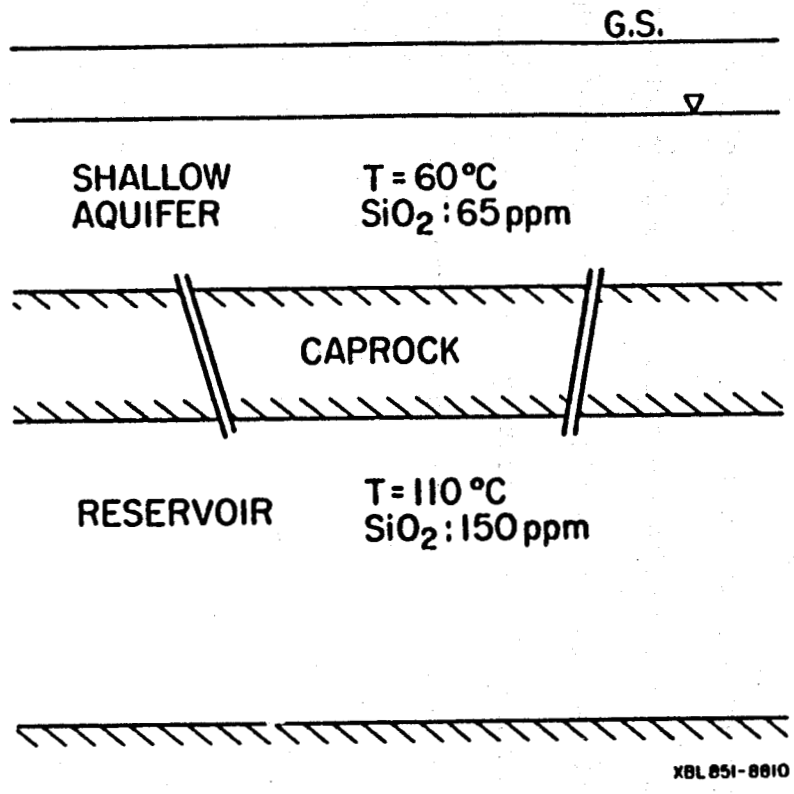

Figure 5-10 A Simplified Conceptual Model of the Ellidaar Geothermal Field, Iceland.

fluids from shallow aquifers. A conceptual model of the reservoir with a shallow aquifer is shown in Figure 5-10. As the temperature gradient in the caprock is conductive it appears likely that the recharge from above is mainly through fractures.

In simulating the conceptual model shown in Figure 5-10, the very simple numerical grid is used as shown in Figure 5-11. It is a two layer radial grid with the whole well field lumped into a single element. Figure 5-12 shows the rate of fluid production for the period 1968-1981. Figures 5-13 to 5-15, show the way in which pressures, temperatures and silica concentrations, respectively, have declined with time. For simplicity, a constant flow rate of $3.5 \times 10^6 m^3$/year over the 16-year period is assumed, so that the seasonal and annual variations are not considered. Consequently, we have not attempted to model the effects of the seasonal variations shown in Figure 5-13.

In this study, the primary purpose is not to develop a predictive model for the Ellidaar geothermal field, but rather to demonstrate the methodology and usefulness of multi-component modeling. After a brief trial and error process, we obtained the results shown in Figures 5-13 to 5-15. All of the matches appear reasonable considering the simple model assumed.

The main results of the history match are as follows. The match with the pressure decline data gives estimates of the permeabilities of the reservoir and the fractured caprock. It is found that in order to match the temperature and the silica concentration decline (Figure 5-14), most of the fluid recharge to the reservoir must come from the shallow aquifer above. The main reservoir is quite

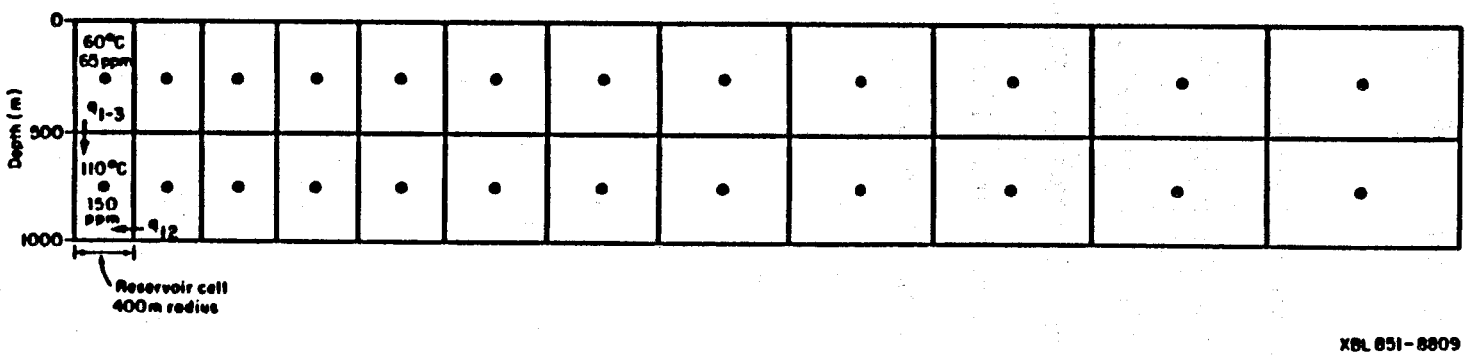

Figure 5-11 The Computational Mesh Used in the Modeling of the Ellidaar Geothermal Field in Iceland.

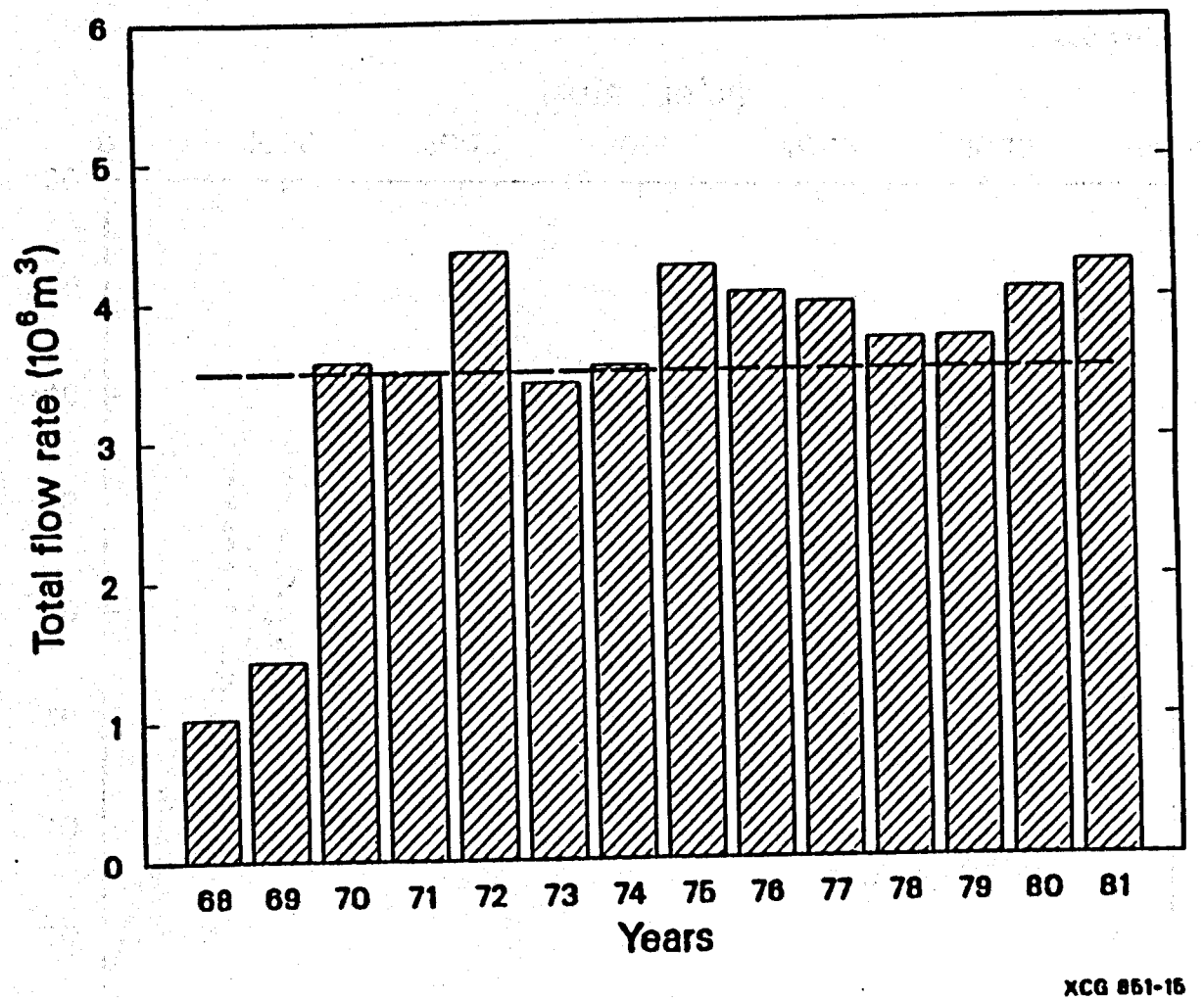

Figure 5-12 Annual Production Rates for the Ellidaar Geothermal Field. The Broken Line Shows the Average Flow Rate Used in the Coupled Modeling.

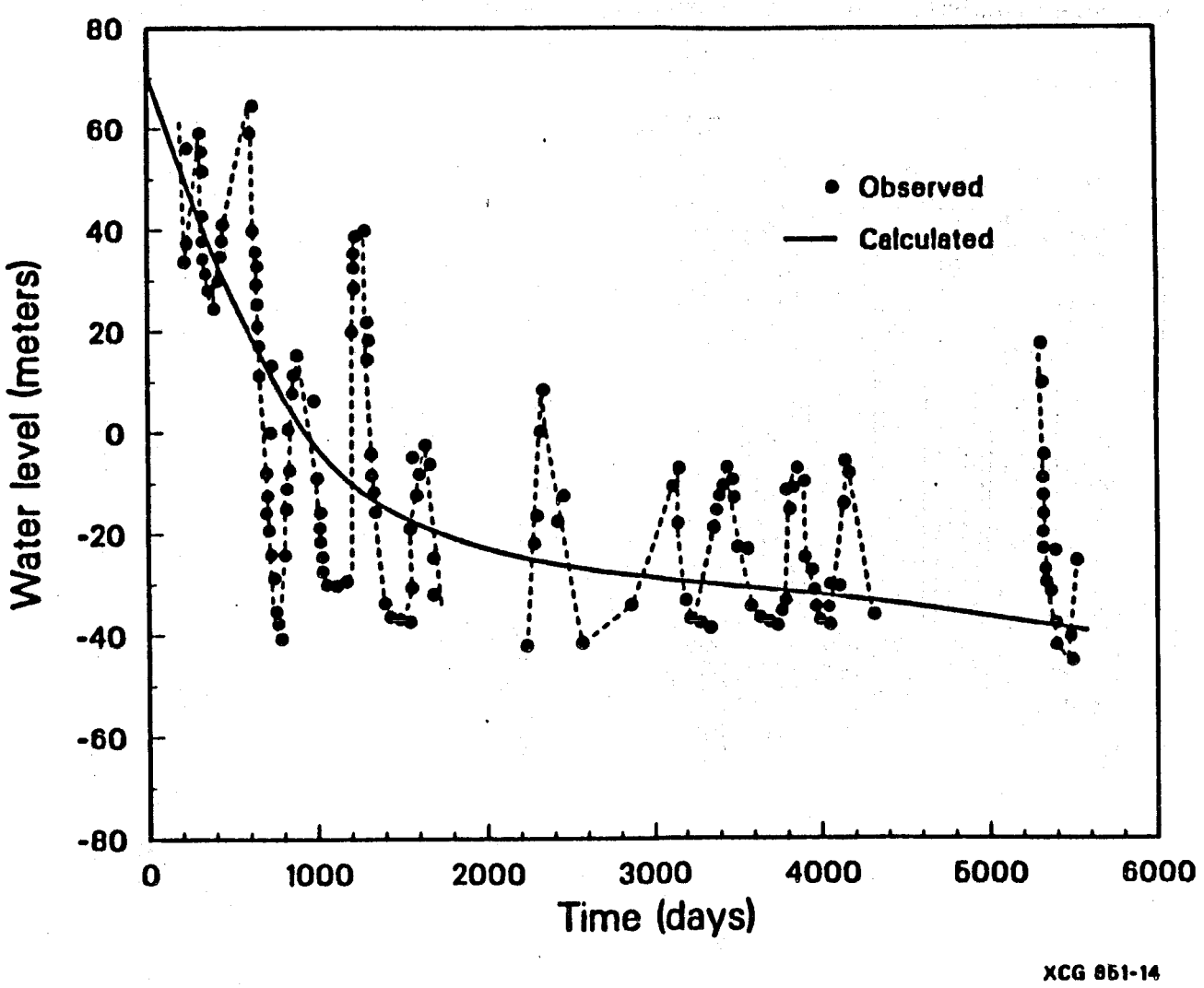

Figure 5-13 Comparison Between Calculated and Observed Pressure Decline at the Ellidaar Geothermal Field in Iceland.

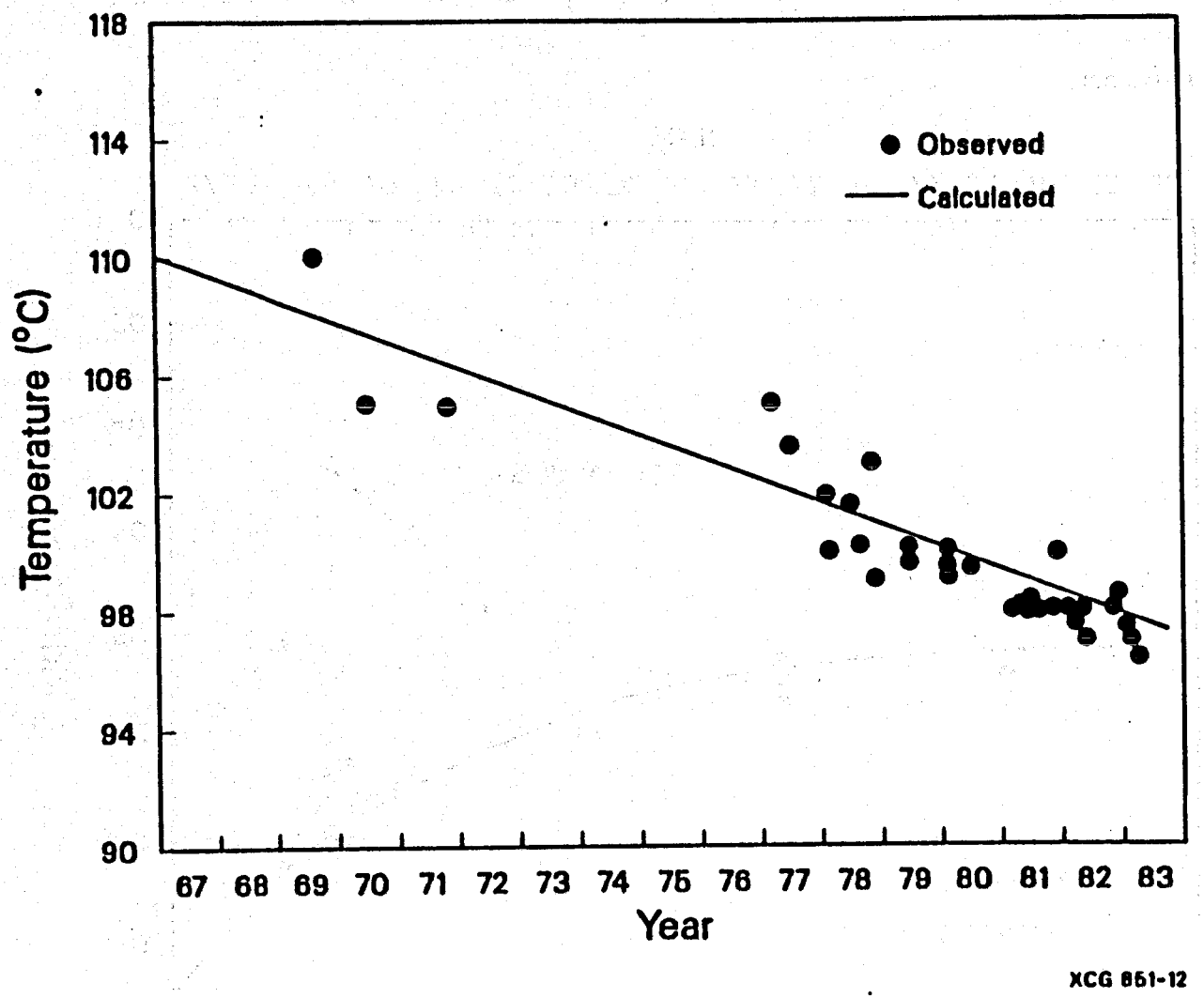

Figure 5-14 Comparison Between Calculated and Observed Temperature Decline at the Ellidaar Geothermal Field in Iceland.

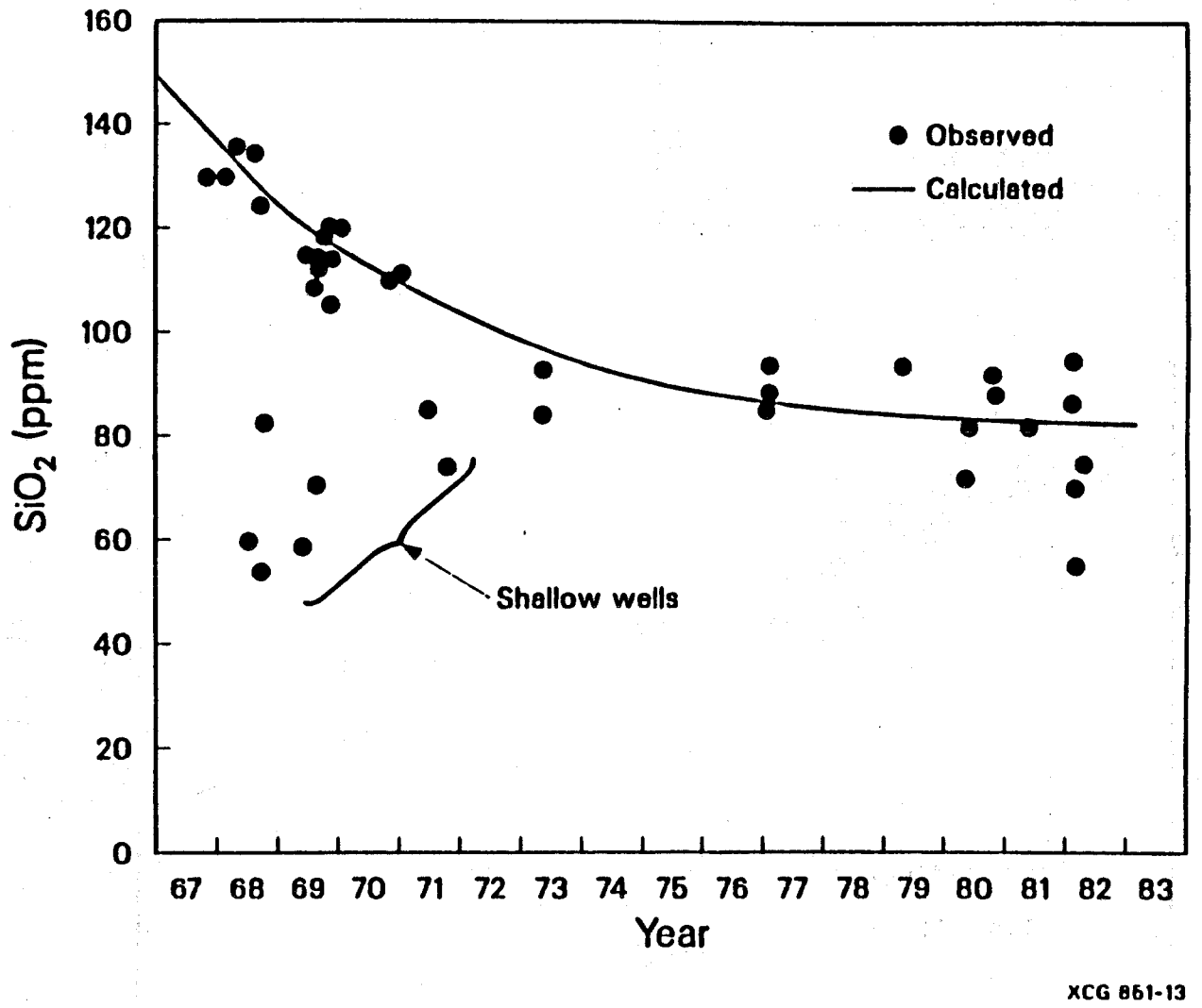

Figure 5-15 Comparison Between Calculated and Observed Silica Concentration Decline at the Ellidaar Geothermal Field in Iceland.

permeable, but the rocks surrounding the well field are much less permeable (<5 md). The fractures providing cold water recharge from above also seem to be quite permeable. The best match with the pressure decline gave a rather high total compressibility, $4\times10^{-7}pa^{-1}$. This high compressibility supports the idea of a shallow unconfined aquifer hydrologically connected to the main reservoir. The match with the temperature decline gives an estimate of the reservoir volume that has undergone cooling due to cold water leakage from above. The average porosity of the reservoir is determined by the match with the silica decline (Figure 5-15). The results indicate an average porosity of 5%, which appears reasonable for the volcanic rocks present at Ellidaar.

Although a very simple conceptual model is used in this study, the results nevertheless illustrate that multi-component modeling can give additional information on reservoir properties and characteristics. For example, this coupled method enables one to obtain a good estimate of reservoir volume as well as porosity, from which reserve estimates can be made. As the different processes are coupled, it is expected that the history match will be more unique and consequently, future predictions more reliable.

5.5. Conclusions

The numerical code PTC has been applied to a problem of natural convection in a porous slab in order to study the effects of the Boussinesq approximation on the temperature and mass flux distributions, as well as overall heat transfer (Nusselt number). The results show that the Boussinesq approximation is reasonable for predicting the overall heat transfer of the system. However, the

mass flux and temperature distributions in the system are significantly affected by the temperature or pressure dependent fluid properties.

A model for simulating silica precipitation and dissolution has been developed. The model has been used for theoretical studies of silica deposition in single fractures. The results show that silica precipitation and the resulting permeability reduction depend strongly on the coupling between the chemical and thermal processes. Various examples are given for different flow rate declines and thermal effects.

A multi-component model has been applied to field data from the Ellidaar geothermal field in Iceland. A simple numerical grid is used for history matching with declines of pressure, temperature, and silica concentration over a 16-year period. The results illustrate that multi-component modeling can yield detailed information about reservoir properties and characteristics.

CHAPTER 6

CONCLUSIONS AND RECOMMENDATIONS

6.1 Conclusions

The main objective of the present study is to develop a methodology to investigate transport phenomena in geologic media. Because transport processes in fractured media are quite different from those in porous media, different mathematical models of transport processes in fractured media are considered. A basic study of uncoupled isothermal and nonisothermal fluid flow in fractured media in this investigation employs the so-called "double porosity" media approach. A semi-analytical model for well test data analysis in naturally fractured media is developed. This model takes into account transient inter-porosity flow, wellbore storage, and skin effects during pressure drawdown and build-up tests for infinite, finite, and outer constant pressure boundary conditions. An approximate analytical solution of an infinite reservoir without wellbore storage and skin effects has been developed for the transient pressure drawdown behavior observed at the production wells. In order to illustrate the applicability of the present model to naturally fractured reservoirs, field data obtained from literature is used to interpret the important reservoir properties. The results show that the inter-porosity flow factor and ratio of storativity obtained from the present model are much smaller than those of the model proposed by Barenblatt et al. and Warren and Root.

For nonisothermal fluid flow in naturally fractured media, proper locations and flow rates for injection wells can be determined from a semi-analytical model

to avoid premature breakthrough of cold water in production wells. Type curves have been developed for optimizing an injection operation to maximize energy recovery from hydrothermal resources located in fractured media.

Since coupled nonisothermal chemical transport processes in geologic media are difficult to solve by any exact analytical methods, a high resolution finite difference method has been developed for solving the convection-diffusion type equation arising from the conservation laws of energy and chemical species. The method consists of a second-order Godunov method and the operator splitting technique. By means of operator splitting, the convection-diffusion type equation can be split into two parts, which can be solved by different numerical methods suitable for each part. The first part, solved by a second-order Godunov method (explicit, monotonized upwind/central difference), is a hyperbolic type equation, which considers only the convection term. The second part, solved by the conventional central finite difference method, is a parabolic type equation, resulting from omission of the convection term from the convection-diffusion type equation. With this solution technique, the results obtained from several benchmark problems show that in contrast to conventional finite difference methods, the numerical diffusion errors and grid orientation effects can be significantly reduced. In particular, the method guarantees oscillation-free results near fronts for high Peclet numbers. These are desirable features for any numerical methods to accurately simulate transport processes in geologic media.

Furthermore, this new method has been incorporated into a two-dimensional code. To illustrate the applicability of the code, some fundamental and practical

problems, including a theoretical study of natural convection in a porous slab and modeling of kinetic silica-water reactions in geothermal systems have been investigated. For natural convection in a porous slab subjected to horizontal temperature differences, the effects of pressure- and temperature-dependent fluid properties on the details of the convection solutions have been studied. The results show that the overall heat transfer behavior is not strongly affected by relaxing the Boussinesq approximation. However, the mass flux and temperature distributions in the system are strongly affected by the non-Boussinesq effects.

To study the effects of silica-water reactions on transient fluid flow behavior, a model for simulating silica precipitation and dissolution has been developed. This model has been used to study the effects of silica deposition on transient flow behavior in a single fracture. The results show that silica precipitation and resulting permeability reduction are strongly dependent on the coupled chemical and thermal processes. To analyze the performance of geothermal systems during the production, a multi-component modeling including transient pressure, temperature and silica concentration history can be employed to obtain a better understanding of reservoir behavior.

6.2 Recommendations

Since the present numerical method is explicit when solving the convection equation, the size of the time step taken during computational procedures must satisfy the Courant-Friedrichs-Lewy condition. It is known that the application of the explicit scheme to steady-state calculations results in rather long computing times. Also, some problems in reservoir simulations require a very fine grid near

wells to obtain accurate solutions. Thus, the explicit scheme would restrict the size of time step severely, and may not be applicable. To retain the characteristic of highly resolved solutions by the explicit second-order Godunov scheme without the disadvantage of a slow convergence rate, an implicit scheme needs to be further developed to get rid of the Courant-Friedrichs-Lewy condition. However, the implicit, second-order, nonoscillatory Godunov scheme needs five-point information in each direction; thus, the construction of the Jacobian matrix is not trivial and the direct solution technique may not be applicable. Therefore, an effective iterative solution technique needs further investigation; most likely the alternate direction solution technique should be considered.

One of various important topics of nonisothermal chemical transport processes is to study double and cross diffusive effects on the processes. These effects may be important in the safety assessments of underground disposal of nuclear waste, and in the analysis of the natural state geothermal systems. The double diffusive effects involves the density variations with temperature as well as chemical concentrations. The cross diffusive effect considers the coupled fluxes of two properties due to irreversible thermodynamic processes. Two well known cross-diffusive effects are the Soret effect and the Dufour effect. To investigate these problems, the equations of state for fluids and the code PTC must be modified.

REFERENCES

Ahlstrom, S. W., Foote, H. P., Arnett, R. C., Cole, C. R. and Serne, R. J., Multicomponent Mass Transport Model- Theory and Numerical Implementation, BNWL-2127, Battelle Pacific Northwest Laboratory, 1977.

Anderson, C. and Concus, P., A Stochastic Method for Modeling Fluid Displacement in Petroleum Reservoirs, LBL-11523, Lawrence Berkeley Laboratory, 1980.

Anderson, M. P., Using Models to Simulate the Movement of Contaminants through Groundwater Flow Systems, Critical Reviews in Environmental Resour. Res., Vol. 17, No. 4, 1075-1081, 1979.

Bankvall, C. G., Natural Convection in Vertical Permeable Space, Warme-und Stoffubertragung, Vol. 7, 22-30, 1974.

Barenblatt, G. I., Zheltov, Iu. P. and Kochina, I. N., Basic Concepts in the Theory of Seepage of Homogeneous Liquids in Fissured Rocks, J. Appl. Math. Mech., Vol 24, 1286-1303, 1960.

Barker, J. A., Block-Geometry Functions Characterizing Transport in Densely Fissured Media, Submitted to Journal of Hydrology.

Batchelor, G. K., Appendix 1 in An Introduction to Fluid Dynamics, London, Cambridge University Press, 615pp, 1979.

Bear, J., On the Tensor Form of Dispersion in Porous Media, J. Geophysical Res., Vol. 66(4), 1185-1197, 1961.

Bejan, A. and Tien, C. L., Natural Convection in a Horizontal Porous Medium Subjected to an End-to-End Temperature Difference, Journal of Heat Transfer, Vol. 100, 191-198, May 1978.

Bell, J. B. and Shubin, G. R., Higher-Order Godunov Methods for Reducing Numerical Dispersion in Reservoir Simulation, Paper Presented at the Reservoir Simulation Symposium, Dallas, Texas, February 10-13, 1985.

Benson, S. and Lai, C. H., Analysis of Interference Data in a Highly Heterogeneous Naturally Fractured Geothermal Reservoir, Accepted for Publication in J. Pet. Tech., 1985.

Blythe, P. A. and Simpkins, P. G., Convection in a Porous Layer for a Temperature Dependent Viscosity, Int. J. Heat Mass Transfer, Vol. 24, 497-506, 1981.

Bodvarsson, G., On the Temperature of Water Flowing through Fractures, J. Geophysical Res., Vol. 74(8), 1969.

Bodvarsson, G., Thermal Problems in the Siting of Reinjection Wells, Geothermics, Vol. 1, No. 2, 1972.

Bodvarsson, G. S., Mathematical Modeling of the Behavior of Geothermal Systems under Exploitation, Ph.D. Thesis, University of California, Berkeley, Lawrence Berkeley Laboratory, LBL-13937, 353pp, 1982.

Bodvarsson, G. S. and Tsang, C. F., Injection and Thermal Breakthrough in Fractured Geothermal Reservoirs, J. Geophysical Res., Vol. 87(B2), 1031-1048, 1982.

Bodvarsson, G. S. and Lai, C. H., Studies of Injection into Naturally Fractured Reservoirs, Geothermal Resources Council Transactions, Vol. 6, 245-248, 1982.

Boris, J. P. and Book, D. L., Flux Corrected Transport I: SHASTA, A Fluid Transport Algorithm that Works, J. Comp. Phys. Vol. 11, 38-69, 1973.

Boris, J. P., Book, D. L. and Hain, K. H., Flux Corrected Transport II: Generalization of the Method, J. Comp. Phys. Vol. 18, 248-283, 1975.

Boris, J. P. and Book, D. L., Flux Corrected Transport III: Minimal Error FCT Algorithms, J. Comp. Phys. Vol. 20, 397-431, 1976.

Boulton, N. S. and Streltsova, T. D., Unsteady Flow to a Pumped Well in a Two-Layered Water-Bearing Formation, Journal of Hydrology, Vol. 35, 245-256, 1977.

Bourdet, B. and Gringarten, A. C., Determination of Fissured Volume and Block Size in Fractured Reservoirs by Type Curve Analysis, Paper Presented at the 55th Annual Fall Technical Conference and Exhibition of the Society of Petroleum Engineers of AIME, Dallas, Texas, September 21-24, 1980.

Bredehoeft, J. D. and Pinder, G. F., Mass Transport in Flowing Groundwater Water Resour. Res., Vol. 9, No. 1, 194-210, 1973.

Burns, P. J., Chow, L. C. and Tien, C. L., Convection in a Vertical Slot Filled with Porous Insulation, Int. J. Heat Mass Transfer, Vol. 20, 919-926, 1977.

Buscheck, T. A., Equation of State for Liquid Water, Internal Memo, Lawrence Berkeley Laboratory, Berkeley, California, 1980.

Caldwell, J. A., The Theoretical Determination of the Fluid Potential Distribution in Jointed Rocks, M.Sc. Thesis, University of Witwatersrand, Johannesburg, South Africa, 1971.

Caldwell, J. A., The Theoretical Determination of the Permeability Tensor for Jointed Rock, Stuttgart, Proceedings , Symposium on Percolation through Fissured Rock, Stuttgart, International Society for Rock Mechanics and International Association of Engineering Geology, 1972.

Carslaw, H. S. and Jaeger, J. C., Conduction of Heat in Solids (2nd ed.), London, Oxford University Press, 510pp, 1959.

Chakravarthy, S. and Osher, S., High Resolution Applications of the Osher Upwind Scheme for the Euler Equations, AAIA Paper Presented at 6th CFD Conference, 1983.

Chen, Z. and Jiang, L., Exact Solution for the System of Flow Equations Through a Medium with Double-Porosity, Scientia Sinica, Vol. XXIII, No. 7, 880-896, July, 1980.

Chorin, A. J., Random Choice Solution of Hyperbolic Systems, J. Comp. Physics, Vol. 22, 517-533, 1976.

Chorin, A. J., Random Choice Method with Applications to Reacting Gas Flow, J. Comp. Physics, Vol. 25, 253-272, 1977.

Cinco-Ley, H. and Fernando Samaniego, V., Pressure Transient Analysis for Naturally Fractured Reservoirs, Paper Presented at the 57th Annual Fall Technical Conference and Exhibition of the Society of Petroleum Engineers of AIME, New Orleans, Louisiana, September 26-29, 1982.

Coats, K. H. and Modine, A. D., A Consistent Method for Calculating Transmissibilities in Nine-Point Difference Equations, Paper Presented at the 7th SPE Symposium on Reservoir Simulation Held at San Francisco, California, November 16-18, 1983.

Colella, P., Glimm's Method for Gas Dynamics, SIAM J. Sci. Stat. Comput., Vol. 3, No. 1, 76-110, 1982.

Colella, P., Concus, P. and Sethian, J., Some Numerical Methods for Discontinuous Flows in Porous Media, Chapter V in The Mathematics of Reservoir Simulation, Edited by R. E. Ewing, SIAM, Philadelphia, 1983.

Colella, P., Multidimensional Upwind Methods for Hyperbolic Conservation Laws, LBL-17023, May 1984.

Colella, P. and Woodward, P. R., The Piecewise-Parabolic Method (PPM) for Gas-Dynamical Simulations, J. Comp. Physics, Vol. 54, 174-201, 1984.

Colella, P., A Direct Eulerian MUSCL Scheme for Gas Dynamics, SIAM J. Sci. Stat. Comput. Vol. 6, No. 1, 104-117, January 1985.

Concus, P. and Proskuroswski, W., Numerical Solution of a Nonlinear Hyperbolic Equation by a Random Choice Method, J. Comp. Physics, Vol. 30, 153-166, 1979.

Dang, Vi-Duong, Steady-State Mass Transfer with Homogeneous and Heterogeneous Reactions, AIChE Journal, Vol. 29, No. 1, 19-25, January 1983.

Dawson, P. R. and McTigue, D. F., A Numerical Model for Natural Convection in Fluid-Saturated Creeping Porous Media, Numerical Heat Transfer, Vol. 8, 45-63, 1985.

Deruyck, B. G., Bourdet, D. P., DaPrat, G. and Ramey, H. J., Interpretation of Interference Tests in Reservoirs with Double Porosity Behavior Theory and Field Examples, Paper Presented at the 55th Annual Fall Technical Conference and Exhibition of the Society of Petroleum Engineers of AIME, New Orleans, Louisiana, September 26-29, 1982.

de Swaan, A. O., Analytic Solutions for Determining Naturally Fractured Reservoir Properties by Well Testing, Soc. Pet. Eng. J., 117-122, June 1976.

De Vahl Davis, G. and Mallinson, G. D., An Evaluation of Upwind and Central Difference by a Study of Recirculating Flow, Computers and Fluids, Vol. 4, 29-43, 1976.

Duff, I. S., MA28- A Set of Fortran Subroutines for Sparse Unsymmetric Linear Equations, AERE Harwell Report R 8730, July, 1977.

Edwards, A. L., Trump- A Computer Program for Transient and Steady State Temperature Distributions in Multidimensional Systems, National Technical Information Service, National Bureau of Standards, Springfield, VA. 1972.

Endo, H. K., Mechanical Transport in Two-Dimensional Networks of Fractures, Ph.D. Thesis, University of California, Berkeley, 203pp, 1984.

Ershaghi, I. and Aflaki, R., Problems in Characterization of Naturally Fractured Reservoirs from Well Test Data, Soc. Pet. Eng. J., Vol. 25, 445-450, June 1985.

Ewing, R. E., Russell, T. F. and Wheeler, M. F., Simulation of Miscible Displacement Using Mixed Methods and a Modified Method of Characteristics, Paper Presented at the 7th SPE Symposium on Reservoir Simulation, Held at San Francisco, California, November 16-18, 1983.

Fried, J. J., Groundwater Pollution, Elsevier Scientific Publishing Company, Amsterdam-Oxford-New York, 930pp, 1975.

Garder, A. O., Jr., Peaceman, D. W. and Pozzi, A. I., Jr., Numerical Calculation of Multidimensional Miscible Displacement by the Method of Characteristics, Soc. Pet. Eng. J., 26-36, March 1964.

Gelhar, L. W., Gutjahr, A. L. and Naff, R. L., Stochastic Analysis of Macrodispersion in a Stratified Aquifer, Water Resour. Res. Vol. 15, No. 6, 1387-1397, 1979.

Gelhar, L. W. and Axness, C. L., Three-Dimensional Stochastic Analysis of Macrodispersion in Aquifers, Water Resour. Res., Vol. 19, No. 1, 161-180, 1983.

George, A., Liu, J. and Ng, E., User Guide for SPARSPAK- Waterloo Sparse Linear Equations Package, CS-78-30, Dept. of Computer Science, University Waterloo, Waterloo, Ontario, 1980.

Gill, W. N. and Sankarasubramanian, R., Exact Analysis of Unsteady Convective Diffusion, Proc. Roy. Soc. Lond. A 316, 340-350, 1970.

Gill, W. N. and Sankarasubramanian, R., Dispersion of a Non-Uniform Slug in Time-Dependent Flow, Proc. Roy. Soc. Lond. A 332, 101-117, 1971.

Glimm, J., Solution in the Large Nonlinear Hyperbolic Systems of Equations, Comm. Pure Appl. Math., Vol. 18, 399-408, 1965.

Glimm, J., Marchesin, D. and McBryan, O., Unstable Fingers in Two Phase Flow, Comm. Pure Appl. Math. Vol. 34, 53-75, 1981.

Glimm, J., Lindquist, B., McBryan, O. A., Plohr, B. and Yaniv, S., Front Tracking for Petroleum Reservoir Simulation, Paper Presented at the 7th SPE Symposium on Reservoir Simulation, Held at San Francisco, California, November 16-18, 1983.

Gray, D. D. and Giorgini, A., The Validity of the Boussinesq Approximation for Liquids and Gases, Int. J. Heat Mass Transfer, Vol. 19, 545-551, 1976.

Gringarten, A. C., Interpretation of Tests in Fissured Reservoirs and Multilayered Reservoirs with Double Porosity Behavior- Theory and Practice, Paper Presented at the SPE International Petroleum Exhibition and Technical Symposium, Beijing, China, March 26-28, 1982.

Hald, O. H., Class Notes for Math. 228A, Dept. of Math., University of California, Berkeley, 1984.

Harleman, D. R. F. and Rumer, R. R., Longitudinal and Lateral Dispersion in an Isotropic Porous Medium, J. Fluid Mechanics, Vol. 16-3, 385-394, July 1963.

Harten, A., Lax, P. D. and Van Leer, B., On Upstream Differencing and Godunov-Type Schemes for Hyperbolic Conservation Laws, SIAM Review, Vol 25, 35-61, January, 1983.

Hickox, C. E. and Gartling, D. K., A Numerical Study of Natural Convection in a Horizontal Porous Layer Subjected to an End-to-End Temperature Difference, Journal of Heat Transfer, Vol. 103, 797-802, 1981.

Horne, R. N., Geothermal Reinjection Experience in Japan, Paper Presented at the 1981 California Regional Meeting of SPE, Bakersfield, California, March 1981.

Itoi, R., MacKawa, H., Iukuda, M., Jinno, K., and Hatanaka, K., Experimental Study on the Silica Deposition in a Porous Medium, Geothermal Resources Council Transactions, Vol. 8, 301-304, August 1984.

Iwai, K., Fundamental Studies of Fluid Flow through a Single Fracture, Ph.D. Thesis, University of California, Berkeley, 208pp, 1976.

Javandel, I. and Witherspoon, P. A., Analytical Solution of a Partially Penetrating Well in a Two-Layer Aquifer, Water Resour. Res., Vol. 19, No. 2, 567-578, 1983.

Javandel, I., Doughty, C. and Tsang, C. F., Groundwater Transport: Handbook of Mathematical Models, American Geophysical Union, Water Resour. Mono. 10, 1984.

Jennings, A. A., Kirkner, D. J. and Theis, T. L., Multicomponent Equilibrium Chemistry in Groundwater Quality Models, Water Reour. Res., Vol. 18, No. 4, 1089-1096, 1982.

Jensen, O. K. and Finlayson, B. A., A Numerical Technique for Tracking Sharp Fronts in Studies of Tertiary Oil Recovery Pilots, Paper Presented at the 7th SPE Symposium on Reservoir Simulation Held at San Francisco, California, November 16-18, 1983.

Karasaki, K., Witherspoon, P. A. and Long, J. C. S., A New Analytical Model for Fracture-Dominated Reservoirs, Paper Presented at the 60th Annual Technical Conference and Exhibition Held in Las Vegas, NV, September 22-25, 1985.

Kazemi, H., Pressure Transient Analysis of Naturally Fractured Reservoir with Uniform Fracture Distributions, Soc. Pet. Eng. J., 451-461, December 1969; Trans., AIME, 256.

Keith, L. A., Delaney, P. T. and Moore, D. E., Permeability Reduction Due to Precipitation of Quartz under Nonisothermal Conditions, Proc. 9th Stanford Geothermal Workshop, 239-245, December 1983.

Konikow, L. F. and Bredehoeft, J. D., Modeling Flow and Chemical Quality Changes in an Irrigated Stream-Aquifer System, Water Resour. Res., Vol. 10, No. 3, 546-562, 1974.

Lai, C. H., Bodvarsson, G. S., Tsang, C. F. and Witherspoon, P. A., A New Model for Well Test Data Analysis for Naturally Fractured Reservoirs, Paper Presented at the 1983 California Regional Meeting Held in Ventura, March 23-25, 1983.

Lai, C. H., Bodvarsson, G. S. and Witherspoon, P. A., Numerical Studies of Silica Precipitation/Dissolution, Presented at the 10th Annual Workshop on Geothermal Reservoir Engineering, Stanford University, January 22-24, 1985.

Lai, C. H., Bodvarsson, G. S. and Witherspoon, P. A., A Second-Order Upwind Differencing Method for Nonisothermal Chemical Transport in Porous Media, accepted for publication in Numerical Heat Transfer, 1985.

Larson, R. G., Controlling Numerical Disperson by Variably Timed Flux Updating in One Dimension, Soc. Pet. Eng. J., Vol. 22, 339-408, 1982.

Lauwerier, H. A., The transport of Heat in an Oil Layer Caused by the Injection of Hot Fluid, Appl. Sci. Res. Sec. A5, 145, 1955.

Li, K. M., Random Choice Method for Treating the Convection-Diffusion Equation, Paper Presented at the 7th SPE Symposium on Reservoir Simulation,

Held at San Francisco, California, November 16-18, 1983.

Lomize, G. M., Filtratsiya V Treshchinovatykh Porodakh, Gosenergoizdat, Moscow, 1951.

Long, J. C. S., Remer, J. S., Wilson, C. R. and Witherspoon, P. A., Porous Media Equivalents for Network of Discontinuous Fractures, Water Resour. Res., Vol. 18, No. 3, 645-658, 1982.

Long, J. C. S., Investigation of Equivalent Porous Medium Permeability in Networks of Discontinuous Fractures, Ph.D. Thesis, University of California, Berkeley, 277pp, 1983.

Long, J. C. S. and Witherspoon, P. A., The Relationship of the Degree of Interconnection to Permeability in Fracture Networks, J. Geophysical Res. Vol. 90(B4), 3087-3098, 1985.

Louis, C., A Study of Groundwater Flow in Jointed Rock and It's Influence on the Stability of Rock Masses, Rep. 10, Imp. Coll. Rock Mech. Res., London, 1969.

Matheron, G. and De Marsily, G., Is Transport in Porous Media Always Diffusive? A Counterexample, Water Resour. Res., Vol. 16, No. 5, 901-917, 1980.

Mavor, M. J. and Cinco-Ley, H., Transient Pressure Behavior of Naturally Fractured Reservoirs, Paper Presented at the SPE 1979 California Regional Meeting, Ventura, April 18-20, 1979.

Najurieta, H. L., A Theory for the Pressure Transient Analysis in Naturally Fractured Reservoirs, J. Pet. Tech. 1241-1250, July 1980.

Narasimhan, T. N. and Witherspoon, P. A., An Integrated Finite Difference Method for Analyzing Fluid Flow in Porous Media, Water Resour. Res., Vol. 12, No. 1, 57-64, 1976.

Neuman, S. P., A Eulerian-Lagrangian Numerical Schemes for the Dispersion-Convection Equation Using Conjugate Space-Time Grids, J. Comp. Physics, Vol. 41, 270-294, 1981.

Odeh, A. S., Unsteady-State Behavior of Naturally Fractured Reservoirs, Soc. Pet. Eng. J., 60-64, March 1965.

Parsons, R. W., Permeability of Idealized Fractured Rock, Soc. Pet. Eng. J. Vol. 10, 126-136, 1966.

Peaceman, D. W., Fundamentals of Numerical Reservoir Simulation, Elsevier Scientific Publishing Company, Amterdam-Oxford-New York, 176pp, 1977.

Pinder, G. F., Mass Transport in Flowing Groundwater, Water Resour. Res., Vol. 9, No. 1, 194-210, 1973.

Potempa, T., A Numerical Model of Two-Dimensional Two-Component, Single Phase Miscible Displacement in a Porous Medium, SIAM J. Sci. Stat. Comput., Vol. 6, No. 3, 582-598, July 1985.

Price, H. S., Cavendish, J. C. and Varga, R. S., Numerical Methods of Higher Order Accuracy for the Diffusion-Convection Equation, Soc. Pet. Eng. J., Vol. 8, 293-303, 1968.

Pruess, K. and Narasimhan, T. N., A Practical Method for Modeling Fluid and Heat Flow in Fractured Porous Media, Paper Presented at the 6th Annual Meeting of SPE, New Orleans, Louisiana, January 31- February 2, 1982.

Pruess, K. et al., Advances in Numerical Modeling of Fractured Geothermal Reservoirs, LBL-15500, 129-132, 1982.

Pruess, K. and Karasaki, K., Proximity Functions for Modeling Fluid and Heat Flow in Reservoirs with Stochastic Fracture Distributions, Presented at 8th Workshop on Geothermal Reservoir Engineering, Stanford University, Stanford, CA., 1983.

Pruess, K. and Bodvarsson, G. S., A Seven-Point Finite Difference Method for Improved Grid Orientation Performance in Pattern Steamfloods, Paper Presented at the 7th SPE Symposium on Reservoir Simulation, Held at San Francisco, California, November 16-18, 1983.

Pyrak, L. R., Myer, L. R. and Cook, N. G. W., Determination of Fracture Void Geometry and Contact Area at Different Effective Stress, Transactions, American Geophysical Union, Vol. 66, 903, November 12, 1985.

Ramey, H. J., Jr., Short-Time Well Test Data Interpretation in the Presence of Skin Effect and Wellbore Storage, J. Pet. Tech., 97-104, January 1970.

Raven, K. G. and Gale, J. E., Water Flow in a Natural Rock Fracture as a Function of Stress and Sample Size, Int. J. Rock Mech. Sci. & Geomech. Abstr. Vol. 22, No. 4, 251-261, 1985.

Redell, D. L. and Sunada, D. K., Numerical Simulation of Dispersion in Groundwater Aquifers, Hydrol. Paper 41, Colorado State University, Ft. Collins, Colo., 1970.

Rimstidt, J. D. and Barnes, H. L., The Kinetics of Silica-Water Reactions, Geochim. Cosmochim, Acta, Vol. 44, 1683-1699, 1980.

Robertson, J. B. and Barraclough, J. T., Radioactive and Chemical Waste Transport in Groundwater at National Reactor Testing Station, Idaho - 20 Year Case History and Digital Model - Proc. Symposium on Underground Waste Management and Artificial Recharge, Vol. 1, 291-322, 1973.

Robinson, B. A., Quartz Dissolution and Silica Deposition in Hot Dry Rock Geothermal Systems, LA-9404-T, Los Alamos Laboratory, July 1982.

Roe, P. L., Numerical Algorithms for the Linear Wave Equation, Royal Aircraft Establishment Technical Report 81047, 1981.

Romm, E. S., Filtratsionnye Svoistva Treshchinovatykh Gornyx Porod, Nedra, Moscow, 1966.

Rubin, J. and James, R. V., Dispersion-Affected Transport of Reacting Solutes in Saturated Porous Media- Galerkin Method Applied to Equilibrium-Controlled Exchanges in Unidirectional Steady Water Flow, Water Resour. Res., Vol. 9, No. 5, 1332-1356, 1973.

Schapery, R. A., Approximation Methods of Transform Inversion for Viscoelastic Stress Analysis, Prcd., Fourth U. S. National Congress of Applied Mechanics, 1075-1085, 1961.

Scheidegger, A. E., General Theory of Dispersion in Porous Media, J. Geophysical Res., Vol. 66(10), 3273-3278, 1961.

Schlichting, H., Boundary Layer Theory, McGraw-Hill, New York, 747pp, 1968.

Schulz, H. D. and Reardon, E. J., A Combined Mixing Cell/Analytical Model to Describe Two-Dimensional Reactive Solute Transport for Unidirectional Groundwater Flow, Water Resour. Res., Vol. 19, No. 2, 493-502, 1983.

Serra, K. V., Reynolds, A. C. and Raghavan, R., New Pressure Transient Analysis Methods for Naturally Fractured Reservoirs, Paper Presented at the SPE 1982 California Regional Meeting, San Francisco, March 24-26, 1982.

Sethian, J. A., Chorin, A. J. and Concus, P., Numerical Solution of the Buckley-Leverett Equations, Paper Presented at the 7th SPE Symposium on Reservoir Simulation, Held at San Francisco, California, November 16-18, 1983.

Sharp, J. C., Fluid Flow through Fissured Media, Ph.D. Thesis, Imperial College, London, 181pp, 1970.

Smith, L. and Schwartz, F. W., Mass Transport, 1, A Stochastic Analysis of Macroscopic Dispersion, Water Resour. Res., Vol. 16, No. 2, 303-313, 1980.

Snow, T. D., A Parallel Plate Model of Fractured Permeable Media, Ph.D. Thesis, University of California, Berkeley, 331pp, 1965.

Snow, T. D., Anisotropic Permeability of Fractured Media, Water Resour. Res., Vol. 5, No. 6, 1273-1289, 1969.

Stehfest, H., Numerical Inversion of Laplace Transforms, Communications of ACM, Vol. 13, 47-49, 1970.

Strang, G., On the Construction and Comparison of Differences Schemes, SIAM J. Numer. Anal., Vol. 5, 506-517, September 1968.

Streltsova, T. D., Well Pressure Behavior of a Naturally Fractured Reservoirs, Paper Presented at the SPE 1982 California Regional Meeting, San Francisco, March 24-26, 1982.

Sweby, P. K., High Resolution Schemes Using Flux Limiters for Hyperbolic Conservation Laws, SIAM J. Numer. Anal., Vol. 21, 995-1011, October 1984.

Taylor, G., Dispersion of Soluble Matter in Solvent Flowing Slowly through a Tube, Proc. Roy. Soc. Lond. A 219, 186-203, 1953.

Truesdell, A. H., D'Amore, F. and Nieva, D., The Effects of Localized Aquifer Boiling on Fluid Production at Cerro Prieto, Geothermal Resources Council Transactions, Vol. 8, 223-229, August 1984.

Tsang, Y. W. and Witherspoon, P. A., Hydromechanical Behavior of a Deformable Rock Fracture Subjected to Normal Stress, J. Geophysical Res., Vol. 86(B10), 9287-9298, 1981.

Tsang, Y. W. and Witherspoon, P. A., The Dependence of Fracture Mechanical and Fluid Flow Properties on Fracture Roughness and Sample Size, J. Geophysical Res., Vol. 88(B3), 2359-2366, 1983.

Valocchi, A. J., Describing the Transport of Ion-Exchanging Contaminants using an Effective K_d Approach, Water Resour. Res. Vol. 20, No. 4, 499-503, 1984.

Van Leer, B., Towards the Ultimate Conservative Difference Scheme IV: A New Approach to Numerical Convection, J. Comp. Physics, Vol. 23, 276-299, 1977.

Vatnaskill, Ellidaar Geothermal Field - The Effects of Exploitation on the Energy Resources (Report in Icelandic), prepared for the Reykjavik Municipal District Heating Systems, December 1982.

Vatnaskill, Ellidaar Geothermal Field - Analysis of Watertable and Temperature Measurements (Report in Icelandic), prepared for the Reykjavik Municipal District Heating Systems, December 1983.

Warren, J. E. and Root, P. J., The Behavior of Naturally Fractured Reservoirs, Soc. Pet. Eng. J., 245-255, September 1963, Trans., AIME, 228.

Watts, J. W. and Silliman, W. J., Numerical Dispersion and the Origins of Grid Orientation Effect - A Summary, Paper 96C, presented at the 73rd Annual Meeting of AIChE, Chicago, 1980.

Weber, J. E., The Boundary Layer Regime for Convection in a Vertical Porous Layer, Int. J. Heat Mass Transfer Vol. 18, 569-576, 1975.

Witherspoon, P. A., Wang, J. S. Y., Iwai, K. and Gale, J. E., Validity of Cubic Law for Fluid Flow in a Deformable Rock Fracture, Water Resour. Res., Vol. 16, No. 6, 1016-1024, 1980.

Witherspoon, P. A., Cook, N. G. W. and Gale, J. E., Geologic Storage of Radioactive Waste- Field Studies in Sweden, Science, Vol. 211, 894-900, 1981.

Yanosik, J. L. and McCraken, T. A., A Nine-Point Finite-Difference Reservoir Simulator for Realistic Prediction of Unfavorable Mobility Ratio Displacement, Soc. Pet. Eng. J. Vol. 18, 253-262, 1979.

Zalesak, S. T., Fully Multidimensional Flux Corrected Transport Algorithms for Fluids, J. Comp. Physics, Vol. 31, 335-378, 1979.

APPENDIX A: Derivation of the Governing Equations for Fluid Flow in Naturally Fractured Media.

In formulating the governing equations, the approach of Warren and Root is employed. The fractures are lumped into to one continuum medium and the rock matrix into another one.

In the radial flow system, one can define a control volume V_n as

$$V_n = \pi\{(r + dr)^2 - r^2\}H \approx 2\pi r dr H \tag{A.1}$$

The interface area A_c between the rock matrix and the fractures in the control volume can be expressed as

$$A_c = 6D^2\left(\frac{V_n}{D^3}\right) = \frac{12\pi r dr H}{D} \tag{A.2}$$

A mass balance equation for the control volume in the fractures can now be written as

$$q_r A - \{q_r A + \frac{\partial}{\partial r}(q_r A)dr\} + (q_z A_c)|_{z=D/2} = \frac{\partial(V_n \phi_2 \rho_f)}{\partial t} \tag{A.3}$$

where A $(2\pi r H)$ is the cross section area in the radial direction, ϕ_2 is fracture porosity, ρ_f is fluid density, t is time, and q_r and q_z are the mass flux in the radial and z directions, respectively, given by

$$q_r = -\frac{k_2}{\mu}\rho_f \frac{\partial P_2}{\partial r} \tag{A.4}$$

and

$$q_z = -\frac{k_1}{\mu}\rho_f \frac{\partial P_1}{\partial z} \tag{A.5}$$

where k_1 and k_2 are fracture and rock matrix permeabilities, respectively, and μ is fluid viscosity. Assume ϕ_2 to be constant so that the right hand side of Eq. A.3 can be expressed as

$$\frac{\partial(V_n \phi_2 \rho_f)}{\partial t} = V_n \{\rho_f \phi_2 c_{fr} \frac{\partial P_2}{\partial t} + \rho_f \phi_2 c_f \frac{\partial P_2}{\partial t}\}$$
$$= V_n \rho_f \phi_2 (c_{fr} + c_f) \frac{\partial P_2}{\partial t} \tag{A.6}$$

where c_f and c_{fr} are fluid and fracture compressibilities, respectively.

Assuming k_2 to be constant and substituting Eqs. A.1, A.2, A.4, A.5 and A.6 into Eq. A.3, one obtains

$$\frac{\partial^2 P_2}{\partial r^2} + \frac{1}{r}\frac{\partial P_2}{\partial r} - \frac{6k_1}{k_2}\frac{1}{D}\frac{\partial P_1}{\partial z}\Big|_{z=D/2} = \frac{\phi_2 c_2 \mu}{k_2}\frac{\partial P_2}{\partial t} \tag{A.7}$$

where $c_2 = c_{fr} + c_f$.

The governing equation describing the mass conservation in the rock matrix can be expressed as

$$q_z A_z - \{q_z A_z + \frac{\partial}{\partial z}(q_z A_z) dz\} = \frac{\partial(A_z\, dz\, \phi_1 \rho_f)}{\partial t} \tag{A.8}$$

where

$$A_z = k_c z^2 \tag{A.9}$$

k_c is a constant, and ϕ_1 is rock matrix porosity. Similar considerations as the fractures yield

$$\frac{\partial^2 P_1}{\partial z^2} + \frac{2}{z}\frac{\partial P_1}{\partial z} = \frac{\phi_1 c_1 \mu}{k_1}\frac{\partial P_1}{\partial t} \tag{A.10}$$

where $c_1 = c_m + c_f$ and c_m is rock matrix compressibility.

Eqs. A.7 and A.10 describe the pressure transient behavior in the fracture and the rock matrix, respectively.

APPENDIX B: Simultaneous Solution for Pressures of the Fracture and Rock Matrix.

Applying Laplace transformation to Eqs. 2.13 through 2.22 yields

$$\frac{\partial^2 \bar{P}_{D2}}{\partial r_D^2} + \frac{1}{r_D}\frac{\partial \bar{P}_{D2}}{\partial r_D} - 3\bar{\lambda}\frac{\partial \bar{P}_{D1}}{\partial \eta}\Big|_{\eta=1} - \omega p \bar{P}_{D2} = 0 \tag{B.1}$$

$$\frac{\partial^2 \bar{P}_{D1}}{\partial \eta^2} + \frac{2}{\eta}\frac{\partial \bar{P}_{D1}}{\partial \eta} - \frac{(1-\omega)}{\bar{\lambda}} p \bar{P}_{D1} = 0 \tag{B.2}$$

$$C_D\, p \bar{P}_{Df} - \frac{\partial \bar{P}_{D2}}{\partial r_D}\Big|_{r_D=1} = \frac{1}{p} \tag{B.3}$$

$$\bar{P}_{Df} = [\bar{P}_{D2} - S\frac{\partial \bar{P}_{D2}}{\partial r_D}]_{r_D=1} \tag{B.4}$$

$$\frac{\partial \bar{P}_{D1}(r_D,\eta)}{\partial \eta}\Big|_{\eta=0} = 0 \tag{B.5}$$

$$\bar{P}_{D1}(r_D,\eta)\big|_{\eta=1} = \bar{P}_{D2}(r_D) \tag{B.6}$$

$$\lim_{r_D\to\infty} \bar{P}_{D2}(r_D) = 0 \tag{B.7}$$

$$\frac{\partial \bar{P}_{D2}(r_D)}{\partial r_D}\Big|_{r_D = r_{eD}} = 0 \tag{B.8}$$

$$\bar{P}_{D2}(r_D)\big|_{r_D = r_{eD}} = 0 \tag{B.9}$$

The general solution to Eq. B.2, expressed in terms of modified Bessel functions, is

$$\bar{P}_{D1} = \frac{A}{\sqrt{\eta}} I_{1/2}(x_1\eta) + \frac{B}{\sqrt{\eta}} K_{1/2}(x_1\eta) \tag{B.10}$$

where A and B are constants and x_1 expressed as

$$x_1 = \sqrt{\frac{(1-\omega)p}{\bar{\lambda}}} = \sqrt{\frac{15(1-\omega)p}{\lambda}} \tag{B.11}$$

After applying boundary conditions given by Eqs. B.5 and B.6 to Eq. B.2, the solution for the pressure in the rock matrix can be expressed as

$$\bar{P}_{D1} = \frac{\bar{P}_{D2} I_{1/2}(x_1 \eta)}{\sqrt{\eta} I_{1/2}(x_1)} \tag{B.12}$$

To solve the equation for the pressure in the fracture and at the wellbore, Eq. B.11 can be used to yield

$$\frac{\partial \bar{P}_{D1}}{\partial \eta}\Big|_{\eta=1} = \frac{\bar{P}_{D2} x_1 I_{3/2}(x_1)}{I_{1/2}(x_1)} \tag{B.13}$$

Eq. B.13 can be further simplified using the recursion formula of Bessel function $I_{3/2}(x_1)$ given by

$$I_{3/2}(x_1) = I_{-1/2}(x_1) - \frac{1}{x} I_{1/2}(x_1) \tag{B.14}$$

$I_{-1/2}(x_1)$ and $I_{1/2}(x_1)$ can be defined by hyperbolic functions as

$$I_{-1/2}(x_1) = \sqrt{\frac{2}{\pi x_1}} \cosh(x_1) \tag{B.15}$$

and

$$I_{1/2}(x_1) = \sqrt{\frac{2}{\pi x_1}} \sinh(x_1) \tag{B.16}$$

Substituting Eqs. B.14 to B.16 into Eq. B.13, one obtains

$$\frac{\partial \bar{P}_{D1}}{\partial \eta}\Big|_{\eta=1} = \frac{\bar{P}_{D2} x_1 I_{3/2}(x_1)}{I_{1/2}(x_1)} = \bar{P}_{D2}[x_1 \coth(x_1) - 1] \tag{B.17}$$

Substituting Eq. B.17 into Eq. B.1 yields

$$\frac{\partial^2 \bar{P}_{D2}}{\partial r_D^2} + \frac{1}{r_D}\frac{\partial \bar{P}_{D2}}{\partial r_D} - [3\bar{\lambda} x_1 \coth(x_1) - 3\bar{\lambda} + \omega p]\bar{P}_{D2} = 0 \tag{B.18}$$

Let

$$\begin{aligned} x_2 &= \frac{3\bar{\lambda} x_1 I_{3/2}(x_1)}{I_{1/2}(x_1)} + \omega p \\ &= 3\bar{\lambda} x_1 \coth(x_1) - 3\bar{\lambda} + \omega p \\ &= \frac{\lambda}{5} x_1 \coth(x_1) - \frac{\lambda}{5} + \omega p \end{aligned} \tag{B.19}$$

The general solution to Eq. B.18 is

$$\bar{P}_{D2} = CK_0(\sqrt{x_2} r_D) + DI_0(\sqrt{x_2} r_D) \tag{B.20}$$

After appling the boundary conditions given by Eq. B.7, the fracture pressure is expressed as

$$\bar{P}_{D2} = CK_0(\sqrt{x_2} r_D) \tag{B.21}$$

Substituting Eq. B.21 into Eqs. B.3 and B.4, respectively, and equating the final results, one obtains

$$CK_0(\sqrt{x_2}) + SC\sqrt{x_2}K_1(\sqrt{x_2}) = \frac{1}{C_D p}\{\frac{1}{p} - C\sqrt{x_2}K_1(\sqrt{x_2})\} \tag{B.22}$$

Rearranging Eq. B.22, C is expressed as

$$C = \frac{1}{p}\{\frac{1}{\sqrt{x_2}K_1\sqrt{x_2} + C_D p\,[K_0\sqrt{x_2} + S\sqrt{x_2}K_1\sqrt{x_2}]}\} \tag{B.23}$$

Substituting Eqs. B.22 and B.23 into Eq. B.4, one obtains the solution of $\bar{P}_{Df}$. Similar procedures can be used for the solution of a finite reservoir.

APPENDIX C: Asymptoic Solution for Pressures of an Infinite Reservoir

In the Laplace domain, the solution of the wellbore pressure for an infinite reservoir without wellbore storage and skin effects can be expressed

$$\bar{P}_{Df} = \bar{P}_{D2} = \frac{K_0(\sqrt{x_2})}{p\,\{\sqrt{x_2}K_1(\sqrt{x_2})\}} \tag{C.1}$$

where $x_2 = \dfrac{3\bar{\lambda}x_1 I_{3/2}(x_1)}{I_{1/2}(x_1)} + \omega p = 3\bar{\lambda}x_1\coth(x_1) - 3\bar{\lambda} + \omega p$ and $x_1 = \sqrt{\dfrac{(1-\omega)p}{\bar{\lambda}}}$.

At small times ($p \to \infty$, $x_1 \to \infty$, and $\coth(x_1) \to 1$), and thus x_2 can be expressed

$$x_2 = 3\bar{\lambda}x_1 - 3\bar{\lambda} + \omega p = 3\bar{\lambda}\sqrt{\frac{(1-\omega p)}{\bar{\lambda}}} - 3\bar{\lambda} + \omega p \approx \omega p \tag{C.2}$$

If the argument x is large, $K_0(x)$ and $K_1(x)$ can be expressed

$$K_0(x) = K_1(x) = \sqrt{\frac{\pi}{2x}}e^{-x} \tag{C.3}$$

Substituting Eqs. C.2 and C.3 into Eq. C.1, one obtains

$$\bar{P}_{Df} = \bar{P}_{D2} = \frac{1}{p\sqrt{\omega p}} \tag{C.4}$$

The inversion of Eq. C.4 from the Laplace domain to real space yields

$$P_{Df} = P_{D2} = \frac{2}{\sqrt{\pi}}\sqrt{\frac{t_D}{\omega}} \tag{C.5}$$

At large times ($p \to 0$, $x_1 \to 0$), $I_{-1/2}(x_1)$ and $I_{1/2}(x_1)$ can be expressed by the asymptotic expansions as

$$I_{-1/2}(x_1) = \sqrt{\frac{2}{\pi x_1}}\left(1 + \frac{x_1^2}{2} + \frac{x_1^4}{24} + \ldots\right) \tag{C.6}$$

$$I_{1/2}(x_1) = \sqrt{\frac{2}{\pi x_1}}\left(x_1 + \frac{x_1^3}{6} + \ldots\right) \tag{C.7}$$

Thus, one obtains

$$x_2 = \frac{3\bar{\lambda} x_1 I_{3/2}(x_1)}{I_{1/2}(x_1)} + \omega p$$

$$= \frac{3\bar{\lambda}\sqrt{\frac{2}{\pi x_1}}\left(x_1 + \frac{x_1^3}{2} + \frac{x_1^5}{24} - x_1 - \frac{x_1^3}{6}\right)}{\sqrt{\frac{2}{\pi x_1}}\, x_1} + \omega p$$

$$= \bar{\lambda} x_1^2 + \omega p = p \tag{C.8}$$

If the argument x is small, $K_0(x)$ cab be expressed as

$$K_0(x_1) = -\gamma + \ln 2 - \ln \sqrt{x_1} \tag{C.9}$$

Similarly, $K_1(x_1)$ cab be expressed as

$$K_1(x_1) = \frac{1}{x_1} \tag{C.10}$$

Substituting Eqs. C.9 and C.10 into C.1, one obtains the solution for the wellbore pressure in the Laplace domain given by

$$\bar{P}_{Df} = \bar{P}_{D2} = \frac{-\gamma + \ln 2 - \ln \sqrt{p}}{p} \tag{C.11}$$

The inversion of Eq. C.11 from the Laplace domain to real space yields

$$P_{Df} = P_{D2} = \frac{1}{2}\{\ln t_D + 0.80909\} \tag{C.12}$$

APPENDIX D: Approximate Solution for the Pressure of an Infinite Reservoir

Without skin and wellbore storage effects, the pressure at the wellbore can be expressed as

$$\bar{P}_{Df} = \frac{K_0\sqrt{x_2}}{p\sqrt{x_2}K_1(\sqrt{x_2})} \tag{D.1}$$

Approximate inversion of Eq. D.1 is possible using the improved Schapery method. As a first step, one approximates

$$P_{Df} \sim [p\bar{P}_{Df}]|_{p=1/e^{\eta t_D}}$$

Hence,

$$P_{Df} \sim \frac{K_0(\sqrt{x_2})}{\sqrt{x_2}K_1(\sqrt{x_2})}\Big|_{p=1/e^{\eta t_D}} \tag{D.2}$$

If x_2 is small, Eq. D.2 becomes

$$P_{Df} \sim K_0(\sqrt{x_2})|_{p=1/e^{\eta t_D}} \tag{D.3}$$

In general, for $t_D \geq 10$ (x_2 is still small), $K_0(x_2)$ can be expressed as asymptotic expansion as

$$K_0(x_2) = -\gamma + \ln 2 - \ln\sqrt{x_2}$$

Within 2% accuracy in comparison to the results of the Laplace numerical inversion, P_{Df} can be expressed as

$$P_{Df} = -\gamma + \ln 2 - \frac{1}{2}\ln\{\frac{\lambda}{5}x_3\coth(x_3) - \frac{\lambda}{5} + \frac{\omega}{e^{\eta t_D}}\} \tag{D.4}$$

where

$$x_3 = \sqrt{\frac{15(1-\omega)}{e^{\eta}\lambda t_D}}$$

The half slope can be observed around the dimensionless time, $t_D = \frac{5\omega}{e^{\lambda}\gamma}$. In this region Eq. D.4 can be further simplified to yield

$$P_{Df} = \frac{1}{4}\{\ln t_D - \ln\lambda(1-\omega) - \ln\frac{3}{80} - 3\gamma\} \tag{D.5}$$

APPENDIX E: The Solution of Temperatures for the Fracture and Rock

In the dimensionless form the governing equations for the temperatures in the fracture and rock are

Fracture

$$-\frac{\partial T_{D2}}{\partial \xi} - 12\frac{\partial T_{D1}}{\partial \eta}\Big|_{\eta=1} = \theta\frac{\partial T_{D2}}{\partial \tau} \tag{E.1}$$

Rock

$$\frac{\partial^2 T_{D1}}{\partial \eta^2} + \frac{2}{\eta}\frac{\partial T_{D1}}{\partial \eta} = \frac{\partial T_{D1}}{\partial \tau} \tag{E.2}$$

The initial and boundary conditions are

$$T_{D1}(\xi,\eta,0) = T_{D2}(\xi,0) = 0 \tag{E.3}$$

$$T_{D2}(0,\tau) = \begin{cases} 0 & \tau < 0 \\ 1 & \tau \geq 0 \end{cases} \tag{E.4}$$

$$T_{D1}(\xi,1,\tau) = T_{D2}(\xi,\tau) \tag{E.5}$$

$$T_{D1}(\xi,0,\tau) = finite \tag{E.6}$$

After applying Laplace transformation to Eqs. E.1 and E.2 with respect to τ, one may obtain,

$$-\frac{\partial \overline{T}_{D2}}{\partial \xi} - 12\frac{\partial \overline{T}_{D1}}{\partial \eta}\Big|_{\eta=1} = \theta \overline{T}_{D2p} \tag{E.7}$$

$$\frac{\partial^2 \overline{T}_{D1}}{\partial \eta^2} + \frac{2}{\eta}\frac{\partial \overline{T}_{D1}}{\partial \eta} = \overline{T}_{D1p} \tag{E.8}$$

subject to the transforms of boundary conditions, Eqs E.4, E.5 and E.6,

$$\overline{T}_{D2}(0) = \frac{1}{p} \tag{E.9}$$

$$\overline{T}_{D2}(\xi) = \overline{T}_{D1}(\xi,0), \tag{E.10}$$

$$\overline{T}_{D1}|_{\eta=0} = finite. \tag{E.11}$$

The general solution to Eq. E.8, expressed in terms of the modified Bessel functions, is

$$\overline{T}_{D1} = \frac{A}{\sqrt{\eta}} I_{1/2}(\sqrt{p}\ \eta) + \frac{B}{\sqrt{\eta}} K_{1/2}(\sqrt{p}\ \eta) \tag{E.12}$$

where A and B are constants. Applying boundary conditions given by Eqs. E.10 and E.11, A and B can be determined.

$$A = \frac{\overline{T}_{D2}}{I_{1/2}(\sqrt{p}\ )} \tag{E.13}$$

$$B = 0$$

Substituting Eq. E.13 into Eq. E.12, one obtains the solution of the temperature in the rock.

$$\overline{T}_{D1} = \frac{\overline{T}_{D2} I_{1/2}(\sqrt{p}\ \xi)}{\sqrt{\xi} I_{1/2}(\sqrt{p}\ )} \tag{E.14}$$

To solve the equation for the temperature in the fracture, one evaluates

$$\frac{\partial \overline{T}_{D1}}{\partial \xi}\Big|_{\eta=1} = \frac{\overline{T}_{D2}\sqrt{p}\, I_{3/2}(\sqrt{p}\ )}{I_{1/2}(\sqrt{p}\ )} \tag{E.15}$$

Substituting Eq. E.15 into Eq. E.7, one may obtain the general solution for the temperature in the fracture

$$\overline{T}_{D2} = A \exp\{ - [\theta p + 12\sqrt{p}\, \frac{I_{3/2}\sqrt{p}}{I_{1/2}(\sqrt{p}\ )}]\xi\} \tag{E.16}$$

where A is a constant. Applying the boundary condition (Eq. E.9), one obtains

$$A = \frac{1}{p}$$

Thus, the solution for the temperature in the fracture can be expressed as

$$\overline{T}_{D2} = \frac{1}{p}\exp\{-[\theta p + 12\sqrt{p}\,\frac{I_{3/2}\sqrt{p}}{I_{1/2}(\sqrt{p})}]\xi\} \tag{E.17}$$

Asymptotic Solutions

From the recursion formula of Bessel functions, $I_{3/2}(x)$ can be expressed as

$$I_{3/2}(x) = I_{-1/2}(x) - \frac{1}{x}I_{1/2}(x) \tag{E.18}$$

If the argument x is large, $I_{-1/2}(x)$ and $I_{1/2}(x)$ can be expressed as

$$I_{-1/2}(x) = I_{1/2}(x) = \frac{e^{x}}{\sqrt{2\pi x}} \tag{E.19}$$

At small times ($p \rightarrow \infty$), one substitutes Eqs. E.18 and E.19 into Eq. E.17 and obtains the equation for the temperature in the fracture in the Laplace domain given by

$$\overline{T}_{D2} = \frac{1}{p}\exp\{-\theta\xi p\} \tag{E.20}$$

Eq. E.20 can be inverted to real space as

$$T_{D2} = U\{\tau - \theta\xi\} \tag{E.21}$$

where U is the unit step function. If the argument x is small, $I_{-1/2}(x)$ can be expressed as

$$I_{-1/2}(x) = \sqrt{\frac{2}{\pi x}}\,(1 + \frac{x^2}{2} + \frac{x^4}{24} + \ldots) \tag{E.22}$$

Similarly, $I_{1/2}(x)$ can be expressed as

$$I_{1/2}(x) = \sqrt{\frac{2}{\pi x}}\left(x + \frac{x^3}{6} + \ldots \right) \tag{E.23}$$

At large times ($p \rightarrow 0$), one substitutes Eqs. E.22 and E.23 into Eq. E.17 and obtains the equation for temperature in the fracture in the Laplace domain given by

$$\overline{T}_{D2} = \frac{1}{p}\exp\{ -(4+\theta)\xi p \} \tag{E.24}$$

The inversion of Eq. E.24 from Laplace domain to real space yields

$$T_{D2} = U\ \{ \tau - (4+\theta)\xi \} \tag{E.25}$$

This report was done with support from the Department of Energy. Any conclusions or opinions expressed in this report represent solely those of the author(s) and not necessarily those of The Regents of the University of California, the Lawrence Berkeley Laboratory or the Department of Energy.

Reference to a company or product name does not imply approval or recommendation of the product by the University of California or the U.S. Department of Energy to the exclusion of others that may be suitable.